#12730

IMPACT OF ADDED INSULATION ON AIR LEAKAGE PATTERNS

By: Dominique Derome
Paul Fazio
Guylaine Desmarais

January 17, 2000

CMHC Project Officer: Sandra Marshall

This project was carried out with the assistance of a grant from Canada Mortgage and Housing Corporation under the terms of the External Research Program (CMHC File 6585-D098). The views expressed are those of the author and do not represent the official views of the Corporation.

Final Report

Impact of added insulation on air leakage patterns

Research team:
Principal investigator: **Dominique Derome**
Collaborator: **Paul Fazio**
Graduate student: **Guylaine Desmarais**

Report written by:
Guylaine Desmarais
Dominique Derome

Presented to:
Sandra Marshall, Senior Researcher
Research Division
Canadian Mortgage and Housing Corp

CMHC Project 6585-D098

January 17th, 2000
Department of Building, Civil, and Env
Concordia University
Montreal

Abstract

Adding insulation to exterior walls may worsen the original wall performance. Depending on the amount and geometry of air leakage in the original wall, added insulation may actually increase the potential for condensation, letting water accumulate in the wood structure and leading to rot.

An experiment was set up to compare the performance of different leaky walls and to investigate their behaviour with insulation added on one side or other of the wood studs. The experiment also maps the path of air leakage. The test conditions represented winter and late spring weather in Montreal.

It was found that the first measure to be considered remains the sealing and air tightening of the existing walls, with special care given to junctions and to punctures. If not sealed, leaky walls were found to accumulate moisture, especially when insulated on the outside.

Acknowledgements

The successful completion of this project required the input of many people in addition to the project team. They deserve to be thanked for their most valuable contributions to the project:

Colleagues:	Andreas Athienitis, Ph.D.
Research support:	Jiwu Rao, Ph.D Dorina Banu Sylvain Belanger
Lab support:	Luc Demers Jacques Payer Joe Hribb Jean-Claude Desjardins Guy Fournier
Students:	Sandrine Bertrand Philippe Brosseau

Executive Summary

Increased levels of insulation are being promoted to reduce energy consumption. Straightforward ways exist to calculate the impact on energy consumption of thermal resistance added to the envelope. However, other impacts of adding insulation, like the potential for condensation due to moisture and air movement through the exterior wall assembly, are often not taken into account. To avoid problems, the post-insulation hygrothermal performance of exterior wall assemblies should be assessed prior to the addition of insulation. To do so however, current computer codes lack the much needed information on the air trajectory through the envelope assembly. This project proposes an experimental procedure to monitor air leakage paths in the context of the retrofitting of existing exterior walls.

The objectives of the experimental work are:

- to develop and validate a mode of characterizing air leakage paths and;
- to study the impact of different insulating strategies on exterior wall assemblies having different air leakage characteristics on the moisture content and temperature distribution patterns in walls when exposed to four months of wetting and drying conditions.

The procedure involves the construction of a full scale test hut inside the environmental chamber where conditions representing Montreal winter and late spring weather are reproduced. Two re-insulation strategies are studied, with three different air leakage patterns, and compared to two insulated base-cases. The construction of the hut is typical of Quebec low-rise wood frame residences, insulated with fiberglass batt insulation or cellulose fiber insulation between the studs.

The two air leakage pattern characterization methods implemented to gain more knowledge about the movement of air through the assemblies were: (1) 3-dimensional grid temperature monitoring and (2) 2-dimensional grid moisture content monitoring.

Results of the temperature monitoring are presented using isotherms at two different planes. The two-dimensional moisture content monitoring grid allows for the development of isohygrons, or contour lines for equal moisture contents. The changes in moisture content in the exterior sheathing and the wood stud are also presented.

The isotherms and isohygrons that were generated demonstrate that there is a correlation between the temperature profiles and the air leakage path, and between the moisture distribution pattern and the air leakage path. The moisture content maps also highlighted the fact that local areas where moisture contents rise well above levels sustaining mold growth exist for some of the assemblies although their average moisture content is lower. Furthermore, it was found that the two re-insulation strategies studied, although they provide the same R-value, performed quite differently in terms of temperatures and moisture accumulation. In the case of adding insulation on the warm side, moisture contents mostly do not rise above 25%, while they go up to 70% when insulation is added on the cold side. It can be conclude that leaky walls tend to behave better when rigid insulation is placed on the warm side on the assembly. Finally, the section where no insulation was added but that was airtight had low moisture contents through the experiment, suggesting that airtightness should be considered before the additions of rigid insulation to reduce energy consumption and reduce the risk of moisture accumulation related problems. It should be kept in mind that these conclusions are applicable to the types of assemblies and materials studied in this research project, i.e. with added insulation with low water vapor permeability and that they cannot be generalized to all existing exterior wall assemblies and all insulation materials.

Résumé

On préconise des niveaux d'isolation accrus afin de réduire la consommation d'énergie. Il existe des façons simples pour calculer les effets que peut avoir l'augmentation de la résistance thermique d'une enveloppe sur la consommation d'énergie. Or, l'ajout d'isolant peut avoir d'autres répercussions, telles que la production de condensation causée par le mouvement d'air et d'humidité à travers le mur extérieur, lesquelles sont rarement prises en considération. Pour éviter les problèmes, il faut évaluer la performance hygrothermique des murs extérieurs, après la pose de l'isolant, avant d'en augmenter la quantité. Toutefois, les codes informatiques actuels ne disposent pas des données essentielles sur la trajectoire de l'air au sein de l'enveloppe. Ce projet a donc pour objectif de suivre, à titre expérimental, les voies de fuites d'air dans un contexte de réfection de murs extérieurs existants.

Ces travaux expérimentaux visaient à :

- mettre au point et valider une façon de caractériser les voies de fuites d'air et à
- étudier l'effet de différentes stratégies d'isolation, pour des murs extérieurs possédant différentes caractéristiques de fuites d'air, sur la teneur en humidité et les schémas de répartition de la température dans les murs lors d'une exposition à quatre mois de conditions de mouillage et de séchage.

La méthode employée a consisté à construire un bâtiment d'essai en vraie grandeur à l'intérieur d'un caisson environnemental reproduisant les conditions climatiques propres à un hiver et à une fin de printemps de Montréal. Deux stratégies d'ajout d'isolant ont été étudiées, comportant trois schémas de fuites d'air différents, puis comparées à deux modèles de référence isolés. Le bâtiment a été construit selon le style des maisons québécoises de plain-pied à ossature de bois. Il a été isolé avec des matelas de fibre de verre ou de fibre de cellulose placés entre les poteaux d'ossature.

Les deux méthodes de caractérisation des schémas de fuites d'air suivantes ont été retenues pour en apprendre davantage sur le mouvement d'air dans les assemblages : (1) contrôle de la température avec grille tridimensionnelle et (2) contrôle de la teneur en humidité avec grille bidimensionnelle.

Les résultats du contrôle de la température sont présentés sous forme d'isothermes sur deux plans différents. La grille bidimensionnelle faisant état de la teneur en humidité permet de réaliser des courbes de niveau représentant les teneurs en humidité égales. Les changements touchant les teneurs en humidité du revêtement d'ossature et des poteaux de bois sont aussi donnés.

Les courbes de niveau représentant les valeurs de température et d'humidité qui ont été produites montrent une corrélation entre les profils de température et les voies de fuites d'air ainsi qu'entre les schémas de répartition de l'humidité et la voie des fuites d'air. Les cartes illustrant les teneurs en humidité font aussi ressortir le fait qu'il existe, dans certains assemblages muraux, des zones localisées où la teneur en humidité augmente bien au-delà des teneurs nécessaires à la prolifération des moisissures, et ce, même si la teneur en humidité moyenne de ces zones est

inférieure. En outre, on a découvert que les deux stratégies d'ajout d'isolant étudiées, bien qu'elles offrent des coefficients R identiques, ont un comportement très différent au chapitre des températures et de l'accumulation d'humidité. Lorsqu'on ajoute de l'isolant du côté chaud, les teneurs en humidité, dans la plupart des cas, n'atteignent pas plus de 25 %, alors qu'elles peuvent atteindre jusqu'à 70 % lorsque l'isolant est mis en place du côté froid. On peut donc en conclure que les murs qui fuient ont tendance à mieux se comporter lorsqu'un isolant rigide est placé du côté chaud de l'assemblage. Enfin, la section qui n'a pas reçu d'isolant supplémentaire, mais qui était étanche à l'air, a présenté de faibles teneurs en humidité tout au long de l'expérience, ce qui laisse supposer que l'étanchéité à l'air devrait être prise en considération avant d'ajouter un isolant rigide pour réduire la consommation d'énergie et diminuer le risque d'éprouver des problèmes liés à l'accumulation d'humidité. Par ailleurs, il faut noter que ces conclusions ne s'appliquent qu'aux assemblages et aux matériaux étudiés durant la recherche dont il est ici question, c'est-à-dire l'ajout d'un isolant possédant une faible perméabilité à la vapeur d'eau. Elles ne peuvent donc pas être étendues à tous les assemblages muraux extérieurs et à tous les matériaux isolants.

CMHC SCHL

National Office
700 Montreal Road
Ottawa ON K1A 0P7
Telephone: (613) 748-2000

Bureau national
700 chemin de Montréal
Ottawa ON K1A 0P7
Téléphone : (613) 748-2000

Puisqu'on prévoit une demande restreinte pour ce document de recherche, seul le résumé a été traduit.

La SCHL fera traduire le document si la demande le justifie.

Pour nous aider à déterminer si la demande justifie que ce rapport soit traduit en français, veuillez remplir la partie ci-dessous et la retourner à l'adresse suivante :

Le Centre canadien de documentation sur l'habitation
La Société canadienne d'hypothèques et de logement
700, chemin de Montréal, bureau C1-200
Ottawa (Ontario)
K1A 0P7

TITRE DU RAPPORT : _____

_____

Je préférerais que ce rapport soit disponible en français.

NOM _____

ADRESSE _____
rue app.

_____
ville province code postal

No de télephone ( ) _____

Table of Contents

List of figures

List of tables

1. Introduction

Increased levels of insulation are being promoted to reduce energy consumption. Different programs have been proposed by government agencies in Quebec and Canada to encourage and assist homeowners to add insulation to existing residential low-rise buildings. For example, Hydro-Quebec launched a program called "Isolaction", while the Ministère Ressources naturelles Québec has one called "PRIME".

Straightforward ways exist to calculate the impact on energy consumption of thermal resistance added to the envelope. However, other impacts of adding insulation, like the potential for condensation due to moisture and air movement through the exterior wall assembly, often are not taken into account. Adding thermal resistance to exterior wall assemblies modifies their temperature gradient and the risk for moisture condensation may increase, especially if warm, moist indoor air is allowed to flow through them. Moisture may then accumulate in the hygroscopic materials (wood, fiberboard sheathing) and the insulation, inducing decay, mold growth, and the reduction of the thermal performance of the insulation.

Moisture from indoor can move through the wall by diffusion or exfiltration. Of the two, exfiltration is the main moisture transfer vehicle (Kumaran 1996), and thus an important cause of moisture related problems. Most air exfiltrates through paths created by cracks, joints between materials, or junctions between components; the latter are often the weak points of the assembly and are critical because of their potential for becoming concentrated areas of deterioration. Furthermore, "it has been demonstrated that walls with point defects on the warm side of the assembly showed moisture accumulation directly opposite the defect on the cold side when tested" (Forest 1989). Yet, the airtightness of residential buildings is currently evaluated only in a global manner. Although useful for energy consumption evaluation, a total air leakage rate for a building provides little information on the actual path taken by the air, and where the potential moisture accumulation areas are.

To avoid problems, the post-insulation hygrothermal performance of exterior wall assemblies should be evaluated prior to the addition of insulation. Computer simulations of combined heat, moisture, and air transfer could be used to study the impact of exfiltration on exterior wall assemblies with added insulation. However, among the short comings of current computer codes is the unavailability of information on the trajectory of air through the envelope assembly. This project proposes an experimental procedure to monitor air leakage paths in the context of the retrofitting of existing exterior walls.

The objectives of the experimental work are:

- to develop and validate a mode of characterizing air leakage paths and;
- to study the impact of different insulating strategies on exterior wall assemblies having different air leakage characteristics on the moisture content and temperature distribution patterns in walls when exposed to four months of wetting and drying conditions.

The procedure involves the construction of a full scale test hut inside the environmental chamber where conditions representing Montreal winter and late spring weather are reproduced. Two re-insulation strategies are studied, with three different air leakage patterns, and compared to two insulated base-cases. The construction of the hut is typical of Quebec low-rise wood frame residences, insulated with fiberglass batt insulation or cellulose fiber insulation between the studs.

The different air leakage pattern characterization methods implemented to gain more knowledge about the movement of air through the assemblies are: (1) 3-dimensional grid temperature monitoring and (2) 2-dimensional grid moisture content monitoring.

Results for these air leakage characterization methods are presented in a graphic manner. The 3-dimensional temperature monitoring grid measures temperatures at two different depths within the assemblies. They are presented using isotherms at these two planes, the cold side and the warm side of the fiberglass batt insulation. The 2-dimensional moisture content monitoring grid allows for the development of isohygrons, or contour lines of equal moisture contents for the fiberboard exterior sheathing.

2. Experimental Facility

The Environmental Chamber is a versatile research facility where the overall hygrothermal performance of exterior walls (with or without doors and windows), and/or roofs can be evaluated. It has been designed to meet the requirements for the guarded hot box standard test method (ASTM C 236-89). For this test, the facility is used in the environmental chamber mode.

2.1. Environmental chamber facility components

- The **cold box**, 7.5 m high by 4.4 m wide by 3.6 m deep, in which temperatures ranging from -40°C to 40°C can be maintained. The conditions are produced using a 5 ton screw compressor, a 12 000 cfm re-circulation fan, and a 25 kW re-heating heater. This box can not be moved from its position. Its walls are made of 150 mm foamed polyurethane boards, laminated between 1 mm aluminum sheets on the outside and 1 mm stainless steel sheets on the inside.
- The **hot box**, 7.5 m high by 4.4 m wide by 6.1 m deep, heated with a 20 kW heater and cooled with a 1 ton cooling unit. Temperatures from 5°C to 50°C can be obtained. It is also equipped with a 600 cfm air re-circulation system, a fresh air supply/return damper, and a humidification system. The hot box is moveable toward and away from the cold box on 4 compressed air pads. Its walls are made of 150 mm foamed polyurethane boards, laminated between 1 mm aluminum sheets on the outside and 1 mm stainless steel sheets on the inside.
- The **data acquisition system**. It has 400 input channels and 10 output channels. Readings are taken every 10 minutes for each measurement point.

Figure 1 illustrates the main parts of the Environmental Chamber Facility, of which the specimen frame and the metering box are not used for this test.

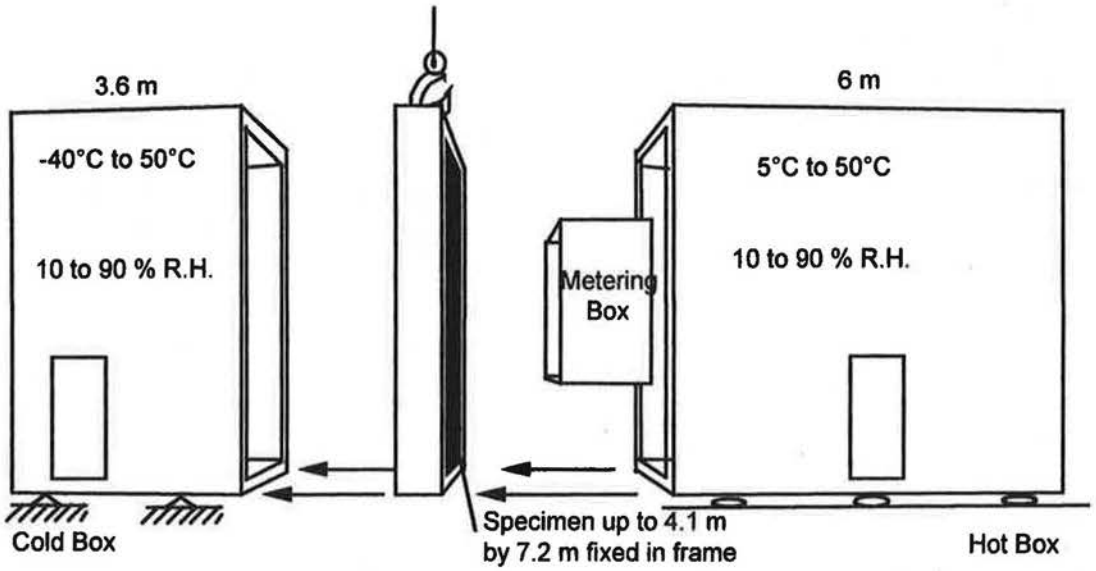

Figure 1. Environmental Chamber Facility.[1]

2.2. Configuration used for present research project.

The facility was used in the climatic chamber mode for this research project. The cold and hot boxes are joined, forming a 7.5 m high by 4.4 m wide by 10.5 m deep climatic chamber, where full scale test huts can be tested. Figure 2 illustrates this configuration.

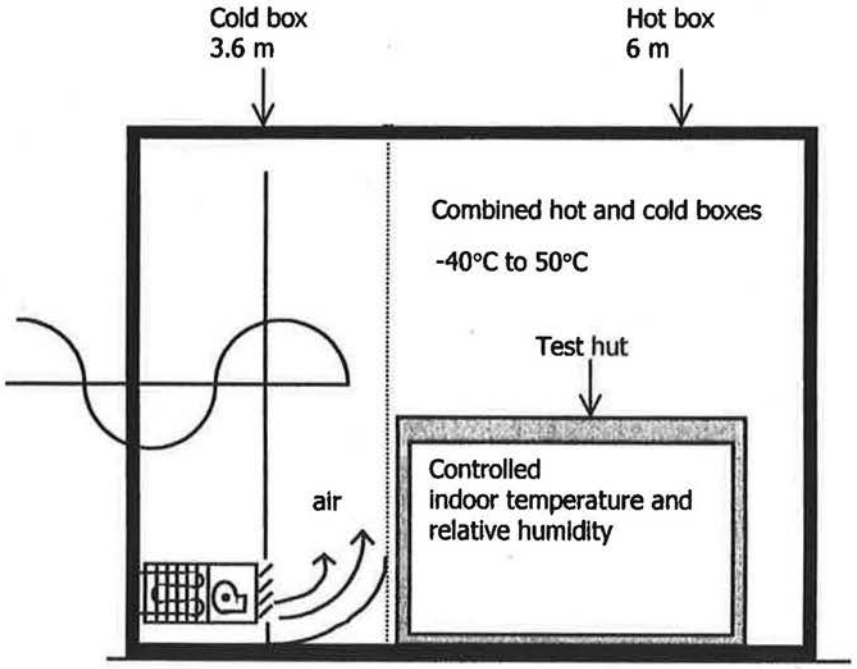

Figure 2. Environmental chamber facility in climatic chamber mode.[2]

[1] From Derome et al, 1997
[2] From Fazio et al, 1997

3. Experimental Protocol

3.1. Scope of experimentation

A 4.2 m long by 2.5 m wide by 3 m high test hut is built inside the environmental chamber. It models the second story of a house, which would normally be subjected to a positive air pressure differential, and therefore exfiltration, during the winter months due to the stack effect.

The test hut is exposed to simulated winter, and then spring, outdoor weather conditions. Real weather data collected for Montreal over 12 years is used to determine the actual conditions in the climatic chamber, while those inside the test hut are based on Standard ANSI/ASHRAE 55-1992 (Thermal Environmental Conditions for Human Occupancy). The baseboard heater and the dehumidifier used to condition the test hut are located in a 1.6 m long by 0.84 m wide by 0.65 m high plywood box in its center. The air is mixed inside this box before circulating in the hut, ensuring more uniform conditions for all sample sections. The installation of the wall-mounted air conditioning unit and the passage of the electrical and sensor wires are concentrated in one section between two studs, where no monitoring is performed.

The test hut includes seven different exterior wall compositions, divided in two groups: those insulated between the wood studs with fiberglass batt insulation (89 mm thick), and those insulated with blown cellulose fiber (89 mm or 140 mm thick). The long walls, perpendicular to the roof joists, are insulated with fiberglass. The shorter end walls are insulated with blown cellulose fiber. Two re-insulation strategies and three different air leakage patterns are applied to the three base cases. In total, 14 exterior wall sample sections are studied. The next page is a schematic plan view of the test hut.

3.2. Test specimens

In total, 14 sample sections, 0.8 m wide by approximately 2.45 m high, are being investigated. A sample section is defined as one complete 0.36 m cavity, flanked on each side by a 38 mm X 89 mm stud and a 0.18 m cavity. Each sample section is completely insulated according to the insulation strategy being investigated, and monitoring is performed only in the 0.4 m central portion. The two half-cavities act as insulated "buffers" between the sample section and the adjacent ones. The sample sections are separated by Oriented Strand Board panels (OSB), 0.016 m thick by 0.3 m wide to prevent air and moisture transfer between the sample sections. The panels are painted with two coats of a special vapor barrier paint to prevent moisture diffusion, and are wider than the assemblies to allow caulking of the finishes against the separators. They are sealed to the bottom and top plates. At the roof level, OSB panels spanning the width of the test hut are sealed to the top plate and to the OSB panels separating the wall sample sections.

Figure 3 shows the wood structure and the separators.

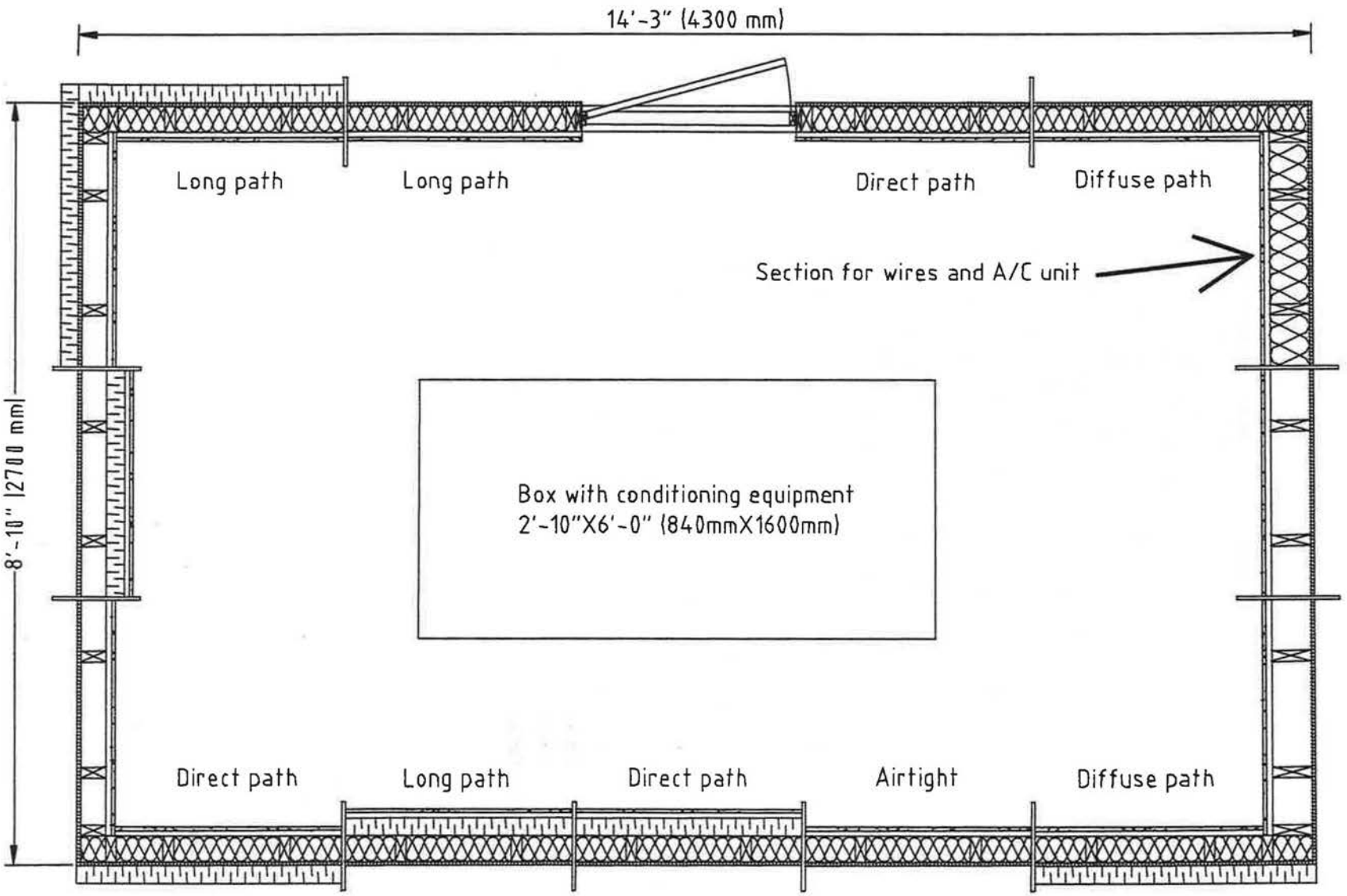
14'-3" (4300 mm)
8'-10" (2700 mm)
Long path
Long path
Direct path
Diffuse path
Section for wires and A/C unit
Box with conditioning equipment
2'-10"X6'-0" (840mmX1600mm)
Direct path
Long path
Direct path
Airtight
Diffuse path

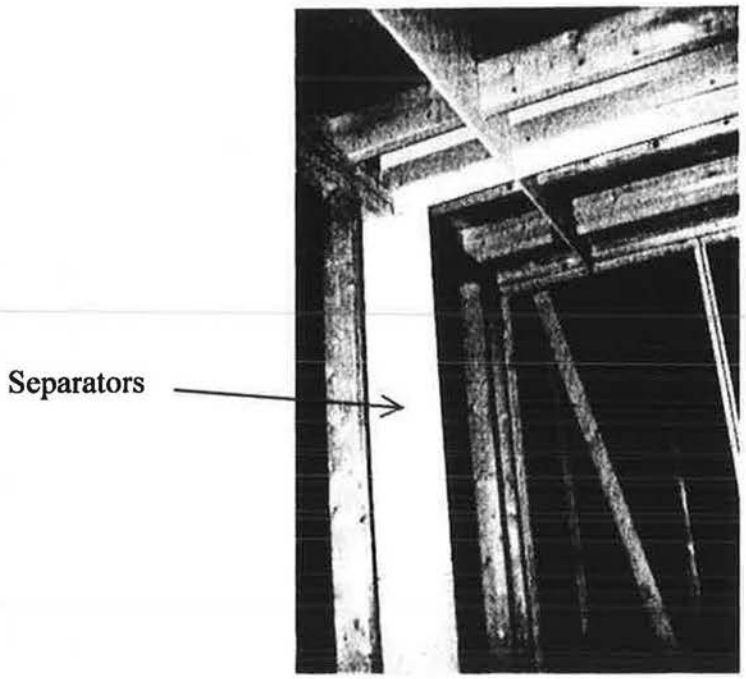

Figure 3. Test hut wood structure and OSB separators.

3.2.1. Composition of the assemblies

The composition of the walls (platform frame system with 38 mm X 89 mm wood studs) is typical of single-family residential construction in Quebec. Statistics from "l'Association Provinciale des Constructeurs d'Habitations du Québec" (APCHQ) were used to select the construction materials.

The junction between the exterior walls and the roof for the sample sections insulated with fiberglass batt insulation is built according to commonly used techniques and materials. The set up simulates typical ventilated roofs. Even though it is not directly monitored, the junction of the roof is included in the overall hygrothermal behavior of the specimens. The sample sections insulated with cellulose fiber are full height but not connected to the roof.

The composition of the roof, from outside to inside, is:

- waterproofing membrane;
- 13 mm plywood;
- 38 mm X 140 mm wood joists @ 400 mm c/c;
- 250 mm air space (ventilated to outside);
- 38 mm X 140 mm wood joists @ 400 mm c/c;
- 250 mm of fiberglass batt insulation;
- 6 mil polyethylene membrane air/vapor barrier;
- 19 mm X 64 mm @ 400 mm c/c wood furring;
- 13 mm gypsum board;
- standard latex paint (two coats).

Base-case walls (simulating typical existing conditions without modifications).

1. Wall insulated with fiberglass batt insulation, with nominal 2" X 4" wood studs:

- Spun bonded polyolefin membrane ("Tyvek");
- 10 mm asphalt impregnated fiberboard;
- 38 mm X 89 mm @ 400 mm c/c wood studs;
- 89 mm fiberglass batt insulation between the studs;
- 6 mil polyethylene membrane air/vapor barrier;
- 19 mm X 64 mm @ 400 mm c/c horizontal wood furring;
- 13 mm gypsum board;
- standard latex paint (two coats).

2. Wall insulated with blown cellulose insulation, with nominal 2" X 4" wood studs:

- Spun bonded polyolefin membrane ("Tyvek");
- 10 mm asphalt impregnated fiberboard;
- 38 mm X 89 mm @ 400 mm c/c wood studs;
- 89 mm blown cellulose fiber insulation between the studs and polyester fiber mesh;
- 19 mm X 64 mm @ 400 mm c/c horizontal wood furring;
- 6 mil polyethylene membrane air/vapor barrier;
- 13 mm gypsum board;
- standard latex paint (two coats).

3. Wall insulated with blown cellulose insulation, with nominal 2" X 6" wood studs:

- Spun bonded polyolefin membrane ("Tyvek");
- 10 mm asphalt impregnated fiberboard;
- 38 mm X 140 mm @ 400 mm c/c wood studs;
- 140 mm blown cellulose fiber insulation between the studs and polyester fiber mesh;
- 19 mm X 64 mm @ 400 mm c/c horizontal wood furring;
- 6 mil polyethylene membrane air/vapor barrier;
- 13 mm gypsum board;
- standard latex paint (two coats).

In these wall compositions, the spun bonded polyolefin "Tyvek" membrane serves as a wind/weather barrier, the asphalt impregnated fiberboard is the exterior sheathing. The wood studs give the structural strength to the wall. The insulation minimizes the heat losses. The polyester mesh is applied to hold the cellulosic fiber insulation in place and to allow the air introduced with the cellulose to escape, preventing air pockets and settling. The wood furring is used, among other reasons, to: minimize the staining of the interior finish that frequently occurs in front of the cold wood studs, protect the air/vapor barrier from being perforated by nails used to hang pictures, and provide a straighter medium to install the interior finish. The polyethylene membrane acts as an air/vapor barrier. The gypsum board is the interior finish, which is then painted with two coats of a standard latex paint.

For three of the sample sections having base-case compositions #1 or #2, rigid extruded polystyrene insulation (38 mm) is added on the indoor side of the assembly, on the warm side of the wood studs and fiberglass batt insulation. The air/vapor barrier membrane, the wood furring, and the interior finish then follow. This method would be used if interior renovations are being performed and removal of the existing interior finish is necessary. The air/vapor barrier can be

evaluated and repaired or replaced if necessary and the airtightness of the assembly can be improved from the inside.

For four sample sections, having base-case compositions #1 or #2, rigid extruded polystyrene insulation (38 mm) is added on the exterior side of the assembly, directly over the existing fiberboard sheathing. For this method, removal of the exterior veneer is necessary and it would therefore be used in a retrofit procedure if the exterior veneer also needs to be replaced. Airtightness can then be improved from the outside.

If both the interior and exterior finishes appear to be in good condition, either of these two re-insulation strategies could be used to increase the thermal resistance of the wall.

Figure 4 shows one sample sections with rigid insulation added on the warm side of the fiberglass batt insulation (before the installation of the air/vapor barrier, the wood furring, and the interior finish), one with rigid insulation added on the cold side of the fiberglass batt insulation (before installation of the spun bonded polyolefin "Tyvek" membrane), and one with cellulose fiber insulation between the studs (before the installation of the interior finish).

a. Section with rigid insulation added on the warm side.

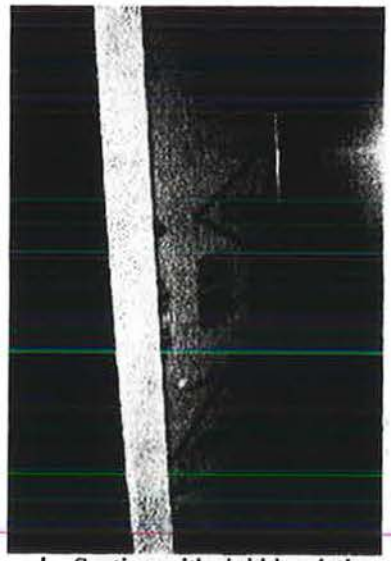

b. Section with rigid insulation added on the cold side.

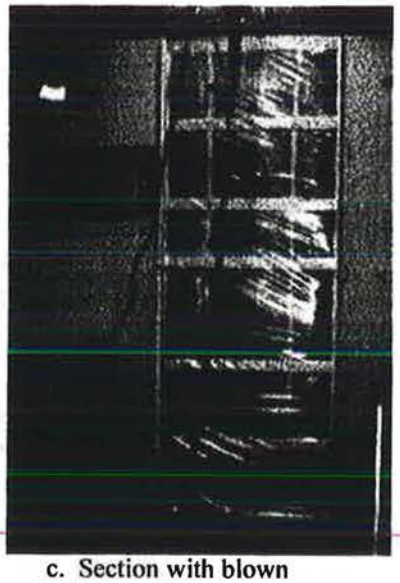

c. Section with blown cellulose fiber.

Figure 4. Insulated sample sections.

3.2.2. Air leakage characteristics

The exterior wall compositions described above are studied with different air leakage characteristics. Many different types of air leakage paths can exist in exterior wall assemblies. Three are studied here:

- Long air exfiltration path. The air flows into the wall through a 2 mm horizontal crack at the bottom of the interior finish and out through a 5 mm horizontal crack at the top of the exterior sheathing, just below the top plate. This is the case when the gap between the interior finish and the floor is not sealed properly.
- Concentrated air exfiltration path. The air flows into the wall through a 20 mm diameter opening in the interior finish (centered between the studs, 300 mm above the floor) and out through the whole surface of the fiberboard sheathing on the exterior side of the assembly. This might occur, for example, when air exits through an electrical outlet but there is not necessarily a corresponding hole on the cold side of the assembly.
- Distributed exfiltration path. The air flows into the wall uniformly through 42 holes, 3 mm in diameter (according to a 150 mm center to center grid) drilled in the interior finish and out through the fiberboard sheathing. There are no holes through the fiberboard sheathing. Although it is not likely to occur in buildings using the usual construction materials (which have a certain airtightness), this type of flow is included because some simulation models only take into account a uniform airflow through the assembly.

These three air leakage characteristics are applied to the sample sections with 89 mm fiberglass batt insulation between the studs. To serve as a reference, one base-case #1 section with no rigid insulation added is sealed so that as little air as possible flows through it. Figure 5 and Figure 6 illustrate the air leakage paths.

For base-cases #2 and #3, only the concentrated exfiltration path is introduced one month into the test, by drilling three holes 10 mm in diameter at the bottom, close to the studs.

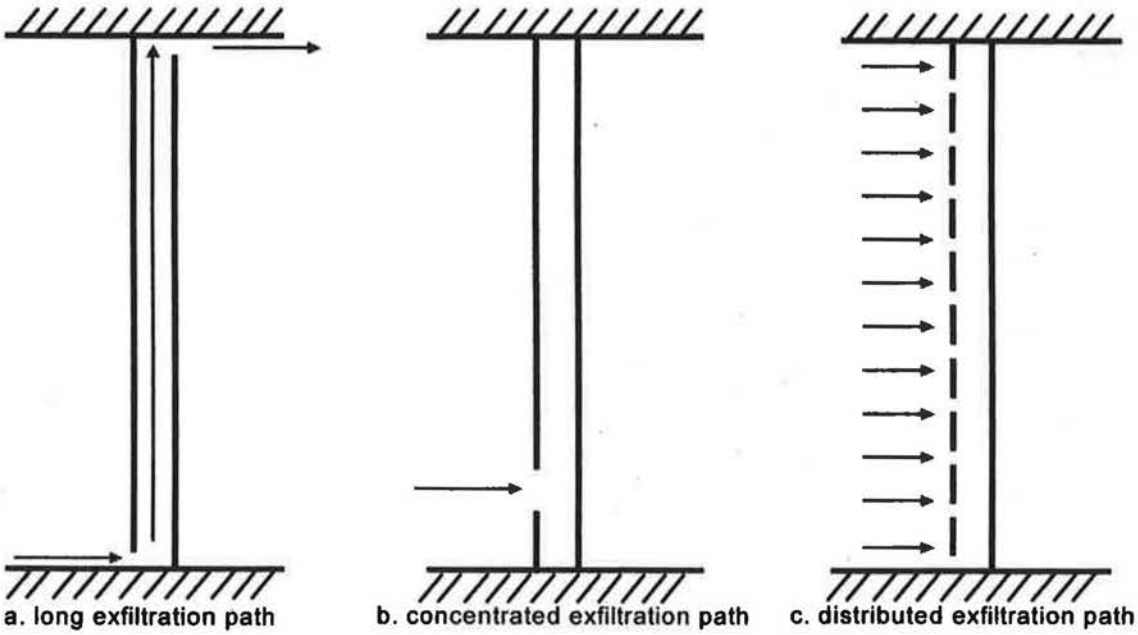

Figure 5. Section view of air leakage paths - Sample sections with fiberglass wool.

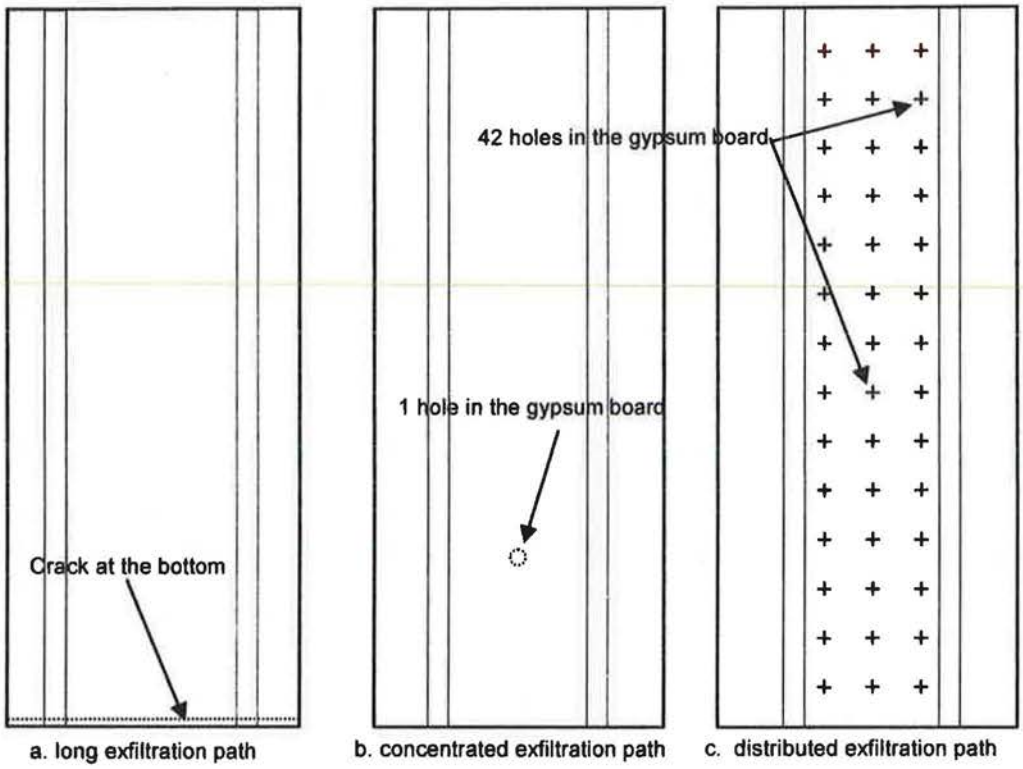

Figure 6. Elevation view of air leakage paths - Sample sections with fiberglass wool.

3.2.3. Summary of sample sections

Table 1. Sample sections parameters

Section ID	89 mm fiberglass	89 mm cellulose	140 mm cellulose	38 mm polystyrene int.	38 mm polystyrene ext.	Long air path	Concentrated air path	Distributed air path	Air tight
1	■					■			
2	■						■		
3	■							■	
4	■				■	■			
5	■				■		■		
6	■				■			■	
7	■			■		■			
8	■			■			■		
9	■								■
10			■						
11			■					■	
12		■						■	
13		■		■				■	
14		■			■			■	

3.3. Test conditions

3.3.1. Climatic conditions

To select the climatic conditions, a list of criteria to be respected was established:

- To get a representative hygrothermal behavior of the exterior wall specimens, the climatic conditions provided in the environmental chamber are based on real outdoor weather conditions for a specific location and the conditions provided inside the test hut are typical of those maintained by occupants under those outdoor conditions.
- Temperature, water vapor pressure, and air pressure differentials had to be imposed simultaneously to represent what is found in real operating conditions.
- The exterior wall assemblies are to be subjected to weather conditions favorable to moisture accumulation in order to study their potential for moisture related problems.
- After moisture has accumulated, the exterior wall assemblies are subjected to weather conditions causing moisture to evacuate, in order to study their mode of drying.
- For the length of each climatic period, the temperature, water vapor pressure, and air pressure are maintained constant. This allows comparison of experimental results with analytical results from a steady-state, 3-dimensional conductive heat transfer model.

3.3.2. Previous moisture transfer laboratory experiments

Experiments including heat, air, and moisture transfer have already been conducted in laboratory settings on various exterior wall assemblies. Table 2 summarizes some of this previous work, which can be used as a basis for the establishment of the climatic conditions to be provided in the present research project. Experiments are listed in reverse chronological order. For the experiments included in Table 2 the duration of the exposure to wetting climatic conditions has varied from 5 days (Trechsel 1985, 1986) to 176 days (Simpson 1994). As for the exterior temperatures, they have varied from 7.2°C, for mild winter conditions (Burch 1995), to -18°C, for extreme Swedish winter conditions (Ojanen, Simonson 1995). The assemblies studied represented mostly wood frame exterior wall assemblies. Ojanen and Simonson (1995) studied a wall junction and a wall/roof junction. Those assemblies were investigated with different insulation strategies, and/or different exterior sheathing, and/or different vapor barriers. The impact of air barriers was also studied in Ojanen and Kohonen (1995), Trechsel (1986), and Trechsel (1985). In some of the experiments, moisture was introduced directly into the assemblies (Ojanen 1995) to study their mode of drying. In others, interior air was allowed to flow through the wall assemblies. For example, Trechsel (1986) made holes in the interior finish (two at the top and two at the bottom) at the beginning of the test, while in another experiment, Simpson (1994) added holes mid-way through the experiment. In both cases, the openings did not represent any specific air leakage path. In his experiment, Trechsel (1986) also provided holes that could be hermetically sealed to allow the introduction of tracer gas, in order to determine the direction of air flow in the cavity.

Table 2. Summary of some previous moisture transfer laboratory experiments.

Authors	Test duration/ conditions	Objective(s)	Test setup	Studied parameters
Zarr, R.R Burch, D.M. Fanney, A.H. (1995)	- int.: 21°C, 50% RH 104 days inc. pre-cond. **1 at 7.2°C steady.-s.** (prep. for 1st cycle) **6 of sine waves** (transfer in dry walls) **34 @ 7.2°C steady-s.** (moisture accumulation) **7 of sine waves** (transfer in moist walls) **14 at 32°C** (drying)	To compare measured heat fluxes and moisture contents to predicted heat fluxes and moisture contents, in order to validate the MOIST mathematical algorithms.	- 12 small wall samples were studied simultaneously in a calibrated hot box. - a circular "carrot" was cut in the middle of each to ensure one-dimensional heat and moisture transfer.	- One-dimensional heat and moisture transfer; - effect of moisture on heat flux; - experimental results compared to calculated results according to ASHRAE and simulated results from "TARP".
Ojanen, T. Kohonen, R. (1995)	- **20 days** @ -10°C, 70% RH - **15 days** @ 3°C, 60% RH. - Int.: 20°C (RH ?) - different ΔP were used for each sample: 3 Pa/m for (1), 65 Pa for (2), and 35 Pa for (3).	- To determine the physical properties of wind barriers having an impact on hygrothermal performance of residential wood frame exterior walls.	- Large scale tests on 3 samples: (1) 1 vertical wall, (2) 1 vertical wall junction, and (3) one wall/roof junction.	- Interior surface of wall assumed to be air tight; - to measure drying potential, moisture introduced in specimens by continuously wetting saturated layer of cellulose between sheathing and air-barrier.
Ojanen, T. Simonson, C. (1995)	- **50 days** @ -18°C, except for 5 thawing cycles. Int.: 22°C, 40% RH	To study the impact of natural convection on moisture accumulation under **extreme winter Swedish conditions** and produce data for a computer model.	- 50 mm mineral wool or expanded polystyrene added on warm side of walls typical of Swedish construction. In some, a gap was left between existing structure and new layer of insulation, in others, the two layers were in contact. A new vapor barrier was added to all specimens. Some existing v.-b. were kept.	- Assembly assumed airtight, but with cracks at the wall-ceiling and wall-floor junctions; - the temperature differential causes natural convection in the space between the existing structure and the new layer of insulation. - outside temperature kept at -18°C
Simpson O'Connor (1994)	- **60 days**, dry cond.: 0°C-80% ext., 20°C, 60%, int. samples intact - **130 days**, wet cond.: 0°C, 55% ext., 20°C, 25%, int. perforated assemblies.	- To compare effect of single & double perforations on moisture distribution and levels in the sheathing, and on the thermal performance of wall elements.	- 2 specimens 2.9 m high by 0.62 m wide. - for the first, the walls were intact, in second half of the test, one is perforated with 1 hole, the other with 2 holes.	- driving potential - perforations
Verschoor, J.D. (1986)	- exterior: -7°C, almost saturated air - int.: 21 °C, 50% RH - pressure differentials of 0, 25 (equivalent to winds of 24 km/h) and of -25 Pa were induced. - until rate of moisture change appeared uniform, 1 to 4 weeks	- To study the impact of 3 different vapor barriers and of negative and positive pressure differentials on the potential of moisture accumulation and condensation.	- specimens: 38mm X 89mm studs; 7 layers of mineral wool, 13mm each (easier observation and installation of TC in insulation), fiberboard, aluminum siding ; - to measure moisture content, the whole assembly had to be rotated and weighed.	- Polyethylene, latex paint, and polyethylene with penetration were vapor barriers studied; - steady-state conditions

Trechsel, H.R. Achenbach, P. Knight, H.J. Lou, G.W. (1986)	**- 5 day periods** - Ext. conditions: -1°C, 70% RH. - Int. conditions: 21°C, 30% RH. - Pressure differentials of 0, 25, and 75 Pa were applied.	To determine the impact of an air barrier on condensation and moisture accumulation, under different pressure differentials due to wind.	- Specimen included 3 panels of 1.2m X 2.7m, with 3 bays. - The central bay had openings: 2 at top, 2 at bottom. 3 more holes (that could be hermetically sealed) were made to allow injection of tracer gas;	- Evaluation of moisture gains and air leakage rate through sheathing; - direction of air flow in cavity. (mild exterior conditions were chosen because previous tests showed that they were more severe for potential moisture accumulation.)
Trechsel, H.R. Achenbach, P. Ebbets, J.R. (1985)	**- 5 days, or until moisture has ceased to increased.** - The conditions represent moderate and cold climates over extended periods of time.	- To determine the impact of an exterior air barrier on the potential moisture accumulation. - To determine the impact of interior RH on the potential for moist. accumulation	- Tests were conducted on 3 1.2m panels, insulated with fiberglass batt insulation, and each covered with a sheathing having a different air leakiness. - The air exchange rate was measured with tracer gas injected in the assembly.	- Indoor air was circulated between center studs. - Tests were first performed without, then with an air barrier placed on the exterior. - For the first series, 2 exterior temperatures were used, for the second, the interior R.H. was varied.
Burch, D.M. Treado, S.J. (1978)	**- 8 weeks** @ -5.6°C **- 8 weeks** @ -14.4°C 24°C warm side, with RH reduced until it reached 23%.	- To study the impact of a vapor barrier.	- A wall was built, part of it was painted with a vapor barrier paint, another was not.	

3.3.3. Weather data.

Actual average daily temperatures collected in Montreal (Quebec) from January 1986 to November 1997 are used to get average monthly temperatures. Those are then compiled to get an overall average temperature for each month of the year. The results are shown in Table 3.

Table 3. Average monthly temperatures.

	1986	1987	1988	1989	1990	1991	1992	1993	1994	1995	1996	1997	Overall monthly averages
January	-9	-8	-8	-7	-4	-10	-11	-9	-16	-6	-11	-10	**-9**
February	-10	-11	-8	-8	-6	-5	-9	-13	-11	-10	-8	-8	**-9**
March	-1	0	-3	-5	-1	-1	-5	-3	-3	0	-2	-4	**-2**
April	9	9	6	5	7	8	5	6	5	4	5	5	**6**
May	14	13	15	15	12	15	13	13	12	13	12	11	**13**
June	17	19	18	19	18	19	18	18	19	20	19	20	**19**
July	20	22	23	22	21	21	19	22	22	22	20	21	**21**
August	19	19	21	20	21	21	19	21	18	20	20	19	**20**
September	14	15	15	16	15	14	15	14	15	13	16	15	**15**
October	8	8	7	9	9	10	7	7	10	11	8	8	**9**
November	1	1	3	0	3	3	2	2	4	-1	0	1	**2**
December	-4	-3	-7	-16	-4	-7	-4	-5	-3	-9	-1		**-6**

3.3.4. Proposed conditions.

To study moisture accumulation and evacuation, the experiment is divided into two distinct climatic periods: a wetting period and a drying period. Moisture accumulates when the temperature, water vapor pressure, and air pressure differentials are the highest, i.e. when the outdoor temperature is the lowest. The air leakage characterization methods are implemented during this winter period. Moisture will start to evacuate when the temperatures inside the assembly increase significantly. This happens when the exterior temperature increases, which is in late spring for Montreal.

For this study, the effects of rain, wind and sun radiation are not taken into account.

3.3.4.1. Wetting period.

The assemblies are subjected to wetting conditions in order to identify those with the greatest and least potential for moisture accumulation problems. Also, by allowing moisture to accumulate, the areas where moisture accumulates in each assembly can be identified.

- Duration: **66 days**.
  In Montreal, the coldest weather occurs from mid-December to the end of February. This accounts for 75 days of testing. After 66 days of testing, the rate of moisture accumulation appeared constant and the wetting trends could be identified. The wetting conditions were then replaced by the drying conditions.
- Exterior conditions: **-8.5°C**.
  The average temperature of the last 15 days of December and the average temperature for January and February are averaged to get an overall outdoor temperature for the wetting period:
  Temperature average for the last 15 days of December: **-7°C**
  Temperature average for January: **-9°C**
  Temperature average for February: **-9°C**
  Overall average: **-8.5°C**
- Interior conditions: **22°C, 50% RH, +4Pa**.
  According to Standard ANSI/ASHRAE 55-1992 (Thermal Environmental Conditions for Human Occupancy), the winter comfort zone lies between 20°C and 24°C for indoor temperature and between 25% and 60% for relative humidity. The temperature in the middle of this range, 22°C, is selected as indoor conditions. The relative humidity of 50%, closer to the higher end of the spectrum, is selected because it represents a worse scenario and will accentuate the moisture related problems.
  A positive air pressure differential of 4 Pa is created inside the test hut to model a typical stack effect for a Montreal winter climate (see calculations in Appendix A).

3.3.4.2. Drying period.

In order to study whether a particular insulation strategy or air leakage characteristic impedes or facilitates drying and to identify the potential problem areas in the exterior wall assemblies, exposure to conditions favorable to moisture evacuation is set to continue until the rate of moisture content changes and the moisture content distribution for each exterior wall specimen is stable (and not necessarily until the materials are dry).

- Duration: **47 days**.
  The drying conditions were maintained until the moisture contents in the assemblies were stable, point at which the drying trends could be established. This took the entire 45 day late-spring period.

- Exterior conditions: **17°C.**
  Spring conditions are selected for the drying period because, having a smaller drying potential, they represent a worse scenario than summer conditions. With a slower drying process, moisture evacuation problems related to the insulation strategies or to the air leakage characteristics should be identified.
  The second half of the month of May, when the exterior temperature significantly increases in Montreal, is the onset of the drying period. Before this time, drying may not occur every day, and when it does occur during the day, it may be reversed at night when the temperature drops. The average temperature of the last 15 days of May is averaged with the average temperature of the month of June to get an overall outdoor average temperature for this 45-day drying period.
  Temperature average of the last 15 of May: **15°C**
  Temperature average of the month of June: **19°C**
  Overall average: **17°C**
- Interior conditions: **23°C, 45% RH, +1 Pa.**
  According to Standard ANSI/ASHRAE 55-1992, the indoor temperature comfort zone for summer is in a higher range than for winter (between 22°C and approximately 27°C). Since the outdoor conditions for this drying period represent spring and not summer, the indoor temperature is chosen where winter and summer conditions overlap, i.e. between 22°C and 24°C.
  The same amount of moisture in the air is maintained, because it is assumed that the occupants would maintain the same rate of moisture generation. From the psychrometric chart, for 23°C this translates into a relative humidity of 45%.
  The positive air pressure differential due to the stack effect is proportional to the temperature differential. Since it is significantly lower, the pressure differential is reduced to 1 Pa (see calculations in Appendix A).

3.4. Monitoring protocol

For the sample sections insulated with fiberglass batt insulation, monitoring is performed in the 0.36 m central portion between the wood studs. This portion is assumed to be vertically symmetrical on each side of its central axis. The temperatures are therefore measured only on one side of the central axis. Moisture contents are measured electronically on one side, and manually on the other. Temperatures and moisture contents are monitored according to a grid determined by the air leakage path of the sample section. The grid is tighter (150 mm) around indoor air entry points, looser (600 mm) for the rest of the expected path. Following this principle, the whole height of the sample sections is monitored for both the long and the distributed air leakage paths, but monitoring is limited to the lower half for the concentrated air leakage path. Figure 7 shows the actual monitoring grid for each of the three air exfiltration paths studied.

For the sample sections insulated with 89 mm or 140 mm of cellulose fiber, monitoring is performed on the wood studs. Figure 8 illustrates the location of electronic (temperatures and moisture contents) and manual (moisture contents) monitoring for these sample sections.

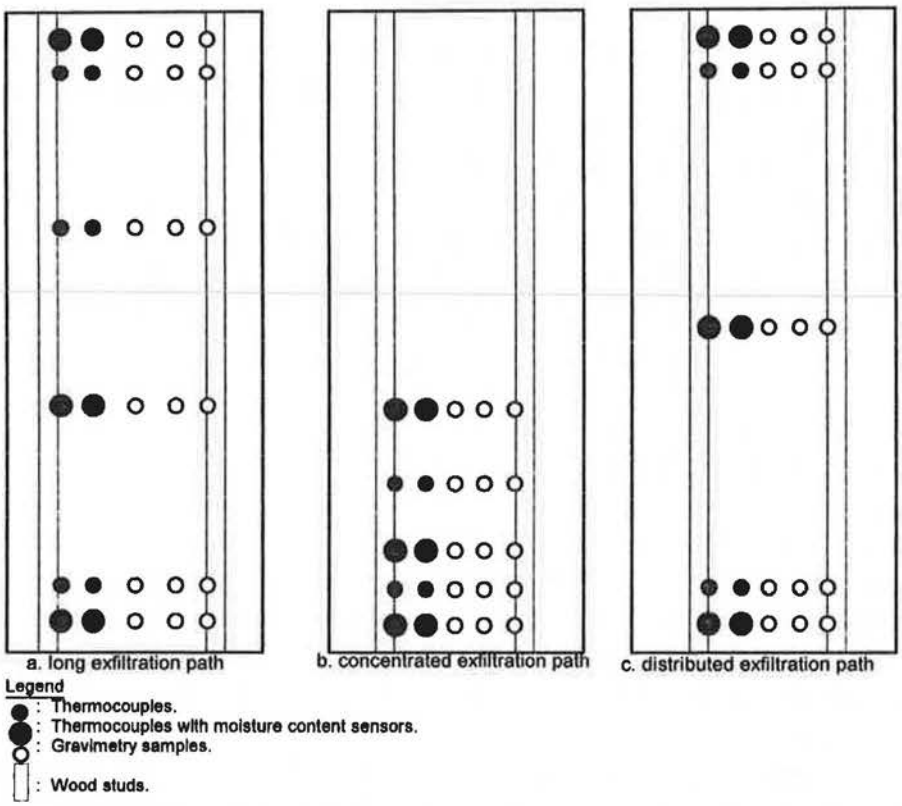

Figure 7. Monitoring grid - Sample sections with 89 mm fiberglass batt insulation.

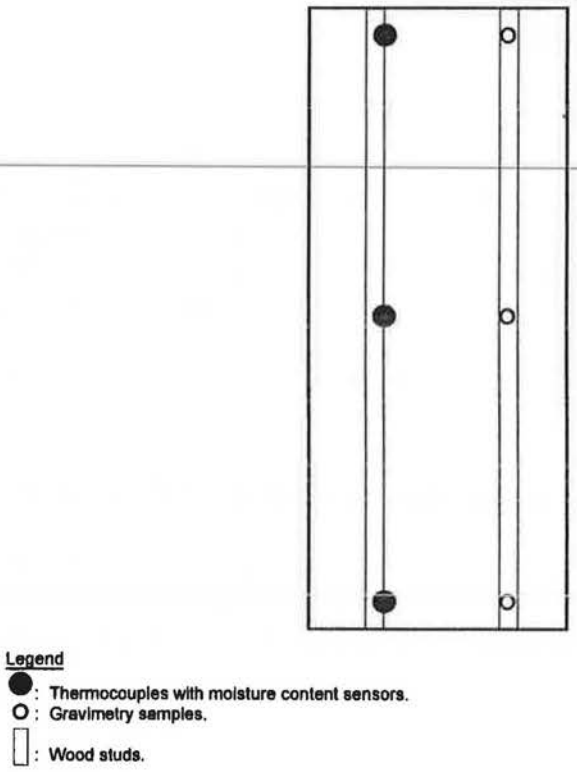

Figure 8. Monitoring grid - Sample sections with 89 mm or 140 mm blown cellulose fiber.

3.4.1. 3-D Grid temperature monitoring

In this research project, the hypothesis that temperatures within an exterior wall assembly can give indications on the movement of air exfiltrating through it is tested. Exfiltrating air warms the materials it comes in contact with, mapping its trajectory. This mapping should be identifiable as long as a sufficient temperature differential exists between outdoor air and indoor air, i.e. during the winter climatic conditions.

Type "T" thermocouples (copper and constantan, which is a copper and nickel alloy) with 0.1°C precision, are used to measure the temperatures within the exterior wall assemblies. Their precision is verified with a temperature controlled (to 0.1%) reference cold water bath. Readings are taken automatically every 10 minutes for the duration of the experiment.

In the sample sections insulated with 89 mm of fiberglass batt insulation, the thermocouples are installed according to a two-dimensional grid, at two planes within the assembly: on the cold side and on the warm side of the fiberglass batt insulation. For all nine sample sections, the cold plane thermocouple layer is installed on the interior surface of the fiberboard sheathing, and the warm plane thermocouple layer is installed on the interior surface of the fiberglass batt insulation. The same grid is repeated for both planes, providing three-dimensional temperature monitoring. Refer to Figure 7 for the thermocouple two-dimensional grid layout. Figure 9 shows thermocouples installed on the cold and on the warm side of the fiberglass batt insulation respectively.

By measuring temperatures in such a way, two-dimensional temperature maps, at two different planes within the building envelope, are produced. From these maps, a pattern for air exfiltration may be extrapolated. Those experimental results are compared to analytical results from a three dimensional finite-difference heat conduction model that gives temperatures of the assembly for conditions excluding exfiltration completely. The temperature maps are presented and discussed in Chapter 5.

For the sample sections insulated with 89 mm or 140 mm of cellulose fiber, the thermocouples are installed on the warm and cold sides of the wood stud, at the bottom, mid-height, and at the top. Refer to Figure 8 for the exact locations of the thermocouples.

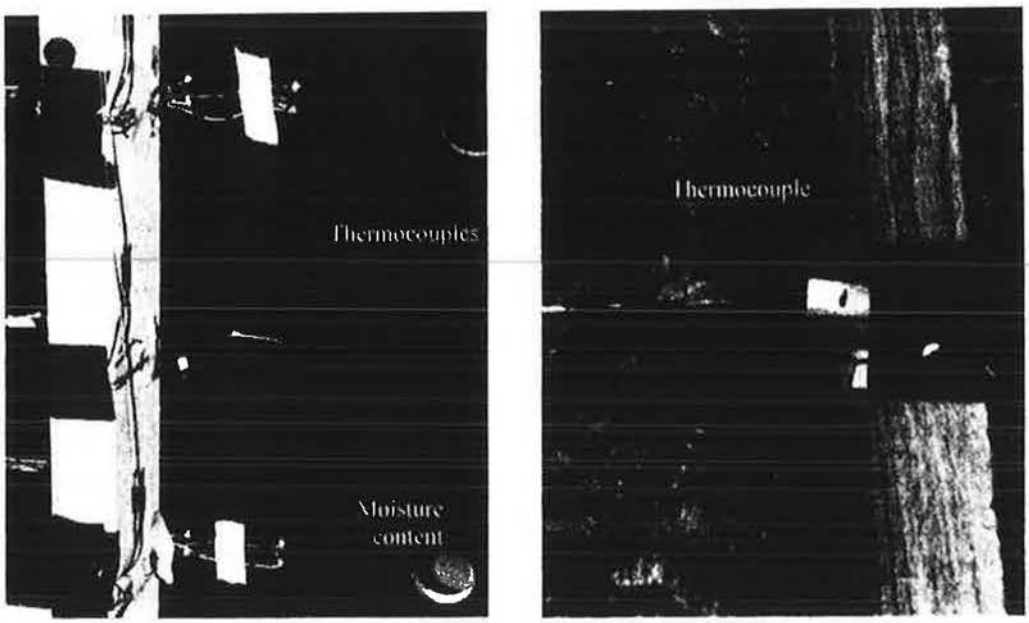

9a. Thermocouples and moisture content sensors on the cold side of the fiberglass batt insulation.

9b. Thermocouples on the warm side of the fiberglass batt insulation.

Figure 9. Thermocouples and moisture content sensors.

3.4.2. 2-D Grid moisture content monitoring

Moisture content monitoring is used to assess where potential moisture related problems are likely to occur in the building envelope. Also, as air exfiltrates, its moisture is deposited in the hygroscopic materials of the assembly. By studying the moisture contents at different locations according to a two-dimensional grid, the results can be presented in a graphic form by drawing curves of equal moisture contents, called "isohygrons". Maps showing the impact of the trajectory of air can be produced, and a pattern of air exfiltration may emerge.

Moisture contents are monitored extensively, both electronically and manually using gravimetry. Both methods are used because they measure different characteristics. When sensors are installed, the moisture content at a specific point in the material is measured. Gravimetry gives an average moisture content for a bigger area of the material being monitored. Refer to Figure 7 for the locations of the moisture content sensors and of the gravimetry samples for the sections insulated with 89 mm of fiberglass batt insulation and to Figure 8 for the sections insulated with 89 mm or 140 mm of cellulose fiber.

3.4.2.1. Electronic monitoring.

The moisture content sensors used for the electronic moisture monitoring of the 12.5 mm thick fiberboard sheathing consist of two metal pins, 1 mm in diameter by 6 mm in length, plated with gold to avoid oxidation. The resistance of the material to electric current, which is inversely proportional to the moisture content, is measured across the two pins inserted in the material. The distance between the two pins is kept constant by making the holes with the pins of a hand held wood moisture content meter. Readings are taken by applying a voltage to the pins, which ionizes the materials. The ionization is proportional to the number and duration of exposures to the voltage and it causes corresponding errors in the readings. This appears to be incompatible with the continuous moisture monitoring required for the 113 days of the experiment. A monitoring system was developed so that short readings are taken automatically from each

sensor every 10 minutes and that each time the polarity of the pins is reversed. This minimizes the error due to the ionization. The moisture content sensors are installed, from inside the test hut, in the fiberboard sheathing to measure the average moisture content of its interior surface layer. Figure 9 shows moisture content sensors.

A moisture content calibration curve is needed for the asphalt impregnated fiberboard sheathing because it is not available. For the calibration procedure, moisture content sensors are installed on five 40 mm X 40 mm fiberboard samples. These samples are placed in a small conditioning chamber, where temperature and relative humidity can be controlled. For the first phase, the temperature is held constant at 17°C, while the relative humidity is increased when fiberboard moisture content equilibrium is attained. The relative humidities produced are: 50%, 75%, 85%, 90%, 95%, and 97%. To get the temperature correction, this procedure is repeated at 4°C for relative humidities of 50%, 75%, 85%, and 92%. Voltage readings are taken from the moisture content sensors each day. After each reading, the samples are weighed. They are dried at the end of the procedure. The maximum fiberboard moisture content obtained in the conditioning chamber (17°C, 97% R.H.) is below those reached during the experiment. To get readings at higher moisture contents, water is sprayed on the fiberboard calibration samples, as if condensation had occurred. The wet samples are placed in sealed plastic bags until the water is uniformly distributed. Voltage readings are then taken and the samples are weighed. Different amounts of water are used, to increase the number of points on the curve. Figure 10 shows the conditioning chamber and the fiberboard calibration samples.

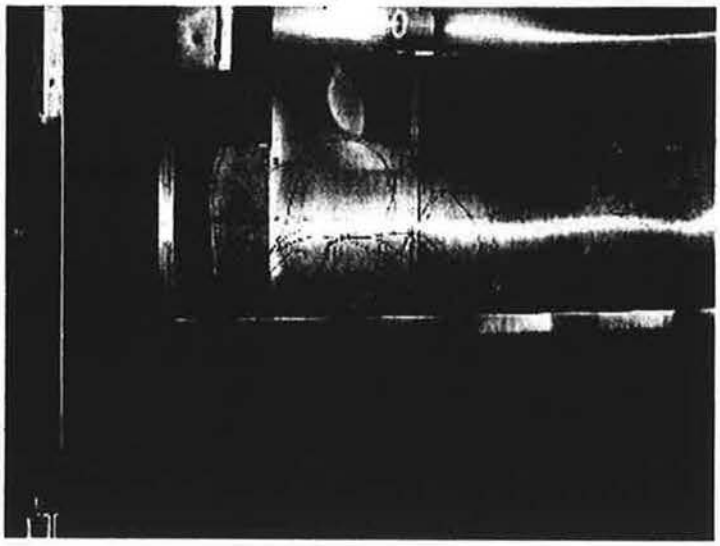

Figure 10. Calibration samples in conditioning chamber.

The actual moisture contents, determined by gravimetry, are then plotted against the voltage readings, to determine the calibration curve, from which voltage readings taken during the test can be translated in moisture contents.

3.4.2.2. Gravimetry.

Gravimetry samples are taken on the cold side of the wood studs and in the fiberboard sheathing for all sample sections. The stud samples are 12.5 mm deep by 12.5 mm high by 38 mm wide. The fiberboard samples are 38 mm in diameter, except for those in front of the studs which are 50 mm to give access to the stud samples. The perimeter of the fiberboard samples is sealed with tape to avoid moisture transfer through this surface. All gravimetry samples are accessible from the outside of the test hut. For the sample sections with 38 mm rigid insulation added on the exterior, a removable piece of the insulation is cut out in front of the gravimetry samples to give access to them. Air leakage around the gravimetry samples has to be avoided in order to minimize the impact of the samples on the behavior of the assembly. However, the perimeter of the gravimetry sample holes cannot be sealed directly because tape or caulking would damage them. Therefore, the fiberboard samples must fit tightly enough so that as little air as possible can flow around them, but not so tight that they cannot not be removed without being damaged. Also, the "Tyvek" polyolefin membrane, with a very low air permeability and a high water vapor permeability, can be used to address the issue. A rectangular window is cut out of the polyolefin membrane in front of the each gravimetry sample row, and the perimeter is sealed with "Tuck Tape" to the fiberboard sheathing. A rectangular piece of the same polyolefin membrane, sealed with "Tuck Tape", is then used to cover this window between and during each of the weightings. An illustration of the gravimetry setup (before the samples are covered) is shown in Figure 11.

The gravimetry samples from the interior side of the wood studs (for the samples sections insulated with cellulose fiber only) are accessible from the inside, through 50 mm holes cut in the gypsum board.

During the experiments, all samples are weighed every week for the first 30 days, and then every 2 weeks for the remainder of the climatic period. Section by section, the gravimetry samples are put in sealed plastics bags for handling, weighed on site using a scale precise to the microgram, and then put back in their respective positions. The sample holes are blocked while the samples are being weighed, to avoid air flow through them. The procedure is completed as fast as possible so that the moisture contents of the samples does not have time to vary significantly. At the end of the experiment the wood samples are oven-dried at 103°C, according to ASTM D 4442-92 "Standard Test Methods for Direct Moisture Content Measurement of Wood and Wood-Base Materials", and the fiberboard samples at 57°C to avoid evaporation of chemical agents.

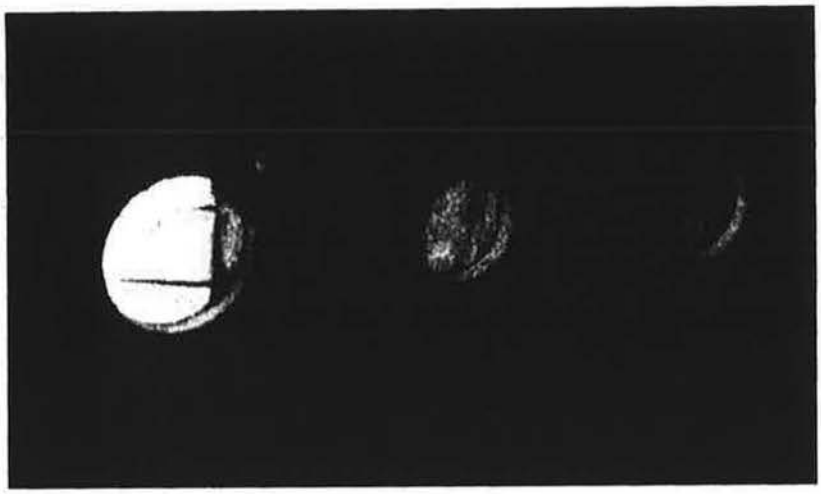

Figure 11. Holes for fiberboard and for wood stud gravimetry samples.

Before the beginning of the experiment, an air exfiltration test was conducted to evaluate the impact of the fiberboard gravimetry samples. For this test, a 60 mm X 60 mm fiberboard sample with Tyvek is placed on an airtight box. Positive air pressures of two, five, six, and 10 Pa are applied inside the box, and the airflow required to maintain these pressures is measured. This procedure is performed five times, with the following five different configurations:

1. setup covered with an airtight polyethylene membrane, to measure the exfiltration rate of the setup itself;
2. setup without polyethylene (the polyethylene membrane is cut out, so as not to disturb the setup), to measure the exfiltration rate of the fiberboard/Tyvek assembly without gravimetry samples;
3. setup with a hole cut out of the Tyvek membrane, to measure the exfiltration rate of the fiberboard sheathing;
4. setup with two holes drilled for gravimetry (identical to those in the test hut sample sections), and with the Tyvek taped as on the test hut sample sections;
5. setup with holes drilled for gravimetry, but without the Tyvek membrane, to measure the exfiltration rate of the fiberboard sheathing with gravimetry samples.

For configurations 1, 2, and 4, the air leakage of the whole setup was so low that at the low air flow rate of 0.01 liter per minute, the air pressure differential would not stabilize. These configurations are therefore considered airtight. For configurations 3 and 5, the results are presented in Table 4.

Table 4. Air leakage measurements for gravimetry sample holes.

	2 Pa	5 Pa	6 Pa	10 Pa
Fiberboard, no gravimetry samples, no Tyvek (3.)	0.37 l/min.	0.96 l/min.	1.53 l/min.	1.89 l/min.
Fiberboard, with gravimetry samples, no Tyvek (5.)	0.38 l/min.	0.98 l/min.	1.56 l/min.	1.93 l/min.

As can be seen, at 5 Pa (the pressure closest to that maintained inside the test hut) the difference between the fiberboard is 0.02 l/min. Transposed to one sample section having 10 or 12 of these holes, the air leakage would be 0.1 l/min. However, all of these holes are covered with a Tyvek membrane, as tested in configuration 4, shown to be airtight.

3.4.3. Global air leakage measurements

The airtightness of each sample section is measured using the standard test procedure ASTM E 283-91 ("Standard Test Method for Determining the Rate of Air Leakage Through Exterior Windows, Curtain Walls, and Doors Under Specified Pressure Differences Across the Specimen") just before the beginning and right after the end of the experiment. Positive air pressure differentials ranging from 10 Pa to 60 Pa are created on the indoor side of the specimens. The air flow necessary to maintain them, which is equal to the amount of air exfiltrating through the specimen, is measured.

Before the procedure, all openings provided in the sample sections insulated with fiberglass batt insulation (crack at the bottom for long path, hole for concentrated path, and grid of holes for diffuse path) are sealed with tape. The wall sample sections are sealed with a polycthylene membrane to isolate them from the other sections.

First, air is blown into the test hut to measure its air leakage rate at the various specified air pressure differentials. The polyethylene covering one sample section to be evaluated is then cut, and the procedure repeated to measure the air leakage rate of the sample section without these openings. The tape covering the openings is removed and the procedure is repeated again to measure the air leakage of the sample section with openings. This is done for each of the 14 sample sections. The difference between the two measurements give the air leakage rate of the opening provided in the interior finish. Air should be flowing mostly through those openings, not around the sample sections (between the gypsum board and the OSB panels). Figure 12 shows some samples sections covered with the polyethylene membrane.

The procedure was performed before the test in April 1998, and repeated after the test in September 1998. The data is processed according to the common form of equation describing air leakage, the "power law" equation (Colliver 1994). Please refer to Appendix B for the details.

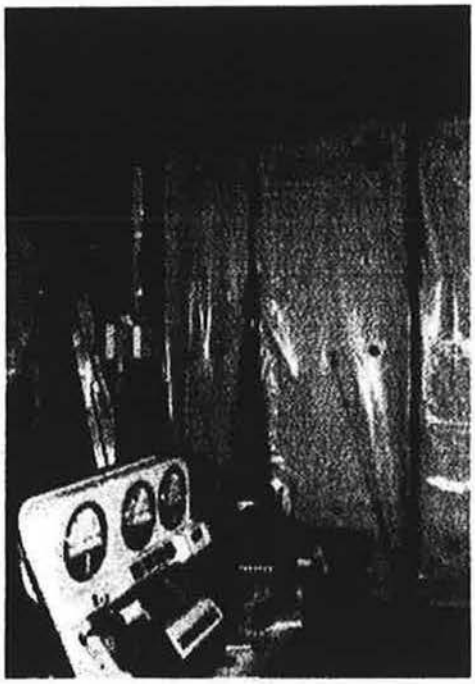

Figure 12. Test hut prepared for air exfiltration rate measurements.

3.4.4. Fine colored dust

After the exposure to the Montreal spring conditions, fine colored chalk dust is added to the air blown into the test hut, pressurized at 10 to 20 Pa. As air passes though the assemblies, the powder is deposited within the fiberglass batt insulation and the cellulose insulation, acting as filters. It was expected that where more air passes, the dust concentration would be higher.

The dust that is selected has to meet certain requirements:

1. Its color has to contrast with that of the insulation.
2. It has to be fine enough to be suspended in air.

It has to be used in a sufficient amount so that it can be detected, but not too much because it may clog the apparatus.

4. Running of the experiment

4.1. Climatic Conditions

The experiment was conducted from May 19th to September 8th, 1998 using consecutively two distinct sets of climatic conditions: a wetting period, from May 19th at 10:00 to July 23rd at 15:00 and a drying period, from July 23rd at 15:00 to September 8th at 11:00

All test hut and chamber temperature readings are plotted over time in Figure 13. Overall, chamber and test hut temperatures were maintained constant during both periods. The repetitive peaks that can be seen for the chamber temperature are caused by the daily manual condenser defrost of the cooling coil during the wetting period. They were of a short duration (15 to 20 minutes) with no significant impact on temperatures and moisture contents. Two events disrupted the running of the wetting portion of the test. A power failure on June 16th caused the computers controlling the climatic conditions and the data acquisition system to shut down. The temperature in the test hut went up to a peak of 35°C. On June 24th, a problem with the compressor, caused the temperature in the chamber to rise, also to a peak of 35°C. In both cases, the overall temperature rise lasted a few hours. There was a third event in which the baseboard heater inside the test hut stopped functioning due to an electrical problem. This caused the temperature in the test hut to go down to 16°C for a very short period.

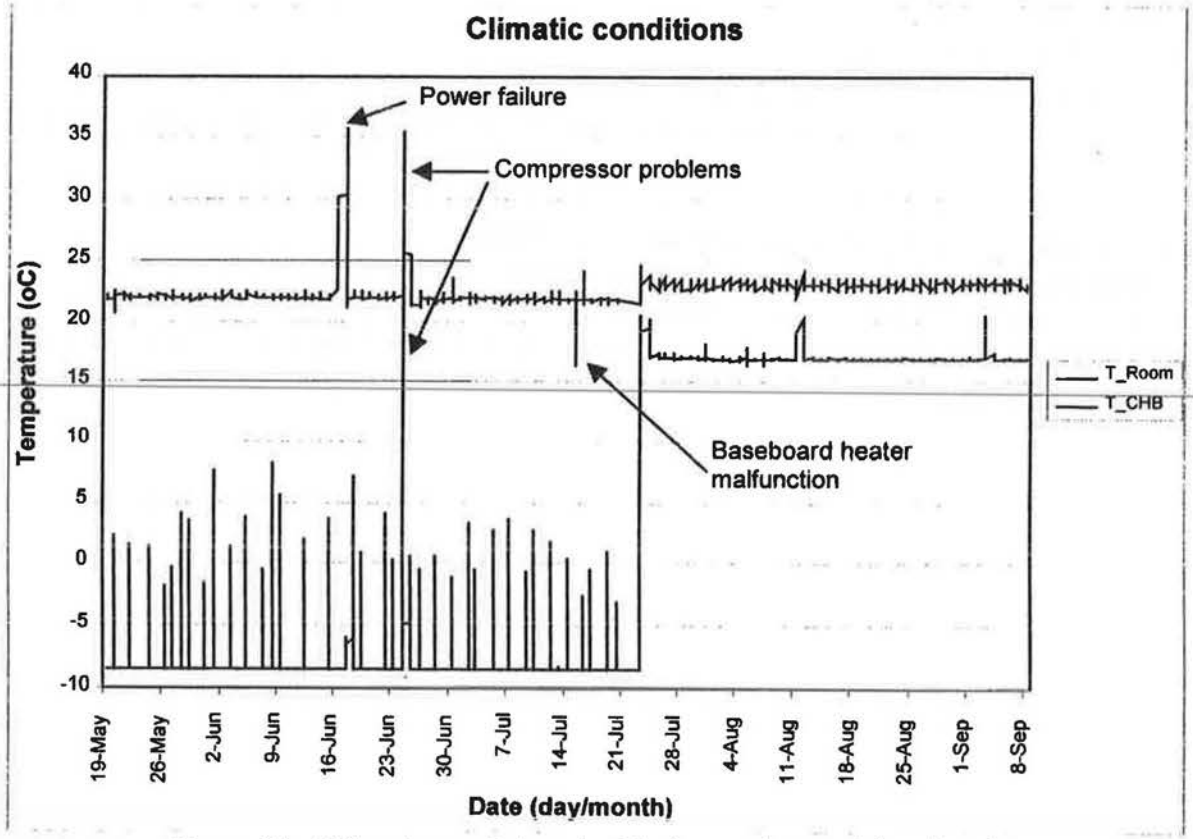

Figure 13. Climatic conditions inside the test hut and the chamber.

4.2. Data Acquisition

4.2.1. Temperatures

Over the course of the experiment, the data acquisition system warned that some thermocouples temporarily gave error readings. This data was removed from the final data file before analysis. Approximately 97% of the temperature data was used for the analysis.

4.2.2. Moisture content sensors

The first part of the wetting period allowed to correct some failed solder joints connecting the moisture content sensors to the data acquisition system. This problem was difficult to determine because in this case, the sensors simply give the equivalent of a very low moisture content. The data from the moisture content sensors is 85% complete.

4.2.3. Gravimetry

The gravimetry samples were weighed 8 times during the wetting period, and 7 times during the drying period for all nine wall sample sections with fiberglass batt insulation. For the assemblies with blown cellulose insulation, they were weighed 5 times during the wetting period and 6 times during the drying period. Table 5 and Table 6 show the actual gravimetry weighing schedules (day/month).

Table 5. Weighing schedule for sample sections with fiberglass batt insulation.

Wetting period								Drying period						
19/05	27/05	3/06	12/06	18/06	26/06	10/07	23/07	24/07	31/07	7/08	17/08	24/08	2/09	8/09

Table 6. Weighing schedule for sample sections with blown cellulose fiber insulation.

Wetting period					Wetting period					
19/05	3/06	19/06	13/07	23/06	24/07	31/07	7/08	24/08	2/09	8/09

4.2.4. Global air leakage measurements.

Air leakage measurements were attempted before and after the test. However, on both occasions and regardless of the care demonstrated during the installation, the data resulting from the pressurization is not conclusive. The complicated geometry of each assembly rendered the sealing of the polyethylene membrane difficult to attain.

4.2.5. Fine colored dust

It was intended to blow fine colored dust in the test hut, under a positive pressure differential so that it would mark the path of air. No way was found to keep the dust suspended and well mixed in the air. It was decided instead to use a theatrical smoke generator. The fan pressurizing the test hut was left on for 40 minutes, at 50 Pa while the test hut was kept full of smoke using the smoke generator. Unfortunately, this smoke left no trace in the insulation, even when looked at with infrared or ultraviolet lights. This provided no significant results.

4.3. Dismantling of the test setup.

The dismantling of the test setup was conducted in three stages, with a visual inspection performed for each:

1. Removal of the interior finish. This allowed to evaluate the state of the insulation between the studs. A gap in the fiberglass batt insulation was found at the top of the base-case assembly with distributed air leakage, shown in Figure 14.
2. Removal of the insulation materials. The cellulose fiber was removed cautiously to observe changes in texture. In a previous test, it was found that cellulose fiber agglomerated where it had been wetted, and that this change in texture was proportional to the moisture content reached. Removing loose insulation (where moisture contents have remained low) while leaving agglomerated patches can therefore give indications of possible air leakage paths and of the moisture content distribution patterns within the loose fill insulation. Figure 15 shows such patches, in the sections with 89 mm of cellulose fiber between the studs.
3. Removal of the sheathing, so that only the wood frame remains. The spun bonded polyolefin membrane and the fiberboard sheathing were removed to expose to wood structure. A visual inspection was then conducted to detect possible fungus staining. Few areas with staining fungi were found indicating that high moisture contents were reached. Figure 16 illustrates an example of staining that was found.

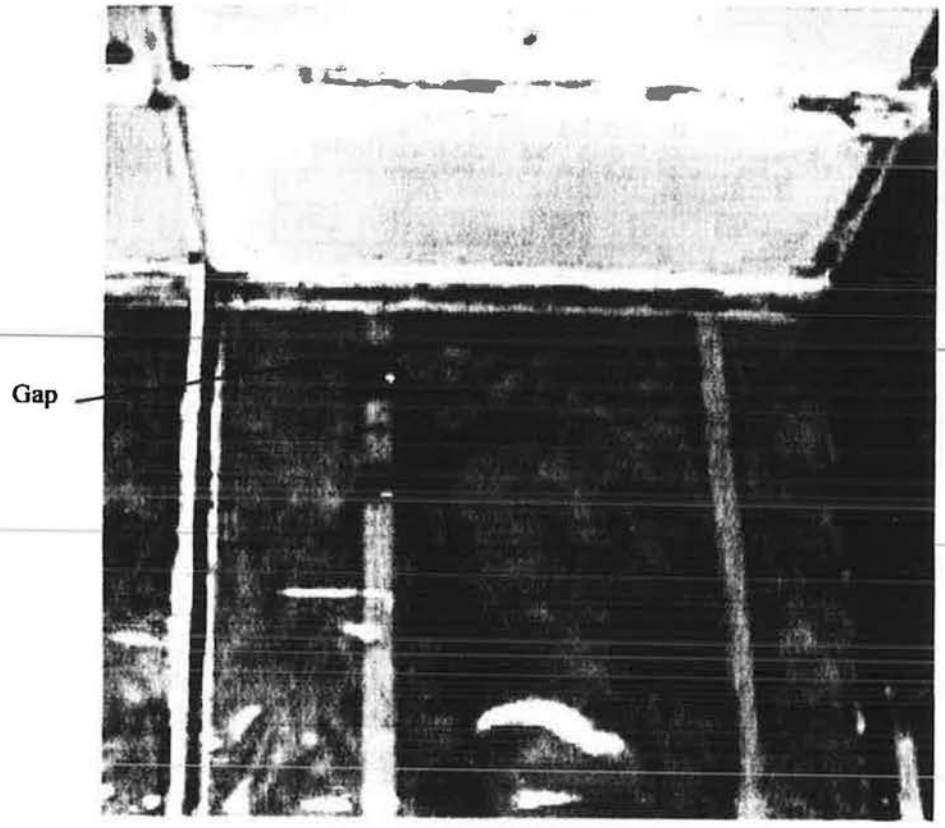

Figure 14. Gap in the fiberglass batt insulation.

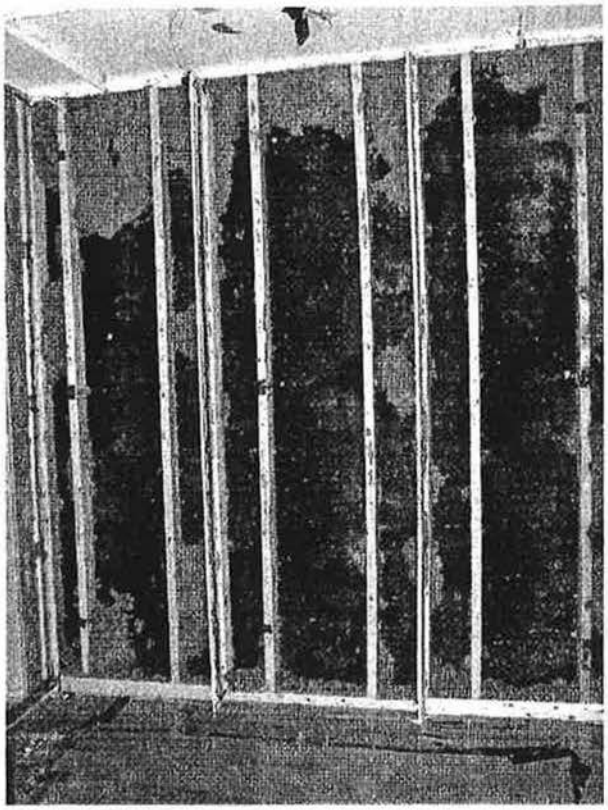

Figure 15. Agglomerations in sections with 89 mm cellulose fiber between the studs.

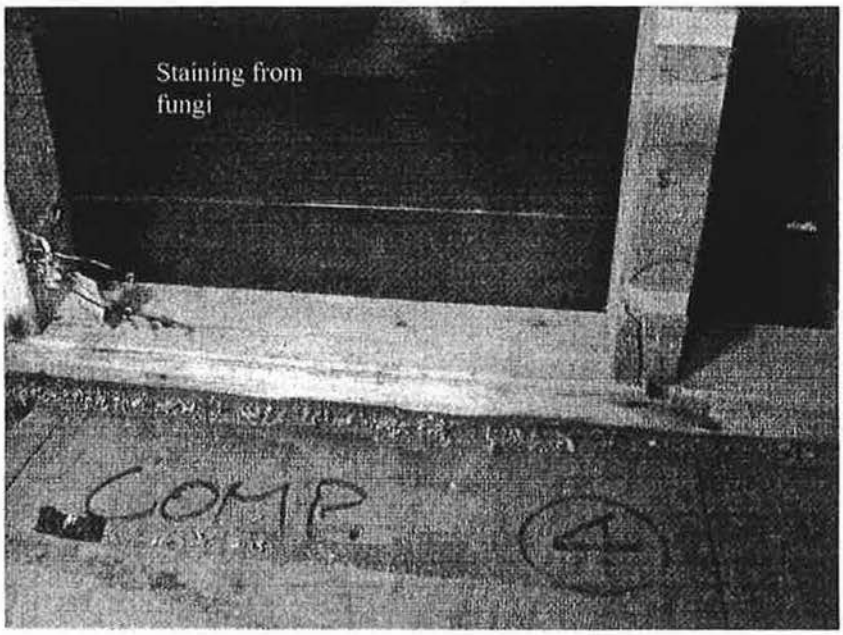

Figure 16. Fungi staining - section with rigid insulation added on cold side, long path.

5. Results and discussion

5.1. Temperature monitoring/modeling.

Adding rigid extruded polystyrene insulation had an strong impact on the warm plane and cold plane temperatures. Throughout the wetting period, the assemblies with rigid insulation added on their cold side had higher measured temperatures, and those with rigid insulation added on their warm side had lower measured temperatures than the base-case assemblies.

5.1.1. 3-D grid temperature monitoring

Temperatures monitored over time are presented in Appendix C for each monitored point. The temperatures were monitored at 267 locations in the 14 wall sample sections (192 for the walls insulated with batt insulation, 75 for the walls insulated with cellulose fiber). One typical graph is included here for discussion, in Figure 17. The dates used are the actual dates when the test was performed and do not refer to the climatic conditions simulated. From the graph, the two testing periods are identifiable by looking at the temperature. Temperature peaks are seen around June 16th and June 25th for all monitored points. They are caused by the two events described in section 4.1. Most monitored points remained at a fairly constant temperature for the duration of each of the two climatic periods. In few instances, the temperature of some of the points, like "WS-6" (the lowest thermocouple on the warm side of the wood stud, in the base-case section with the long air leakage path) shown in Figure 17, was varying although the conditions were held constant for most of the duration of the climatic periods. This might indicate the presence of natural convection loops within the assemblies.

The subsequent analysis looks at the data after steady state was established, during the first climatic period. For the sake of this discussion, the temperatures at the indoor surface of the fiberglass batt insulation will be referred to as "warm plane" temperatures and those at the outdoor surface of the fiberglass batt insulation as "cold plane" temperatures.

Temperature averages for each monitoring point between May 26th and 30th, when no significant moisture build up had occurred but temperature equilibrium had been reached, were used for the analysis. In addition, to find out the impact of moisture accumulation in the assemblies, average temperatures from July 10th, when moisture accumulation was high, were also studied.

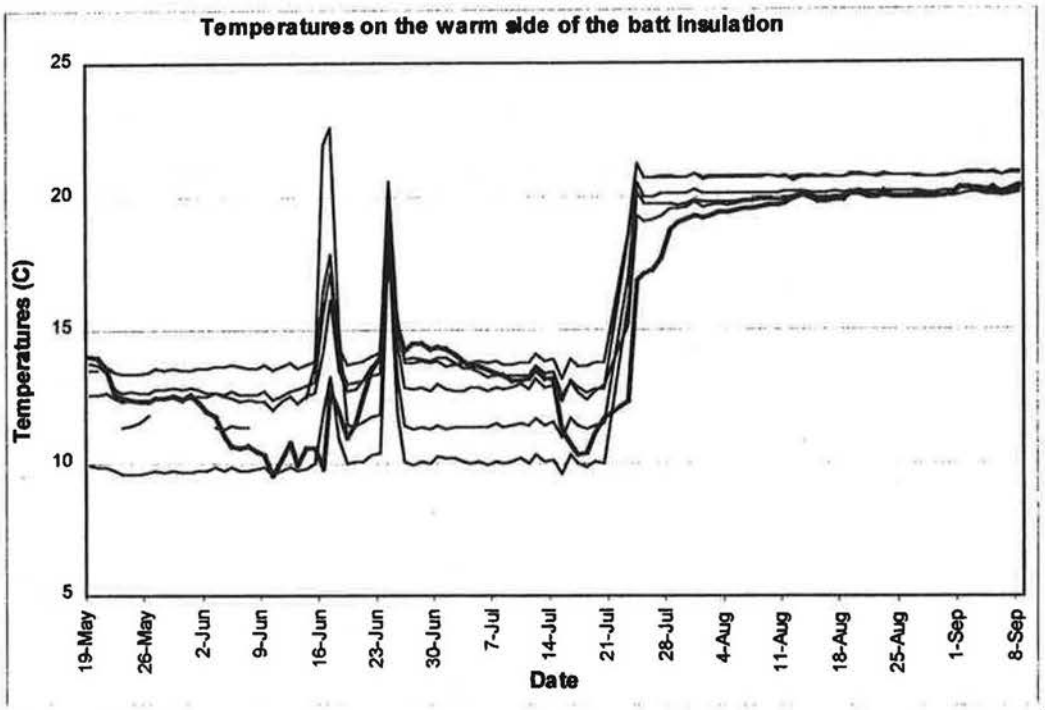

Figure 17. Monitored temperatures - base-case assembly, long air leakage path.[3]

In Figure 18, the measured temperature gradients across the wood studs and the fiberglass batt insulation for three sample sections with no added rigid insulation are plotted at three different heights, 300 mm, 900 mm, and 2100 mm, for the May 26th to 30th period. Temperature gradients calculated using the three-dimensional conductive heat transfer model are also plotted on this figure. This representation allows comparison of the monitored temperature gradients across the edge of the studs and across the batt insulation at different heights for different air leakage patterns, and monitored versus calculated temperature gradients. This figure shows the effect of the thermal bridges caused by the wood studs. Temperature gradients are greater through the batt insulation than across the wood studs, this effect being pronounced for the airtight section.

At the 900 mm and 2100 mm levels, the temperatures are higher in both planes for the long leakage path than for the concentrated leakage path and the airtight section, indicating that the air is warming the materials as it flows up. At the 300 mm level, which is the height of the concentrated leakage opening and warm air entry point, higher temperatures are found in the concentrated path wall. The difference in temperature gradients between the different air leakage paths is more pronounced across the studs than across the insulation. This is most likely due to the thermal bridge effect caused by the studs. Before the installation of the interior finish, the construction was checked to ensure that there was no gap between the studs and the fiberglass batt insulation, so that no air could flow along the studs.

The calculated temperature gradients are slightly greater than the measured temperature gradients across the insulation and markedly greater across the edge of the studs. One explanation would be the presence of convection between the batt insulation and the studs.

[3] These curves show temperatures over time. The peaks due to the compressor failure (around June 16th and June 26th) are visible on this chart. The darker temperature curve, for thermocouple WS-6 at the bottom, shows variations that the lighter temperature curves (at different heights in the section) do not.

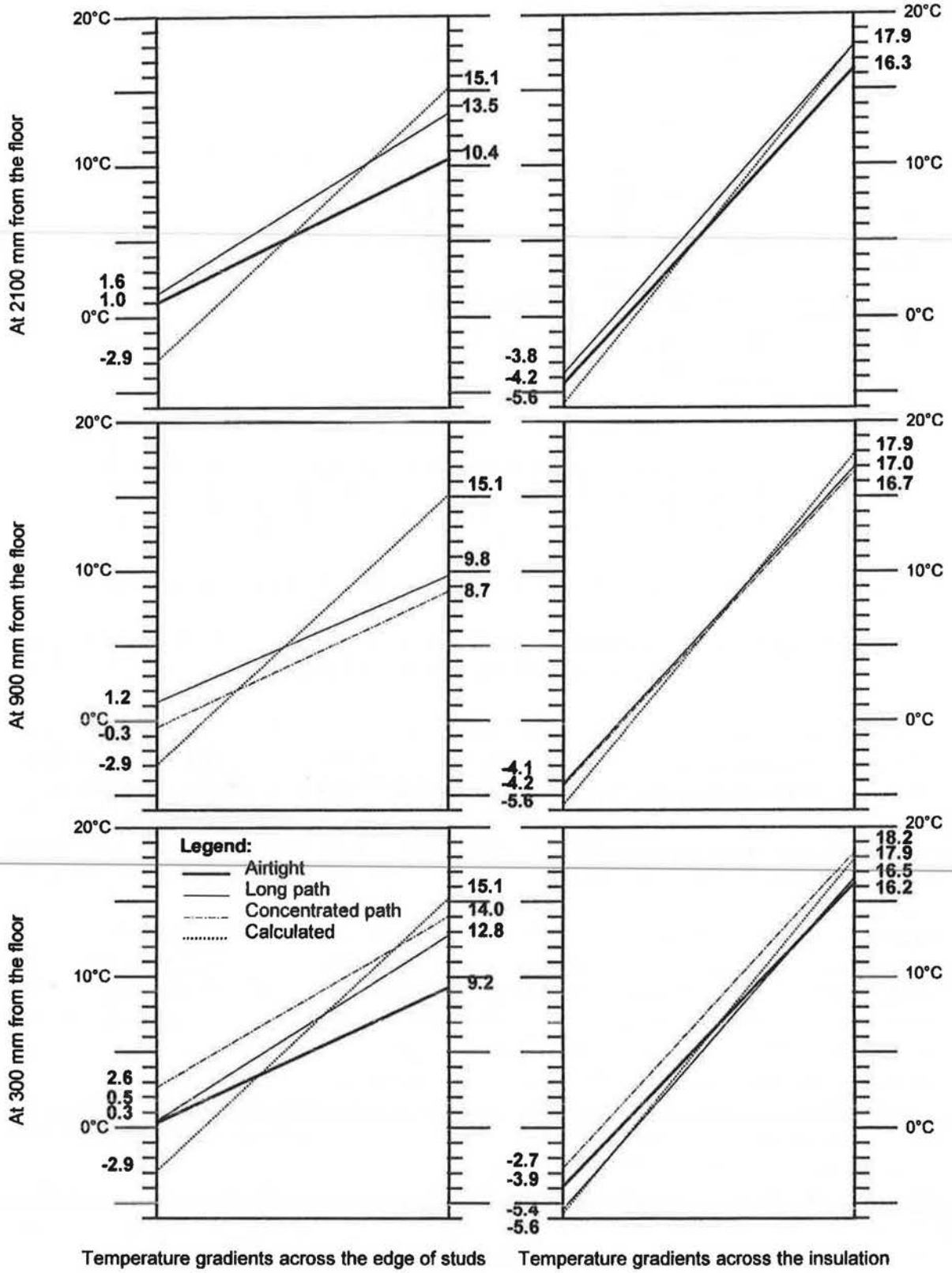

Figure 18. Monitored and calculated temperature gradients - base-case assemblies.

The following isotherms are generated using the May 26th to 30th average temperatures. They are plotted over an elevation view of the sample sections. The numbers on the isotherms are the temperatures in Celsius.

Figure 19 shows the warm and cold plane isotherms for the airtight section, with no rigid insulation added. It can be seen that the isotherms on the warm plane are generally parallel (Figure 19a), indicating that the vertical temperature gradient is small. This pattern that is produced is analogous to that of conductive heat transfer, without the influence of convective heat transfer. For the cold plane however (Figure 19b), the temperatures are slightly warmer in the top half of the section.

Isotherms for the sections with the long air exfiltration path are presented in Figure 20. Temperatures at the warm plane of the sections with the base-case composition and with insulation added on the cold side are warmer toward the top (Figure 20a and Figure 20b). In the case of the section with rigid insulation added on the warm side, the temperatures are warmer at the bottom (Figure 20c). At the cold plane, the temperatures are colder at the top for the section with rigid insulation added on the cold side (Figure 20e), but slightly warmer at the top for the base-case section and for the one with rigid insulation added on the warm side (Figure 20d and Figure 20f).

Figure 21 shows isotherms for the sections with the concentrated air exfiltration path. Isotherms for these sections are generated for the lower half only because there are no monitoring points in the top half. For the base-case assembly, the warm plane temperatures are warmer around the indoor air entry point (Figure 21a). For the section with rigid insulation added on the cold side, the warm plane temperatures are warmer just above the opening (Figure 21b), while they are warmer just below and on each side of the opening for the section with rigid insulation added on the cold side (Figure 21c). At the cold plane (Figure 21d to Figure 21f), temperatures are slightly colder opposite the air entry point, although the patterns are not as clearly defined as those for the warm plane temperatures.

The isotherms for the sections with the distributed air exfiltration path, found in Figure 22, show that the temperatures are colder at the bottom and warmer at the top, at both the warm and cold planes.

These maps confirm that temperatures are warmer for the sample sections with insulation added on the cold side and colder for the sections with insulation added on the warm side than those of the base-case assembly. Also, the temperature distribution patterns within the assemblies are related to the air leakage path, indicating that some correlation exists between the temperature distribution and the air leakage path. This suggests that temperature monitoring according to a 3-dimensional grid could be used to characterize the path of exfiltrating air.

In Figure 23 to Figure 26, isotherms from monitored temperatures at the beginning of the wetting period (from May 26th to May 30th) when the wall sample sections were dry can be compared with isotherms from monitored temperatures toward the end of the wetting period (July 10th) when moisture had accumulated. Both for the warm plane and cold plane temperatures, no significant change in temperature profiles can be detected between these two time periods.

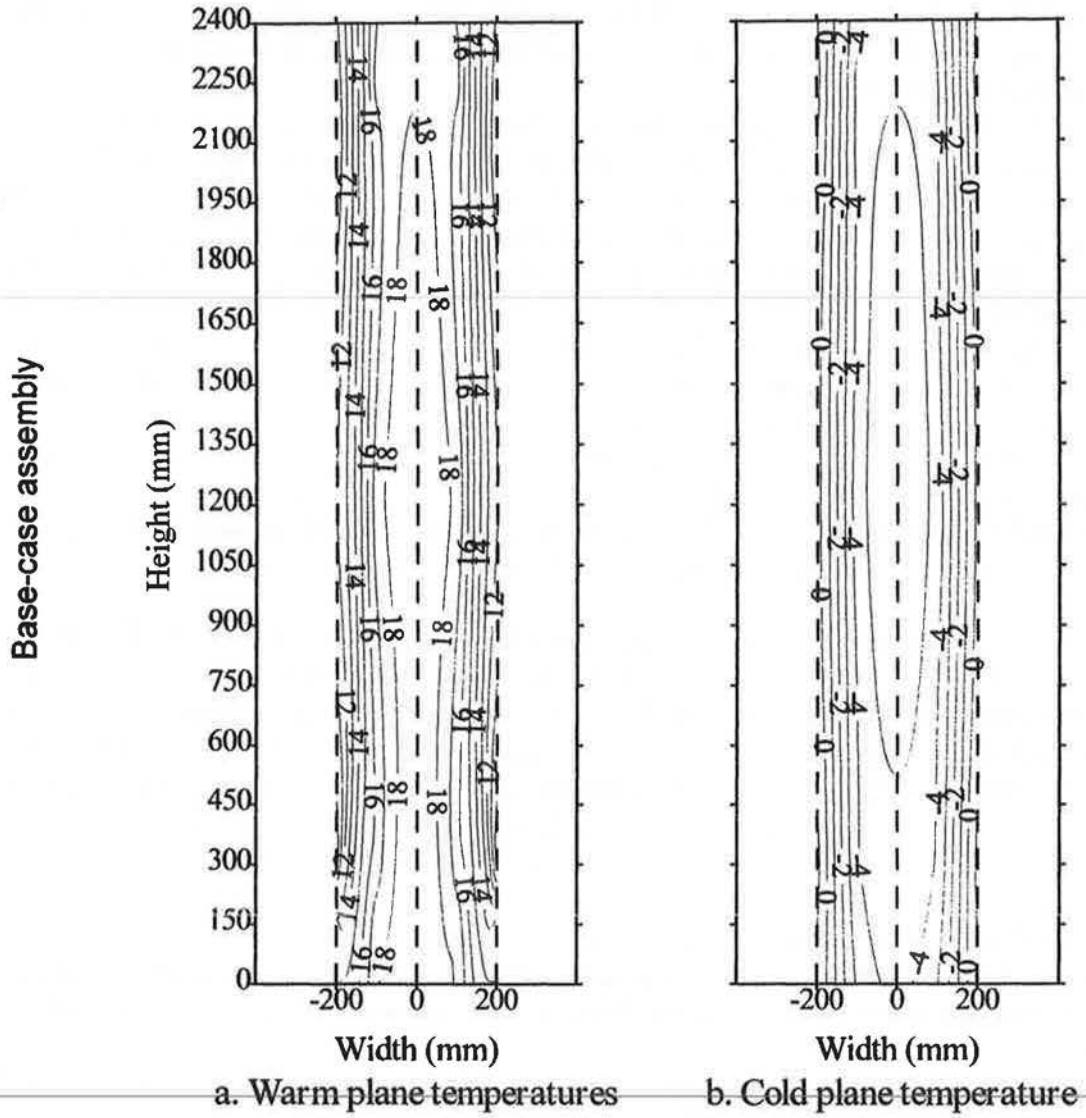

Figure 19. Isotherms for the airtight section - May 26th to 30th (°C).

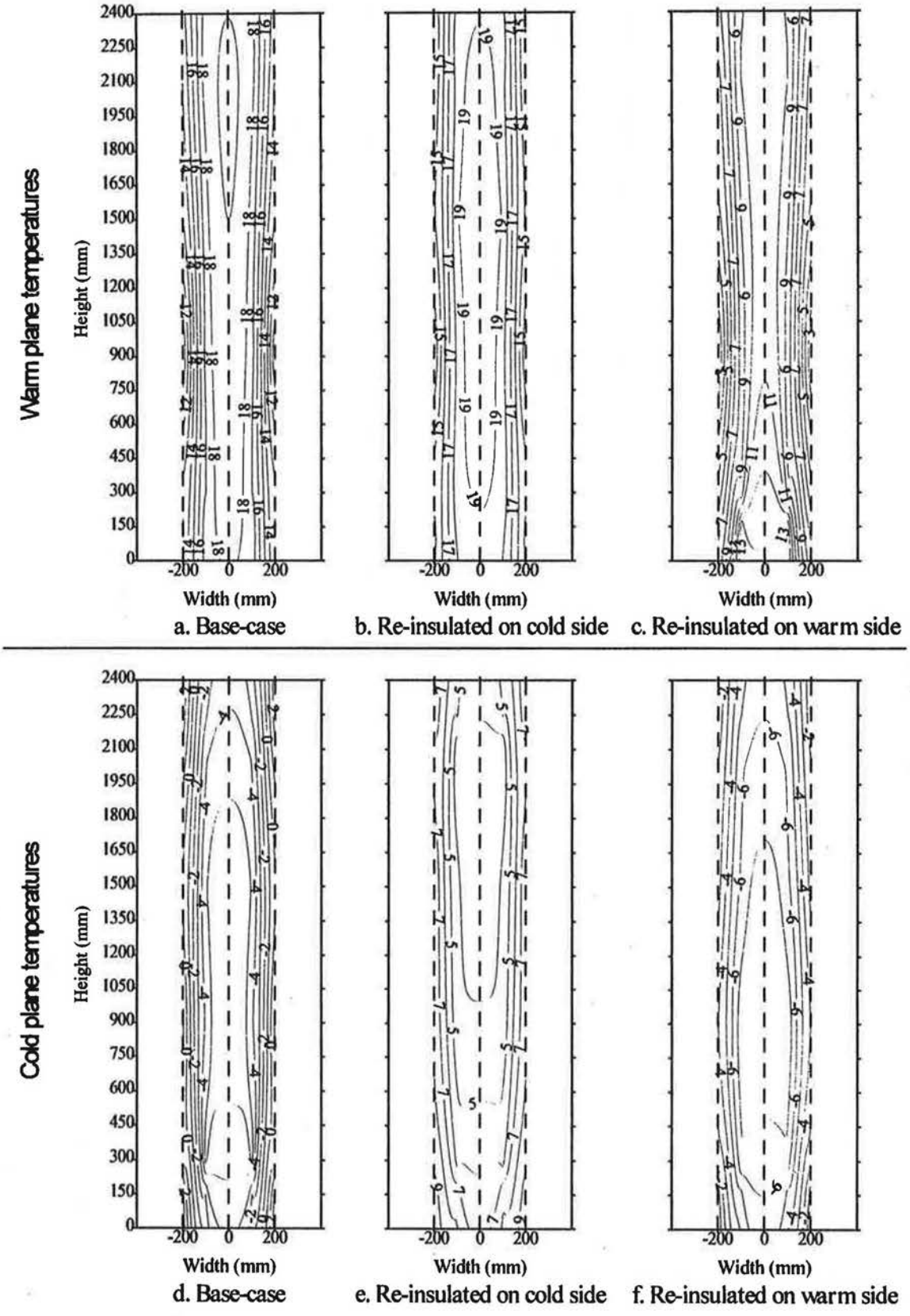

Figure 20. Isotherms for sections with the long air exfiltration path - 26th to 30th (°C).

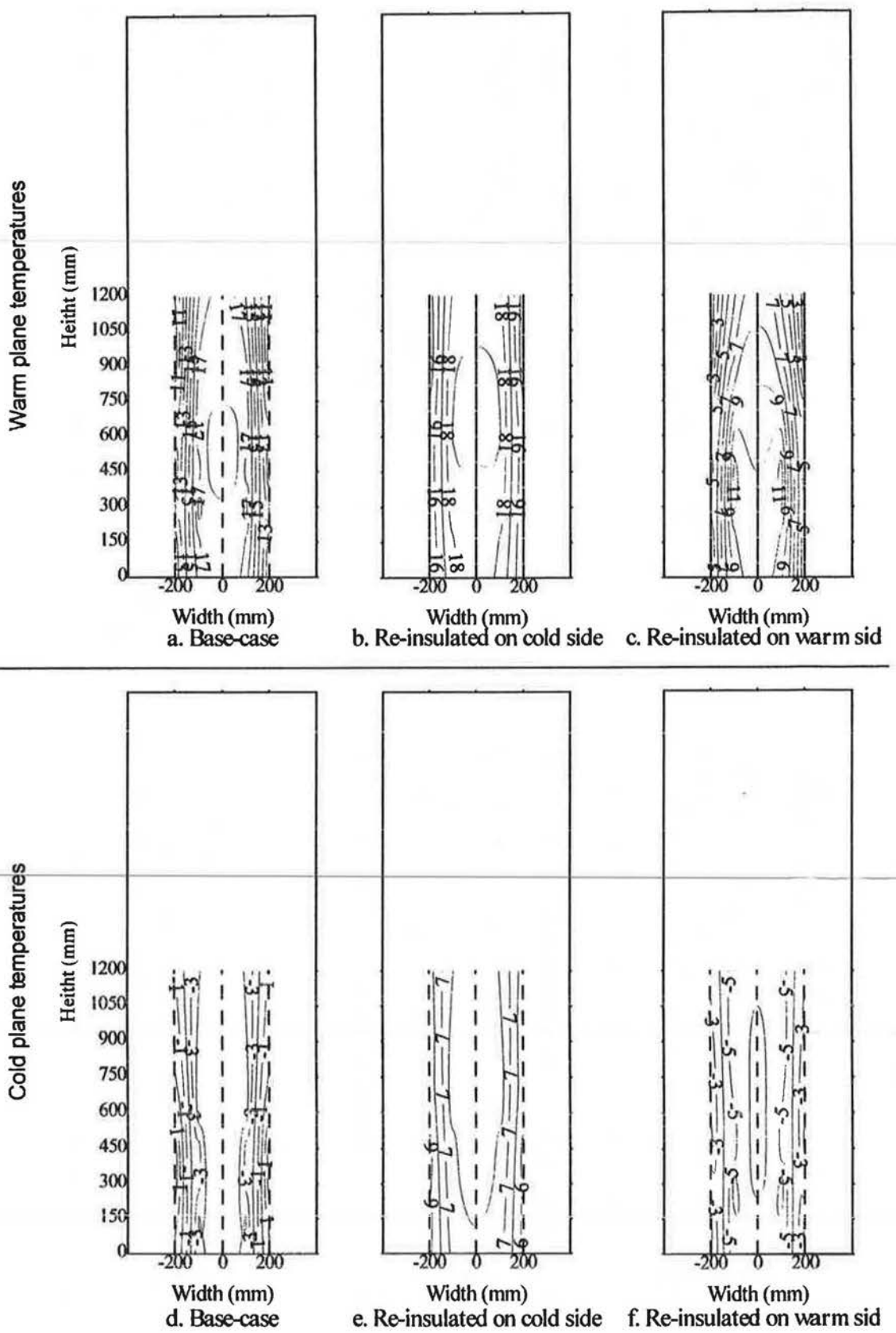

Figure 21. Isotherms for sections with the concentrated air exfiltration path - May 26th to 30th (℃).

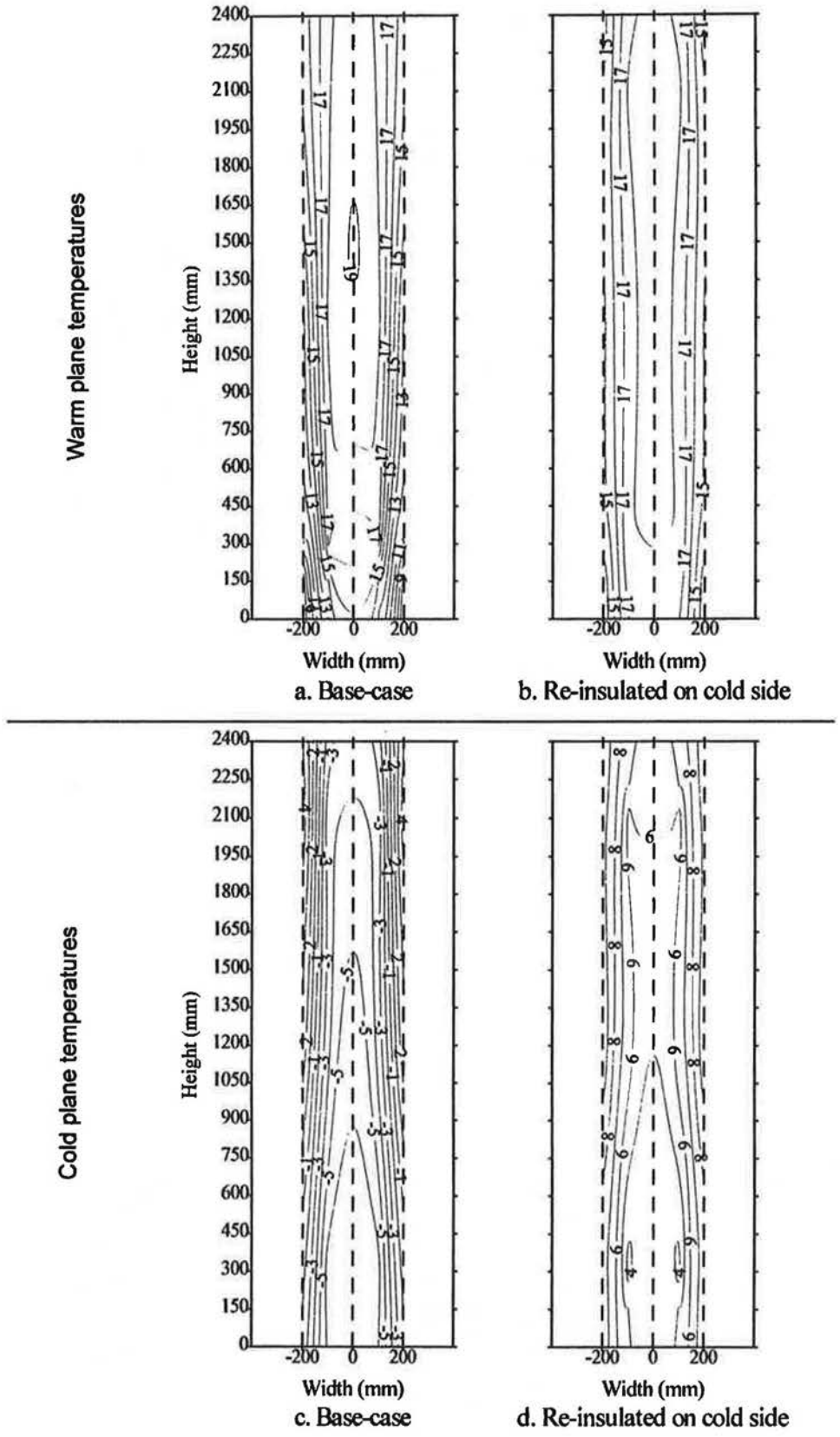

Figure 22. Isotherms for sections with the distributed air exfiltration path - May 26th to 30th (°C).

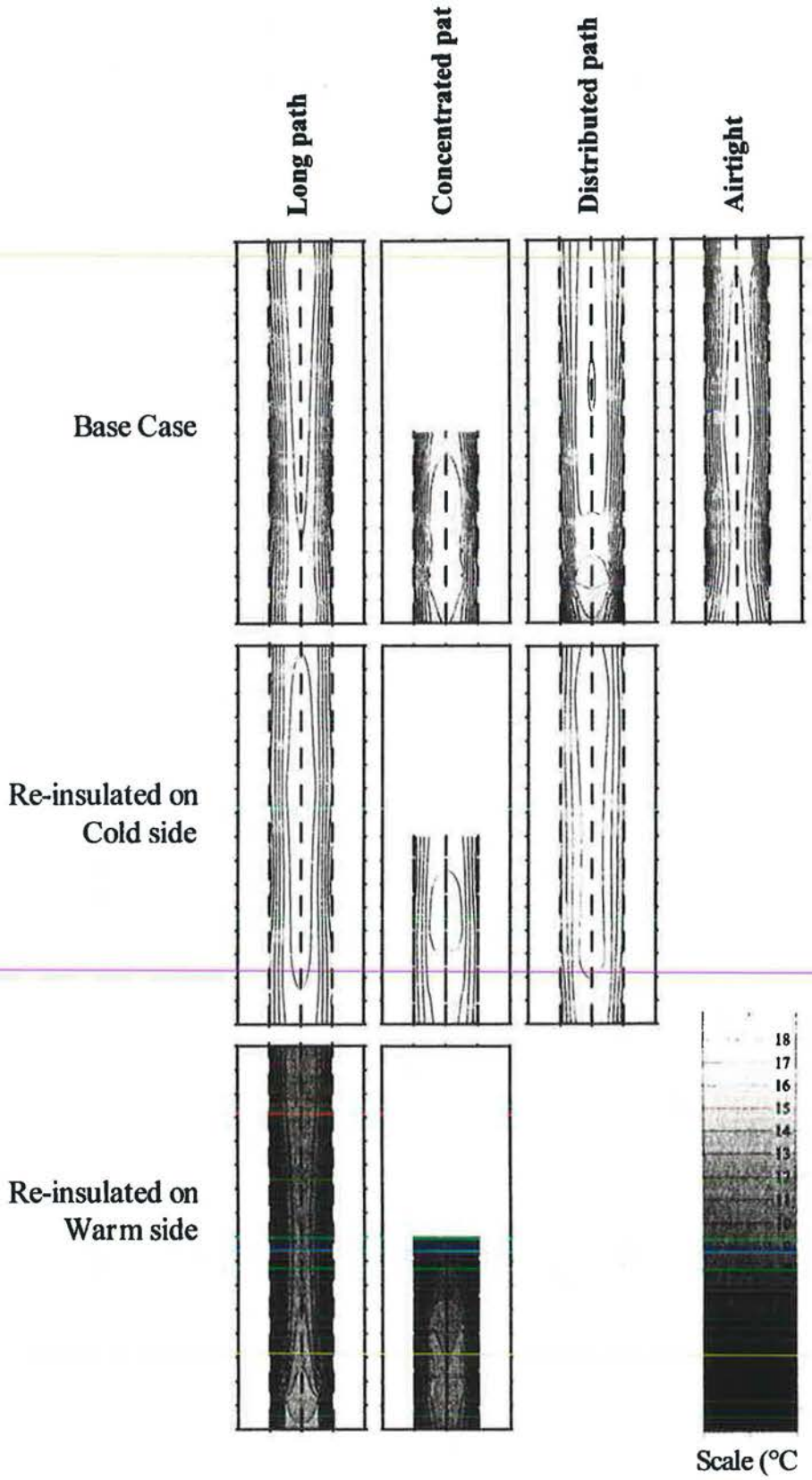

Figure 23. Warm plane isotherms for the May 26th – May 30th period.

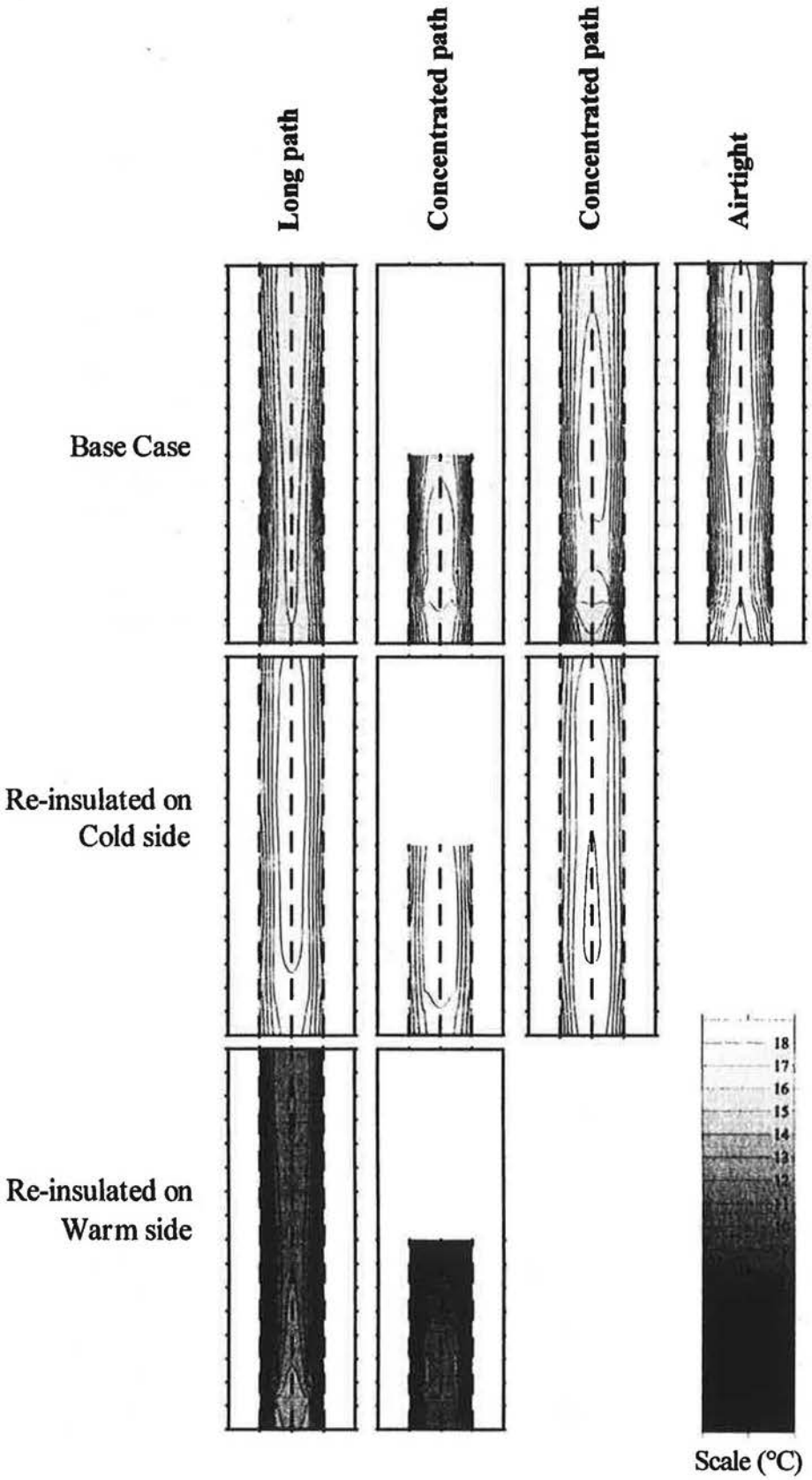

Figure 24. Warm plane isotherms for July 10th.

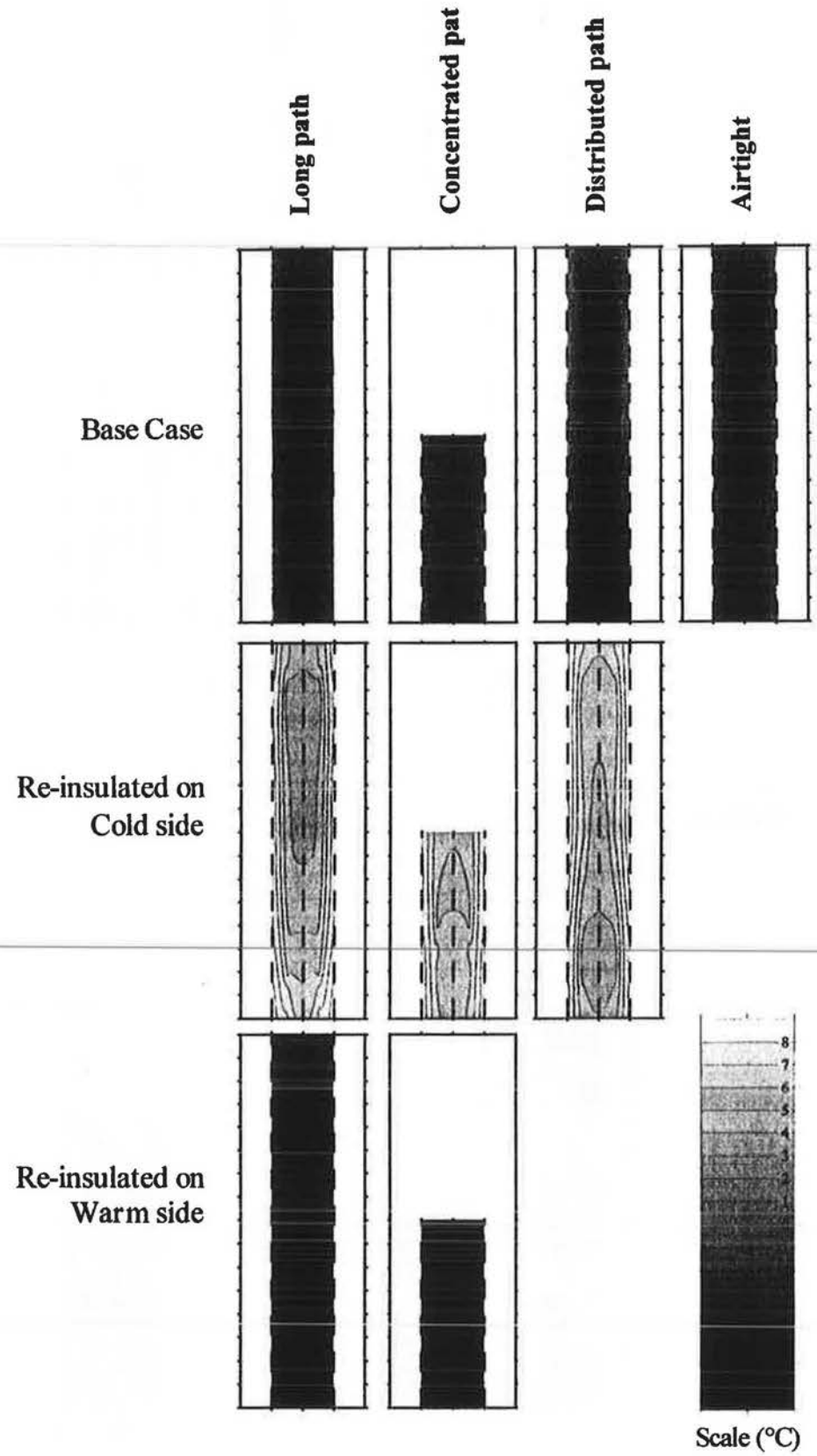

Figure 25. Cold plane isotherms for the May 26th - May 30th period.

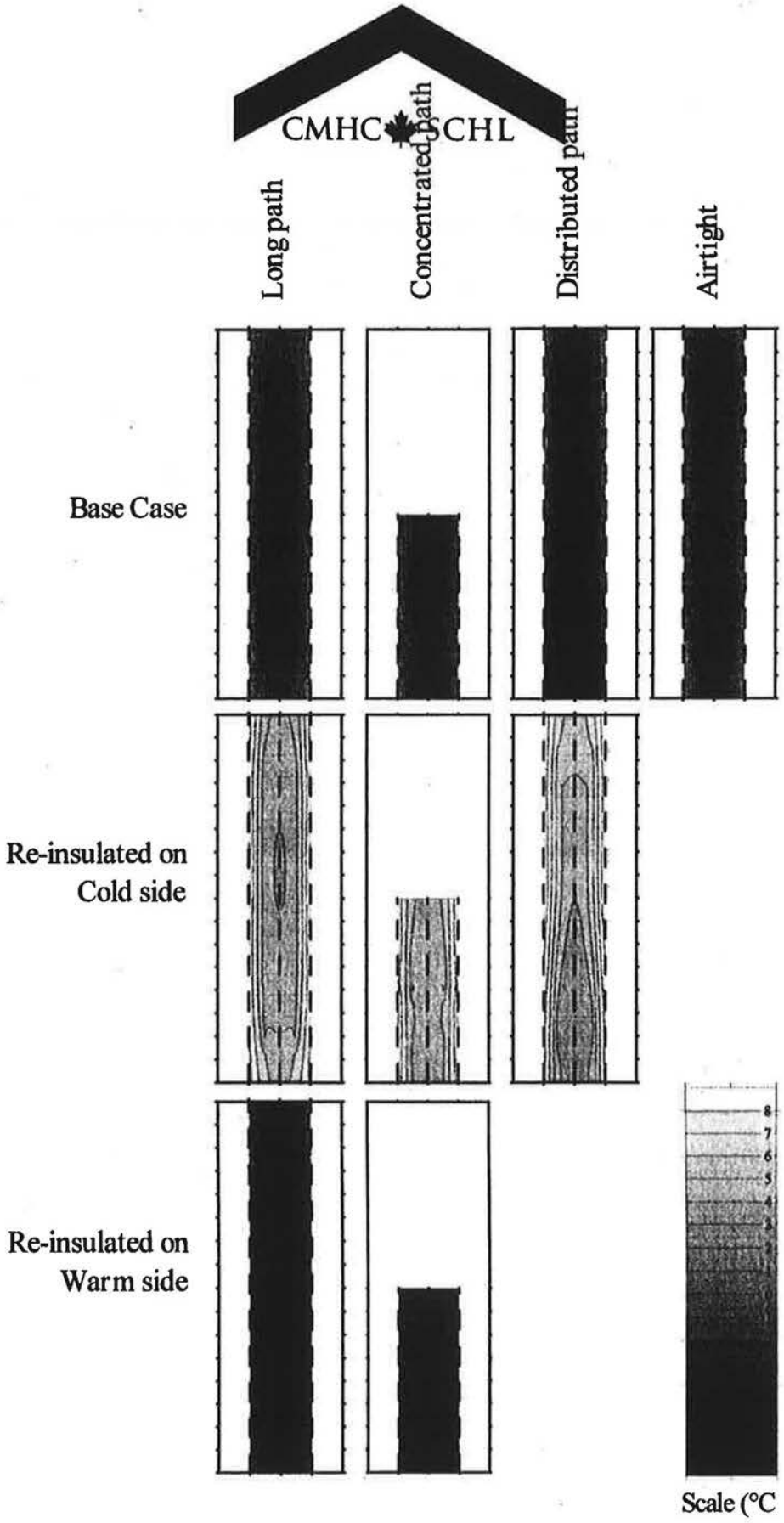

Figure 26. Cold plane isotherms for July 10th.

5.1.2. 3-D conductive heat transfer modeling

A steady-state modeling approach using 3-dimensional finite-difference element was used to simulate the heat transfer through the assemblies insulated with fiberglass batt, in order to calculate their warm and cold plane temperatures. The calculations are based on the steady-state two-dimensional conductive heat transfer model described in "An Electronic Mathcad Book", by A. Athienitis (1994). To fit the cases studied, this model has been expanded to include up to 96 control volumes and to be three-dimensional. As an example, a sketch of the control volume representation for the base-case assembly is presented in Figure 27. The calculations are performed for a 200 mm by 200 mm area. It is assumed that adiabatic conditions exist at the boundaries of this area. Vertically, the defined area goes from the center of the sample section, between the studs, to the center of the stud. Horizontally, it goes from the center of the space between the wood furring, to the center of the wood furring. The compositions are also divided in different layers, corresponding to the different materials in the assemblies. The fiberglass batt insulation is split in two layers to improve accuracy. The material conductivities ("k" value, in W/ (m^2 * °C)) used in the calculations were taken from the manufacturers for both insulation materials and the fiberboard. For the gypsum board and the wood, the values were taken from the ASHRAE Handbook of Fundamentals, 1993.

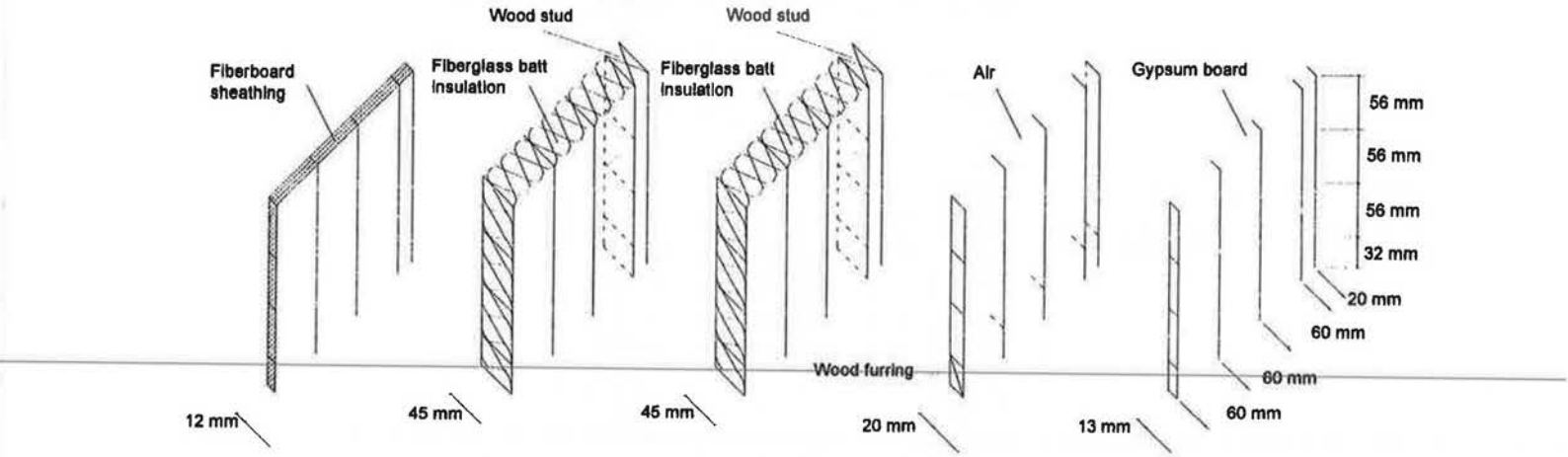

Figure 27. Control volume representation of the base-case assembly.

As in the monitored results, the calculated temperatures for the assembly with rigid insulation added on its cold side are higher, and those for the assembly with rigid insulation added on its warm side are lower than for the base-case assemblies. Adding the 38 mm of rigid insulation to the base-case composition also reduces the average temperature gradient across the batt insulation and the wood studs. The average gradient for the base-case assembly is approximately 22°C, while it is only 14°C for the assemblies with rigid insulation added on the cold side or on the warm side.

The isotherms generated from the calculated temperatures at the cold and warm planes for all three compositions are shown in Figure 28. In all cases, the predominant temperature gradient is horizontal, and the isotherms parallel to the wood studs. The vertical temperature changes seen for the warm planes of the base-case assembly and of the assembly with rigid insulation added on the cold side are due to the horizontal wood furring. In the base-case assembly (Figure 28a), the warm plane of the batt insulation is warmer behind the wood furring, which acts as a short thermal bridge. For the assembly with rigid insulation added on the cold side (Figure 28b) the temperatures are slightly warmer in the space between the studs and the furring. The impact of the wood furring is more pronounced for the base-case assembly, where the small oval shapes delimit areas that are 1°C warmer than the rest of the surface, than for the other section, where the irregular "donut" shapes delimit areas that are 0.5°C warmer than the rest of the surface. The wood furring does not have any impact on the warm plane temperatures for the assembly with rigid insulation added on the warm side of the batt insulation (Figure 28c) or on the cold plane temperatures of any assembly (Figure 28d to Figure 28f).

The model is also used to calculate the overall R-Value for the defined area for both base-case assemblies, insulated with 89 mm of fiberglass batt insulation or of blown cellulose fiber. The R-Value for the base-case assembly with fiberglass batt insulation is 2.45 (m^2 * °C)/W. When rigid insulation is added, either on the cold side or the warm side of this base-case assembly, the R-Value jumps to 3.81 (m^2 * °C)/W, an increase of 55%. For the base-case assembly insulated with blown cellulose insulation, the R-Value is 2.32 (m^2 * °C)/W, which becomes 3.66 (m^2 * °C)/W when insulation is added either on the warm or on the cold side. This is an increase of 66%.

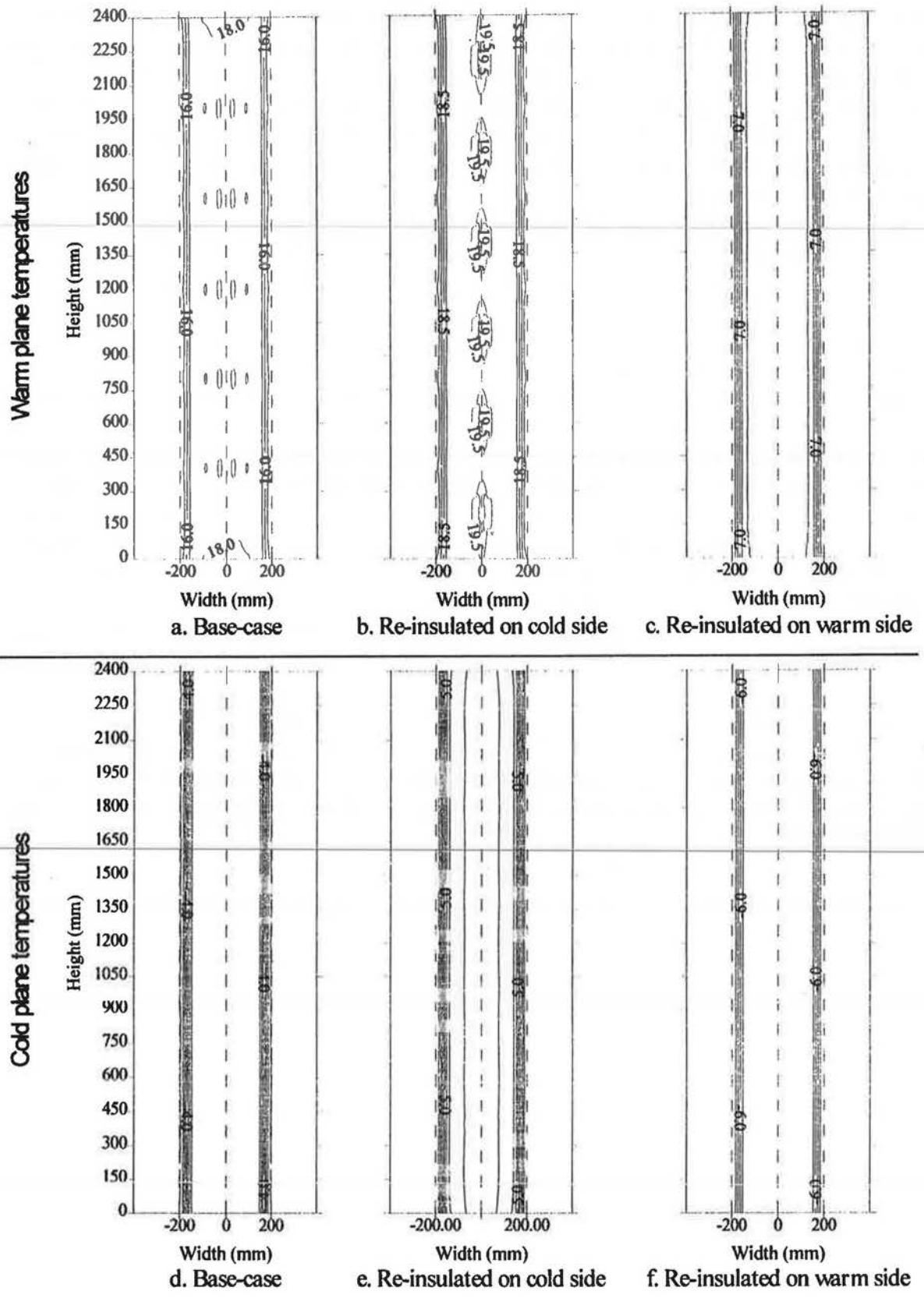

Figure 28. Isotherms for the 3-dimensional conductive heat transfer model (℃).

5.1.3. Preliminary air leakage pattern characterization effort.

Comparison of isotherms generated from the model results (Figure 28) to those obtained from the monitoring of assemblies with air leakage (Figure 19 to Figure 22), allows visualization of the effect of air leakage on temperatures within the assemblies. The curves presented in Figure 29 are generated using the difference between the measured warm plane temperatures of the sample sections with the long air exfiltration path and their corresponding calculated temperatures, which exclude air leakage. The negative numbers mean that the calculated temperature is warmer than the measured temperature. The difference between the measured and calculated temperatures illustrates the impact of the air leakage within the assembly.

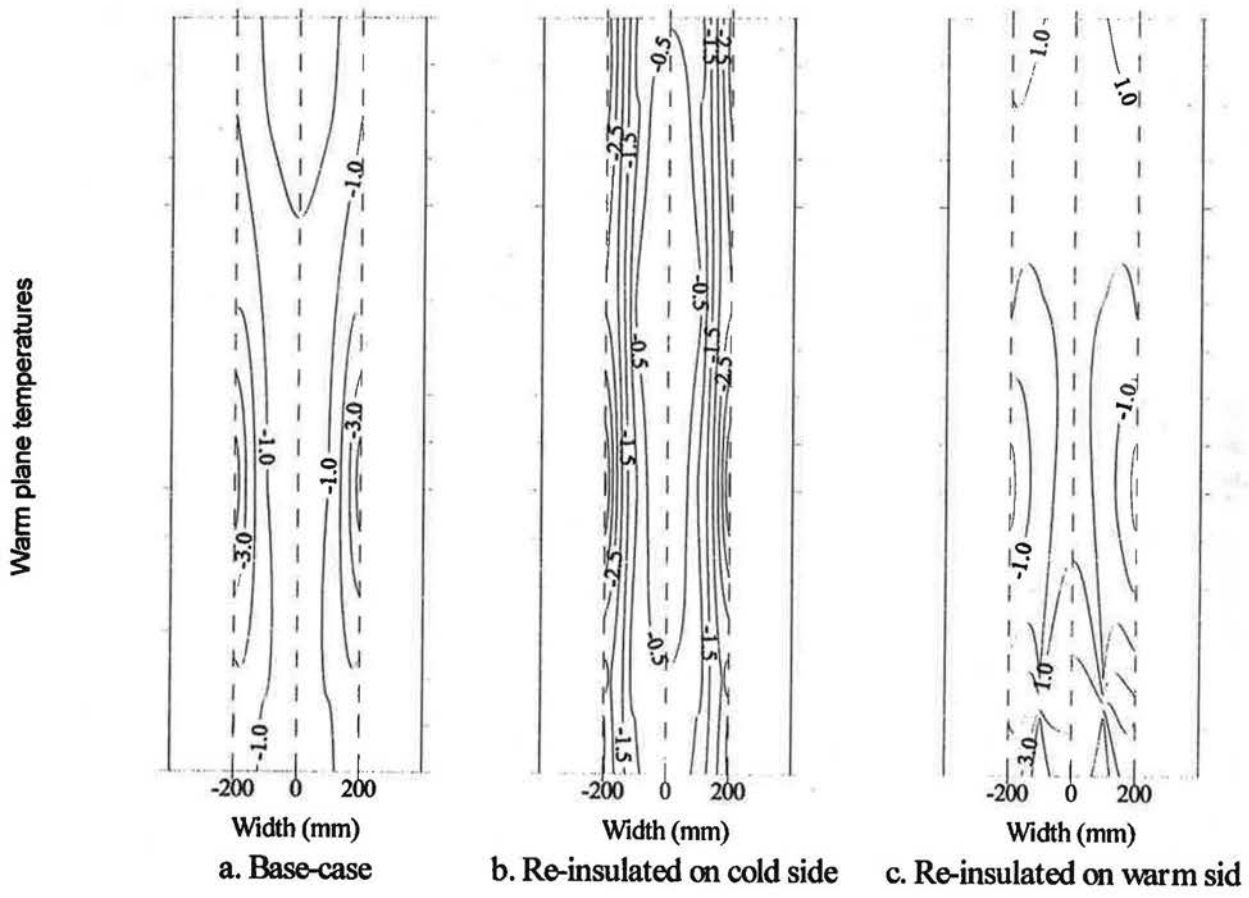

Figure 29. Differential isotherms for sections with the long exfiltration path (°C).

5.2. 2-D grid moisture content monitoring.

The moisture contents in the fiberboard sheathing panel were monitored with 237 gravimetry samples and with 59 electronic moisture content pins. The following analysis will focus on the gravimetric results for the sections with fiberglass batt insulation between the studs. Figure 34 to Figure 42 show the changes in gravimetric moisture content in the fiberboard sheathing panels during the whole length of the test for the assemblies with batt insulation.

The data collected on July 10th (day of the 7th weighing, and 53rd day into the test) was chosen to produce contour lines of equal moisture content, called isohygrons. As seen in Figure 34 to Figure 42, this data corresponds to high or near peak moisture content for all gravimetry samples. These isohygrons are found in Figure 30 to Figure 33. The numbers on the curves are the moisture contents in percentage per dry weight.

During the June 18th weighing procedure, the gravimetry samples from the top of the airtight section were accidentally interchanged with those from the top of the section with distributed air leakage, rigid insulation added on the cold side. By comparison with neighboring samples, the data used to generate the isohygrons for the airtight section were corrected to eliminate the effect of this event. The resulting isohygrons are presented in Figure 30. The moisture contents are very low, and there is no significant vertical moisture content gradient.

Isohygrons for the sections with the long air leakage path are shown in Figure 31. In all cases, the fiberboard moisture content is higher at the bottom, at the air entry point. This vertical gradient is most accentuated for the section with rigid insulation added on the cold side of the batt insulation (Figure 31b), where moisture contents range from 60% at the bottom to about 5% at the top, while the range for the other two is from approximately 20%-25% at the bottom to 10% at the top.

For the sections with the concentrated air leakage pate, isohygrons were generated only for the lower part because there were no monitoring points in the top half. In these sections, presented in Figure 32, moisture is concentrated at the height of 450 mm, just above the 20 mm circular air entry point. The section with insulation added on the cold side reaches the highest moisture contents (Figure 32b). The circular pattern of moisture accumulation, following the shape of the hole in the interior finish, is clear for the base-case assembly (Figure 32a) and the section with rigid insulation added on the warm side (Figure 32c) but less obvious for this section (Figure 32b) where moisture contents are also higher above this height. This indicates that warm air is flowing up, its moisture is condensing at the indoor face of the rigid insulation and is then absorbed by the fiberboard sheathing. It was indeed observed during the test that the indoor face of the rigid insulation was covered with drops of water.

Figure 33 shows isohygrons for the sections with the distributed air leakage path. For the base-case assembly (Figure 33a), moisture contents range from 15% to 25%, being higher at the top of the section. This vertical moisture content gradient is caused by a gap in the batt insulation at the top of the section (see Figure 14). When the holes to allow air leakage were drilled, the drill caught the insulation which twisted and got displaced, leaving this gap. It was suspected from the beginning because of the cold temperature readings for this location, but it was decided not to open the section to make the correction. The section with rigid insulation added on the cold side (Figure 33b) has slightly higher moisture contents than for the base-case assembly (Figure 33a), ranging from around 18% to 28%. The moisture contents are higher toward the center of the cavity, and slightly toward the top of the section.

As can be seen, a correlation exists between moisture distribution patterns in the fiberboard sheathing and the air leakage pattern. Moreover, by representing moisture contents with this method, local problem areas can be easily identified. The isohygrons also demonstrate that these problem areas are generally linked to the entry point of warm indoor air into the cavity.

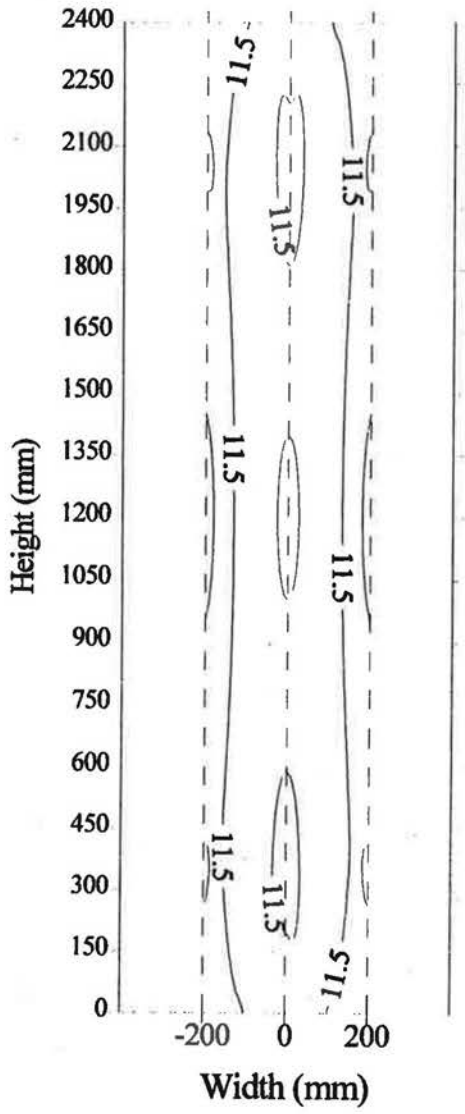

Figure 30. Isohygrons for the airtight section (% M).

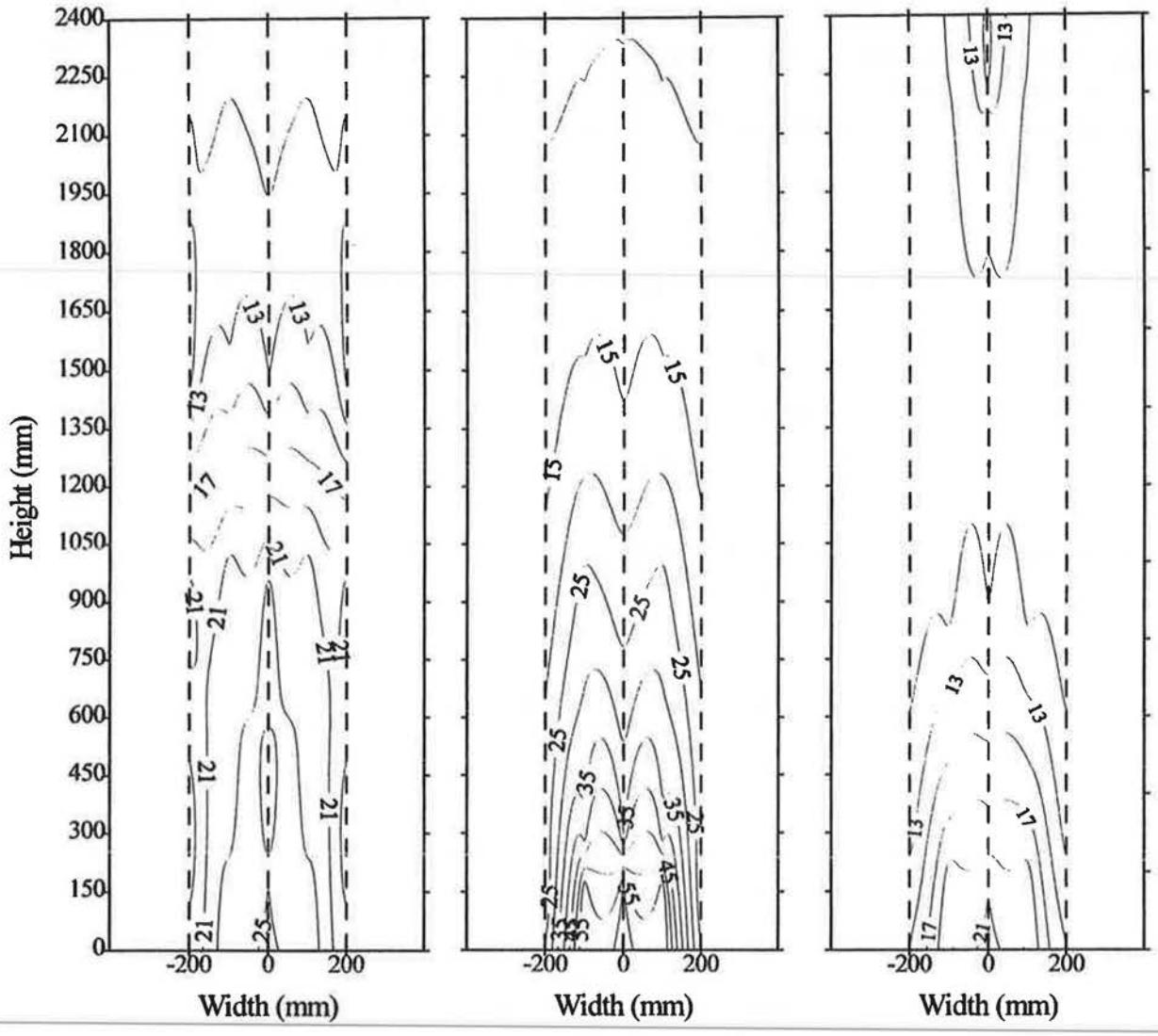

a. Base-case b. Re-insulated on cold side c. Re-insulated on warm sid

Figure 31. Isohygrons for sections with the long air leakage path (% M).

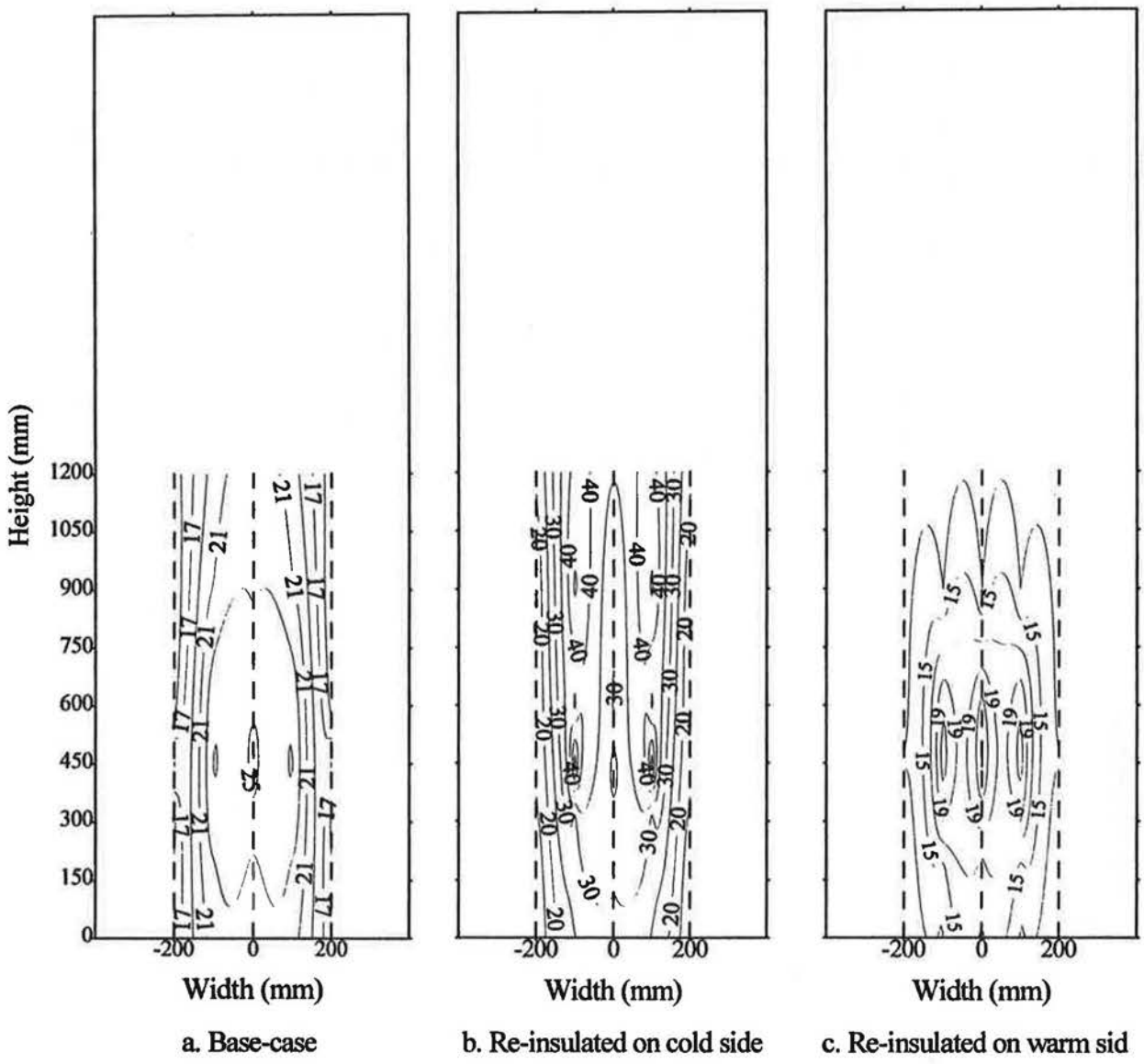

Figure 32. Isohygrons for sections with the concentrated air leakage path (% M).

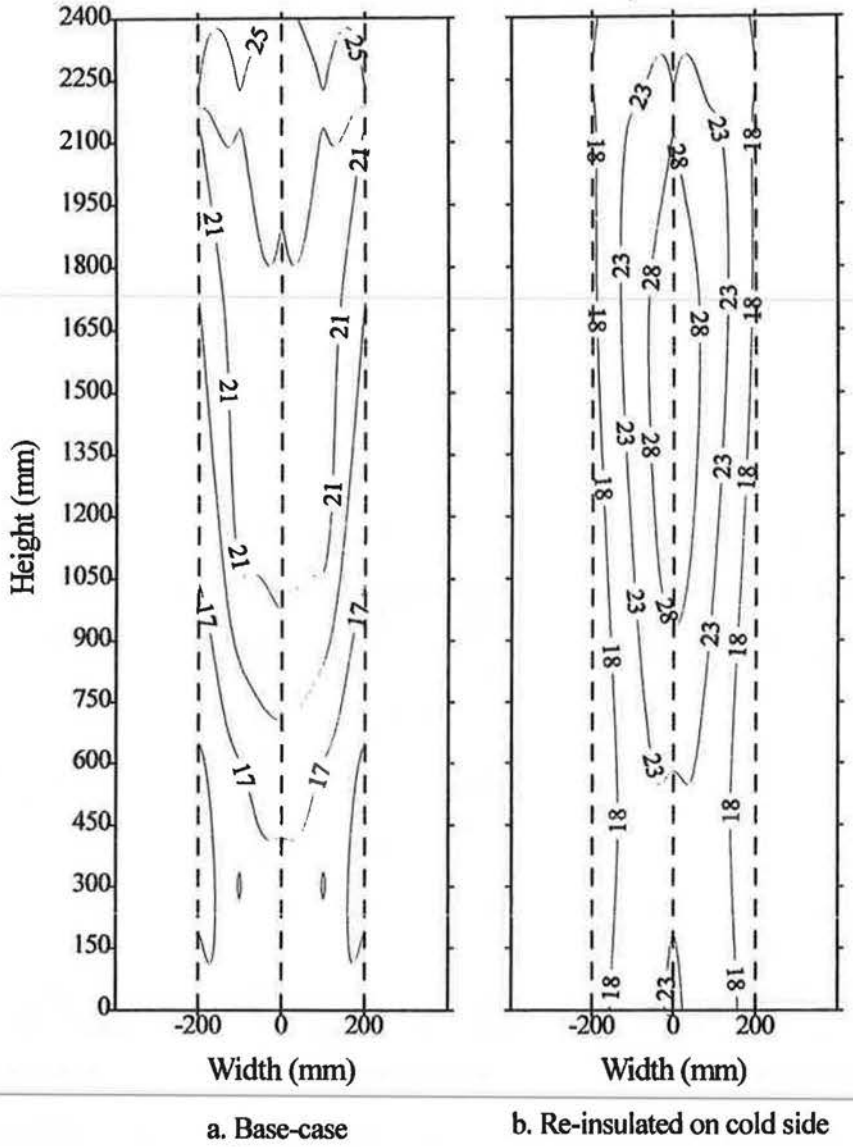

Figure 33. Isohygrons for sections with the distributed air leakage path (% M).

The moisture contents in the fiberboard sheathing and in the cold side of the wood studs are plotted over time and presented in Figure 34 to Figure 42. Please note that three scales of moisture contents are used. In most cases, a range of 0% to 40% moisture content per dry weight was used. For two charts, Figure 38a and Figure 39a, a range of 0% to 75% was used, and in one case, Figure 37b, a scale of up to 110% was necessary.

The section with the least moisture accumulation is the airtight section, base-case assembly (Figure 34). Moisture contents did not rise above 20%. This section also had the least moisture content variation. The peaks, due to the misplacement of the samples discussed previously, show that moisture contents vary rapidly in fiberboard (Figure 34a), and more slowly in wood (Figure 34b). Moisture contents in the studs and in the fiberboard in front the studs (Figure 34b) also increased slightly more than those in the fiberboard between the studs (Figure 34a). At the end of the drying period, the moisture contents of all samples were close to their original value, 2% higher on average. It can be concluded that the drying potential for this wall is good since no moisture related problems was observed.

The other sections with the base-case assembly: long air leakage path (Figure 35), concentrated air leakage path (Figure 36), and distributed air leakage (Figure 37), also performed fairly well. Most moisture contents did not rise above 25%. In the case of the section with the distributed path however, the moisture contents at the top of the studs reached very high moisture content (Figure 37b). The cause of this is the gap in the insulation at the top of the section, shown in Figure 14. Warm, moist indoor air was entering this gap through the 3 mm holes, and condensing on this part of the stud. Otherwise, after the initial accumulation the moisture contents were relatively stable, and when the temperature was increased for the drying period, they dropped very rapidly to just above the initial level. For the section with the long path however, moisture contents in the stud and in the fiberboard in front of the studs (Figure 35b) dropped more slowly and did not finish drying.

A similar trend is observed for the section with rigid insulation added on the cold side and long air leakage path (Figure 38b). The moisture contents were also much higher, up to 70% (Figure 38a) compared to just about 25% in the base-case assembly, long air leakage path (Figure 35a). The section with rigid insulation added on the cold side and concentrated air leakage path (Figure 39) reached high moisture contents as well, up to a maximum of 55%. For these two sections with rigid insulation added on the cold side, the moisture contents did not seem to reach a plateau, as in the other cases. The moisture contents increased until the drying period was started. These high moisture contents and the steady increase can be explained by the fact that the temperature at the interface between the fiberboard sheathing and the rigid insulation was above freezing, but below the dew point of the indoor air, at 11°C for the prevailing indoor conditions. When moisture, transported by exfiltrating air, reached this point it condensed on the indoor face of the rigid insulation and was absorbed by the fiberboard and the wood. When the piece of rigid insulation was removed to access the gravimetry samples, water was observed on its indoor surface. For the section with the distributed air leakage, the moisture contents went up to 35% (Figure 40). For all sections with rigid insulation added on the cold side, the moisture contents at the drying period remained approximately 5% to 7% higher than before testing, suggesting that their drying potential is slightly lower. This applies especially to the fiberboard in front of the studs and to the studs (Figure 38b, Figure 39b, and Figure 40b).

The moisture contents in the sections with rigid insulation added on the warm side (Figure 41 and Figure 42) did not rise above 25%, with the exception of three locations in the stud of the section with the concentrated path (Figure 42b) right after the climatic condition change. During the experiment, frost was observed on the exterior surface of the fiberboard sheathing. When the outdoor temperature was increased, this frost melted and momentarily increased the moisture contents in the stud and the sheathing in front of the stud. This effect, although less pronounced, can also be observed in the base-case with distributed air leakage path (Figure 37b).

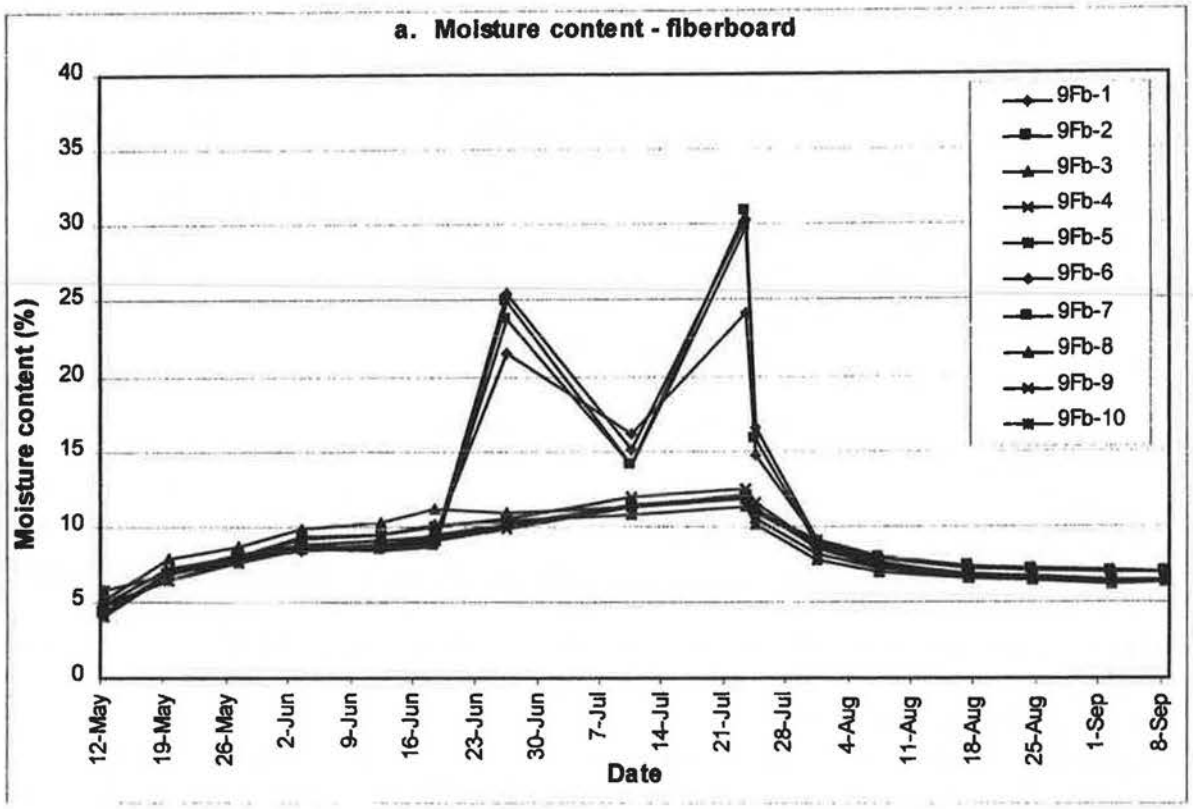

Figure 34. Airtight section.

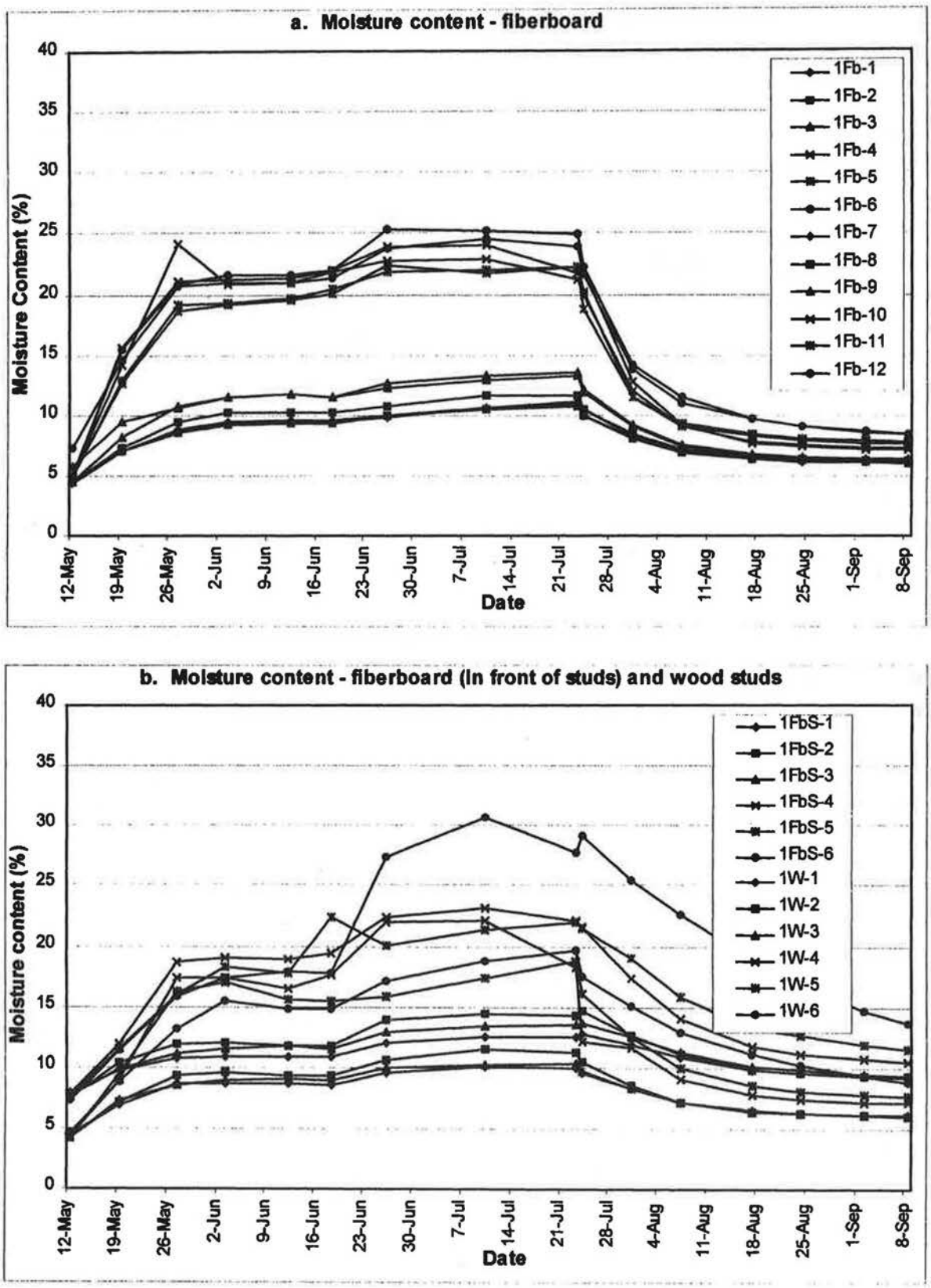

Figure 35. Section with base-case assembly, long air exfiltration path.

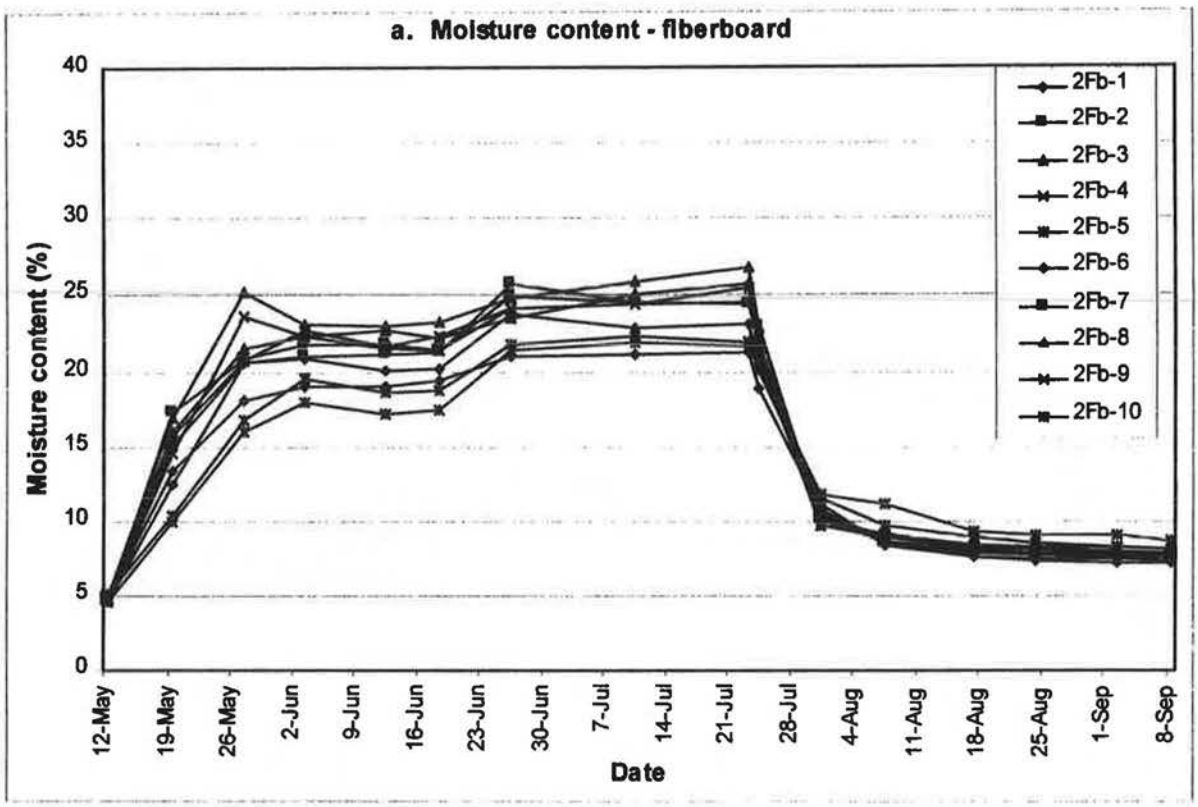

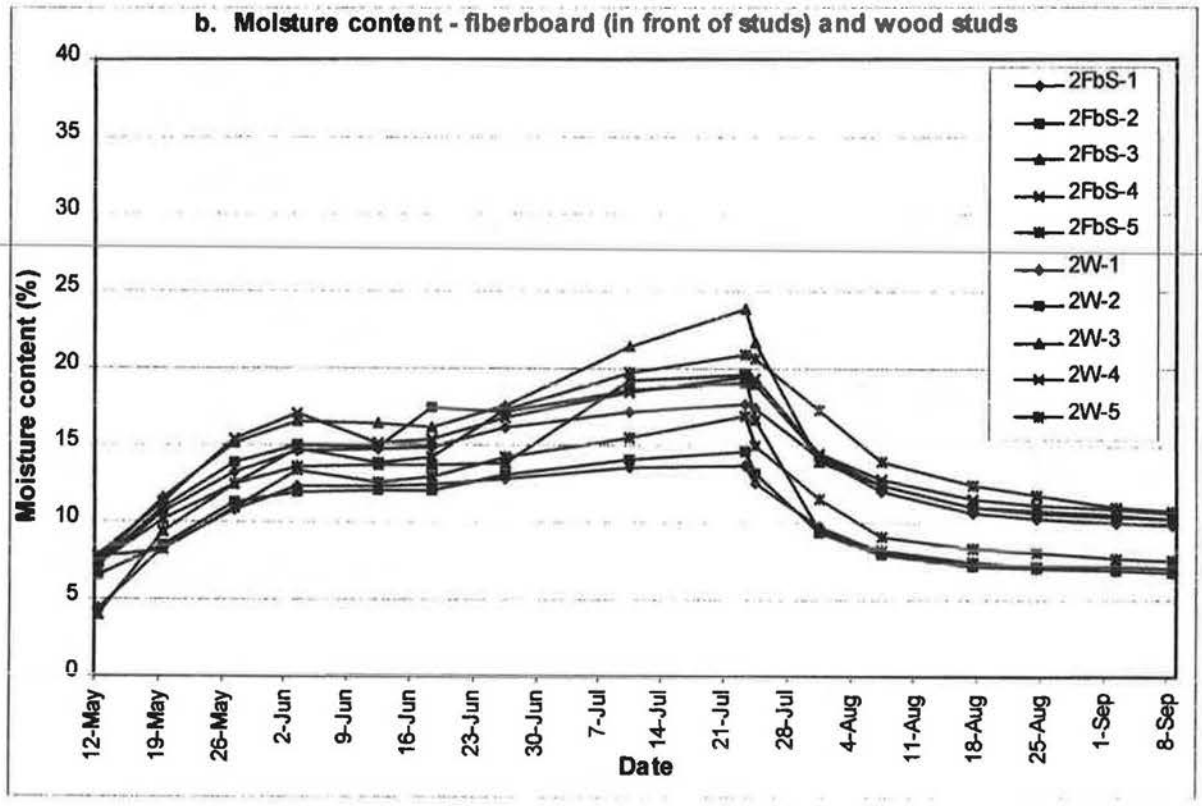

Figure 36. Section with base-case assembly, concentrated air exfiltration path.

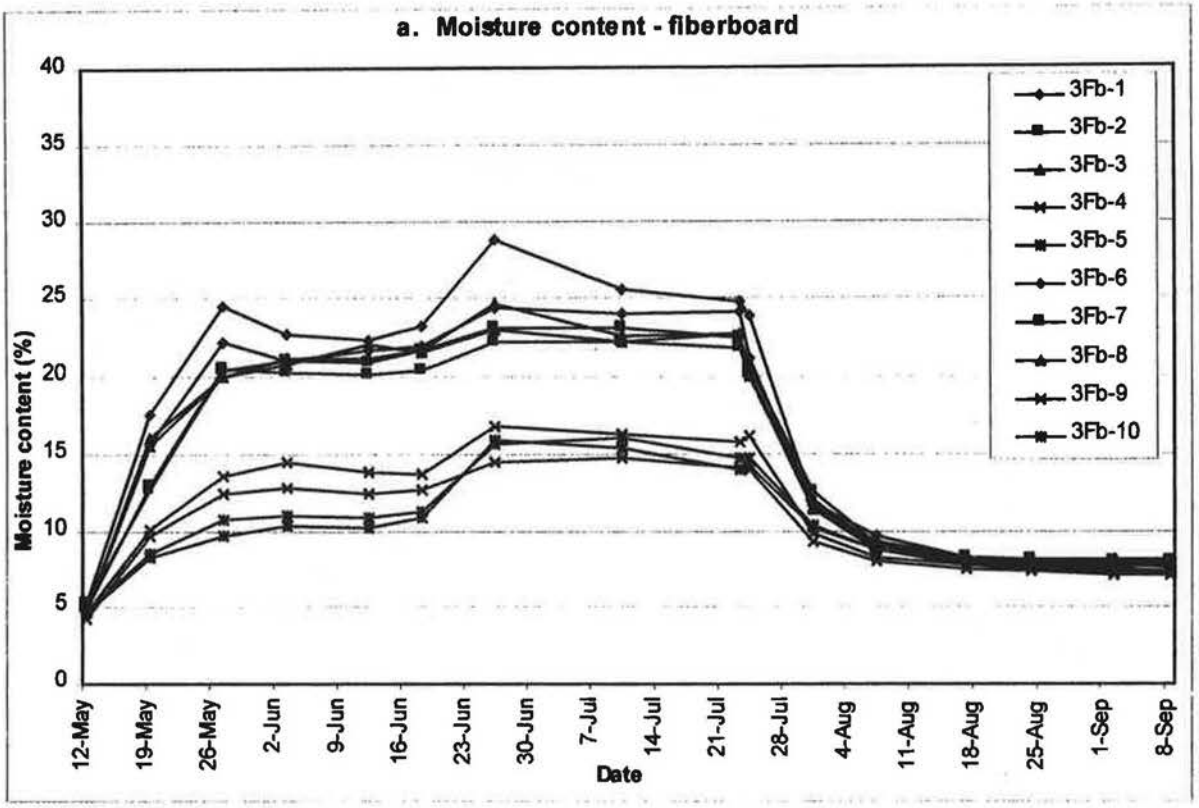

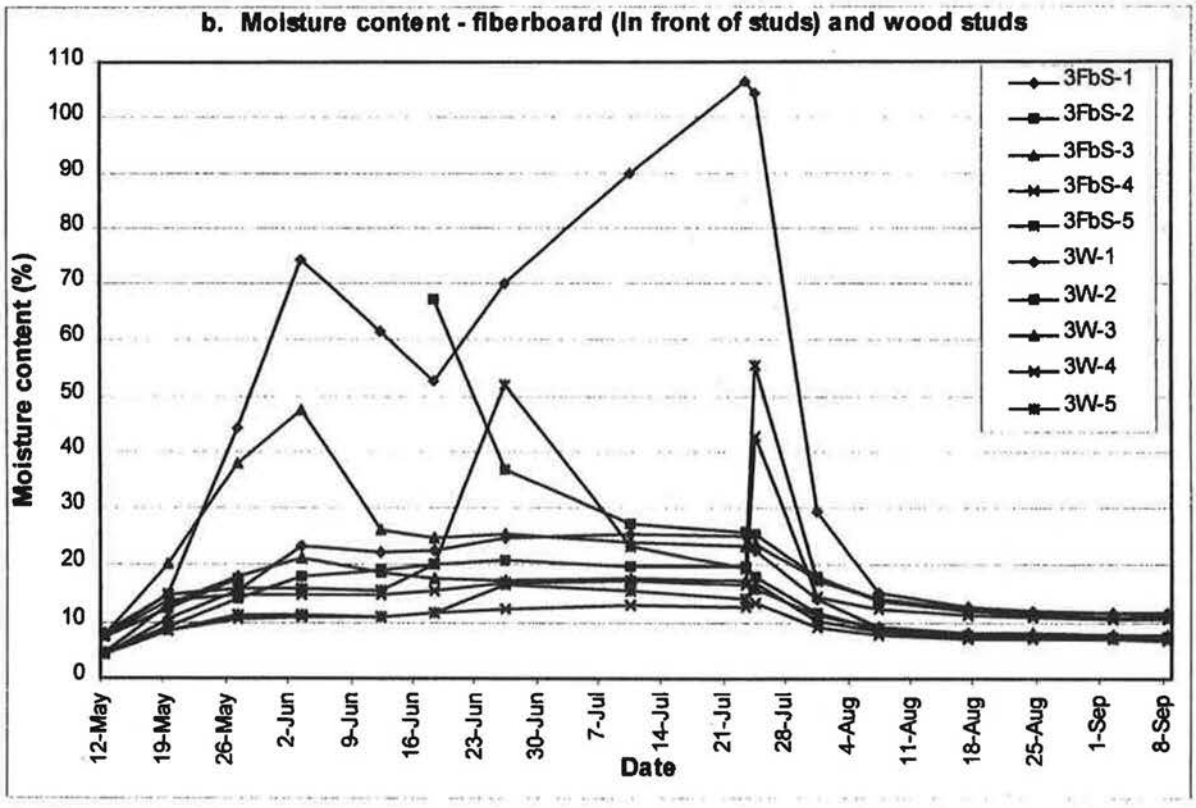

Figure 37. Section with base-case assembly, distributed air leakage path.

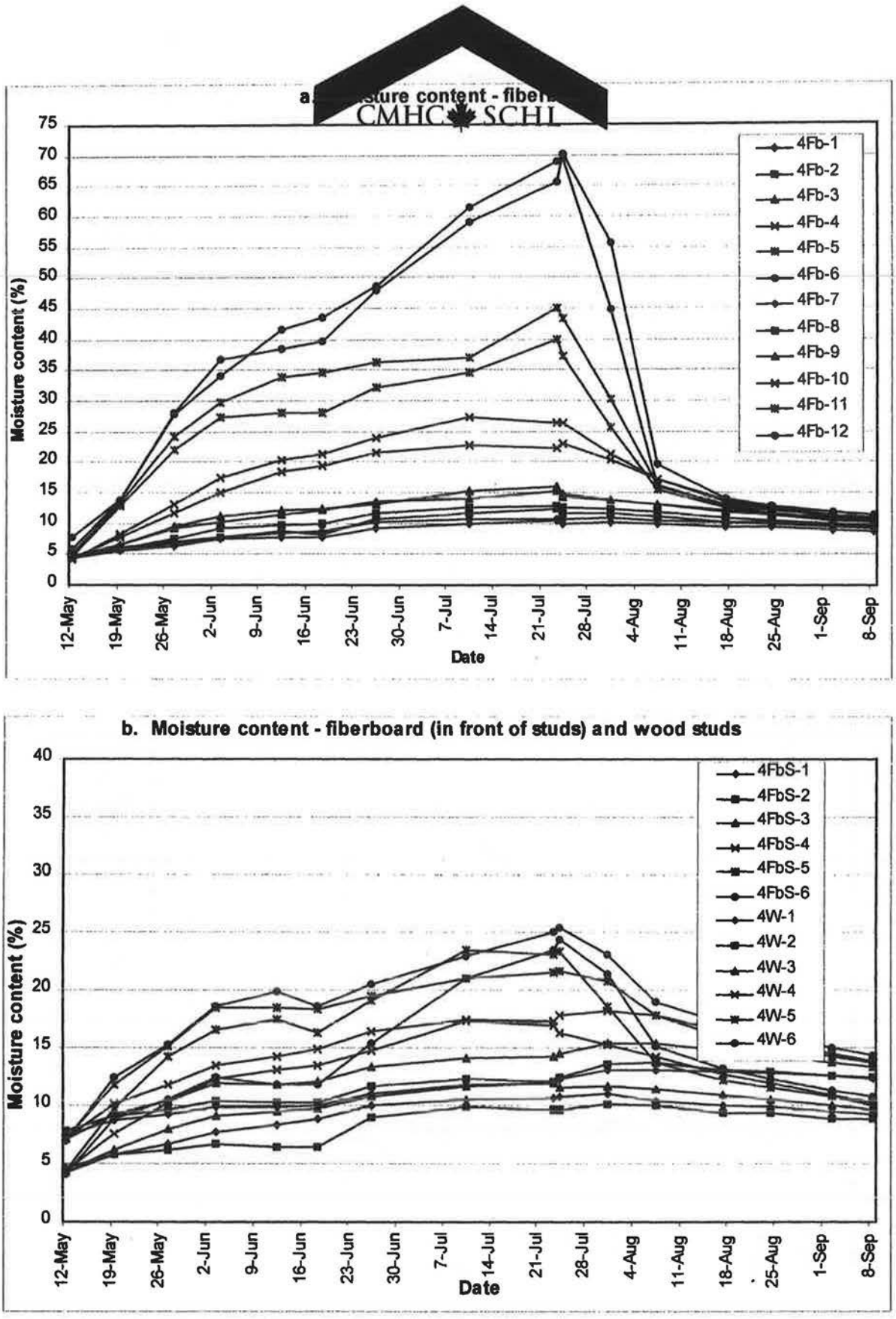

Figure 38. Section with rigid insulation added on the cold side, long air leakage path.

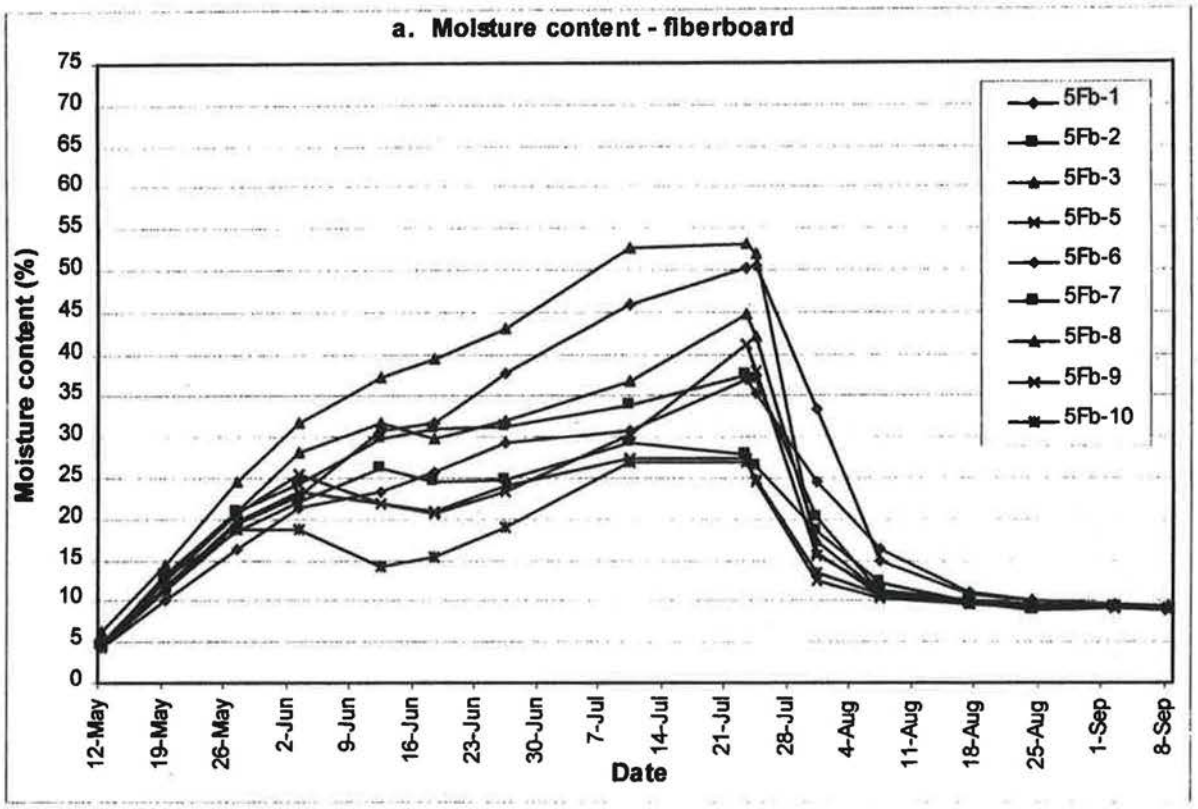

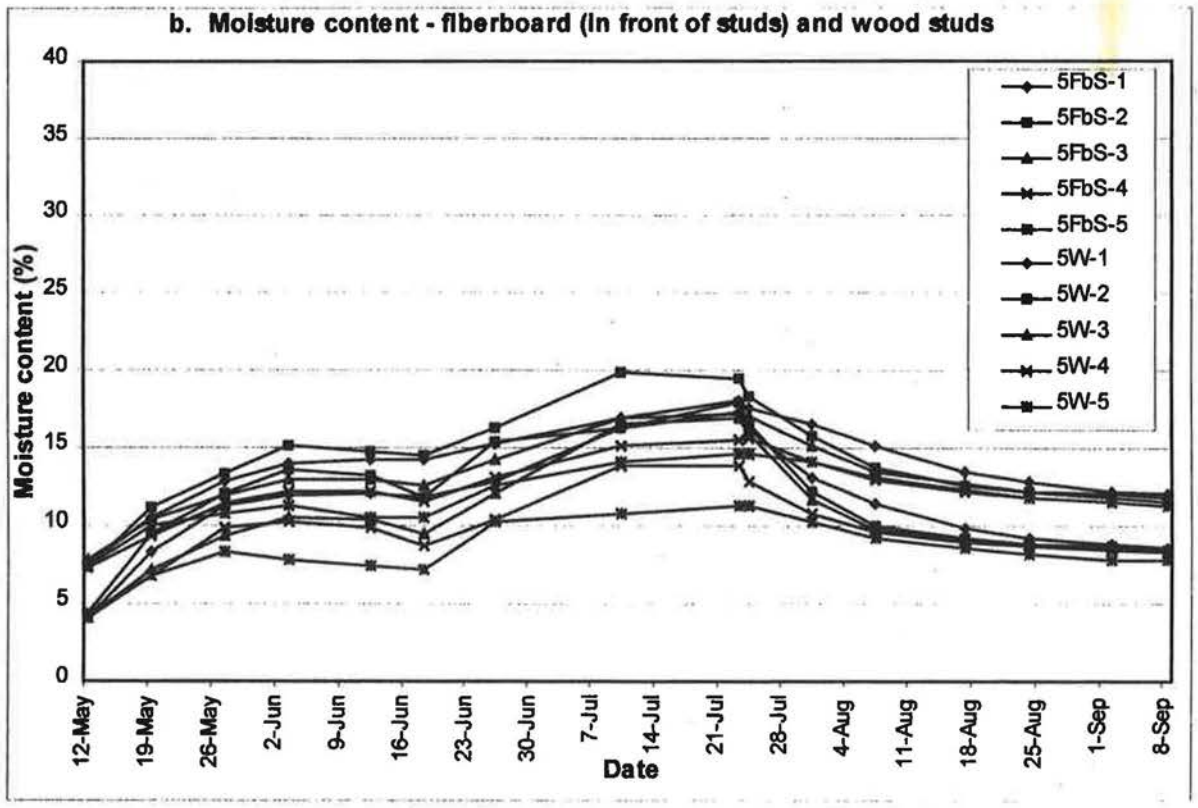

Figure 39. Section with rigid insulation added on the cold side, concentrated air leakage path.

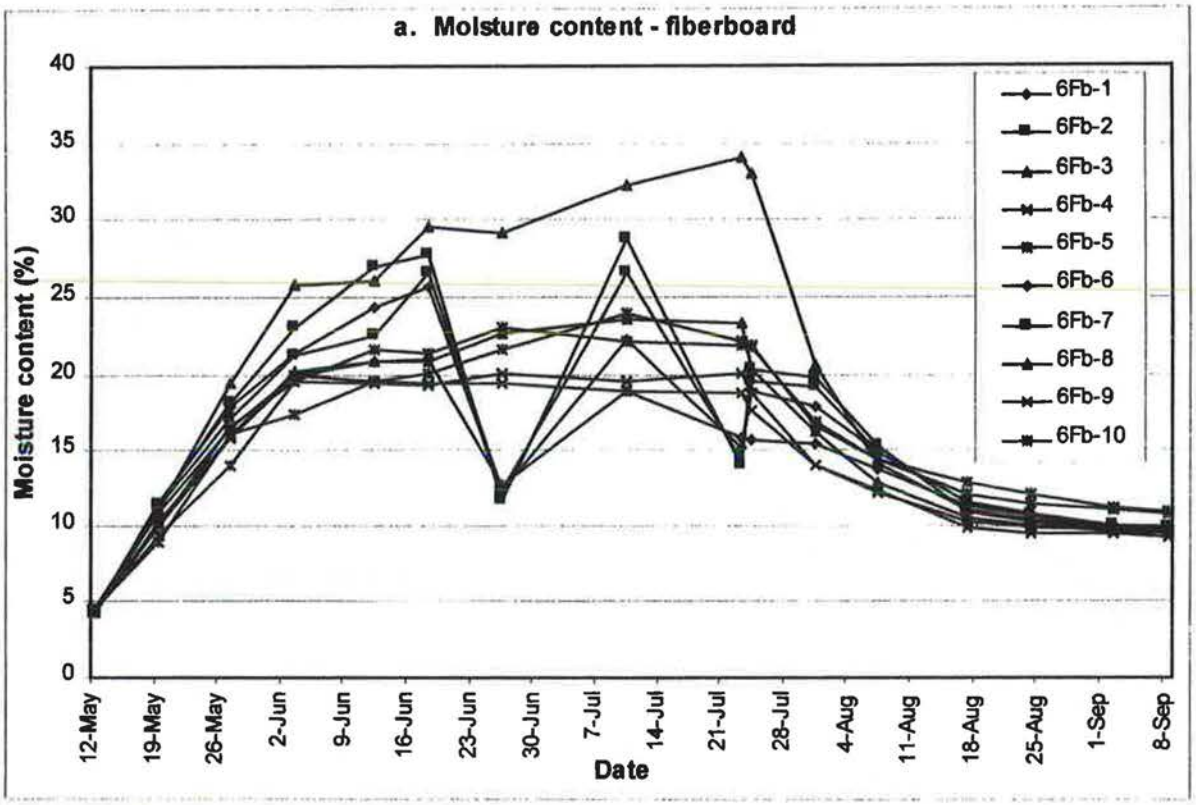

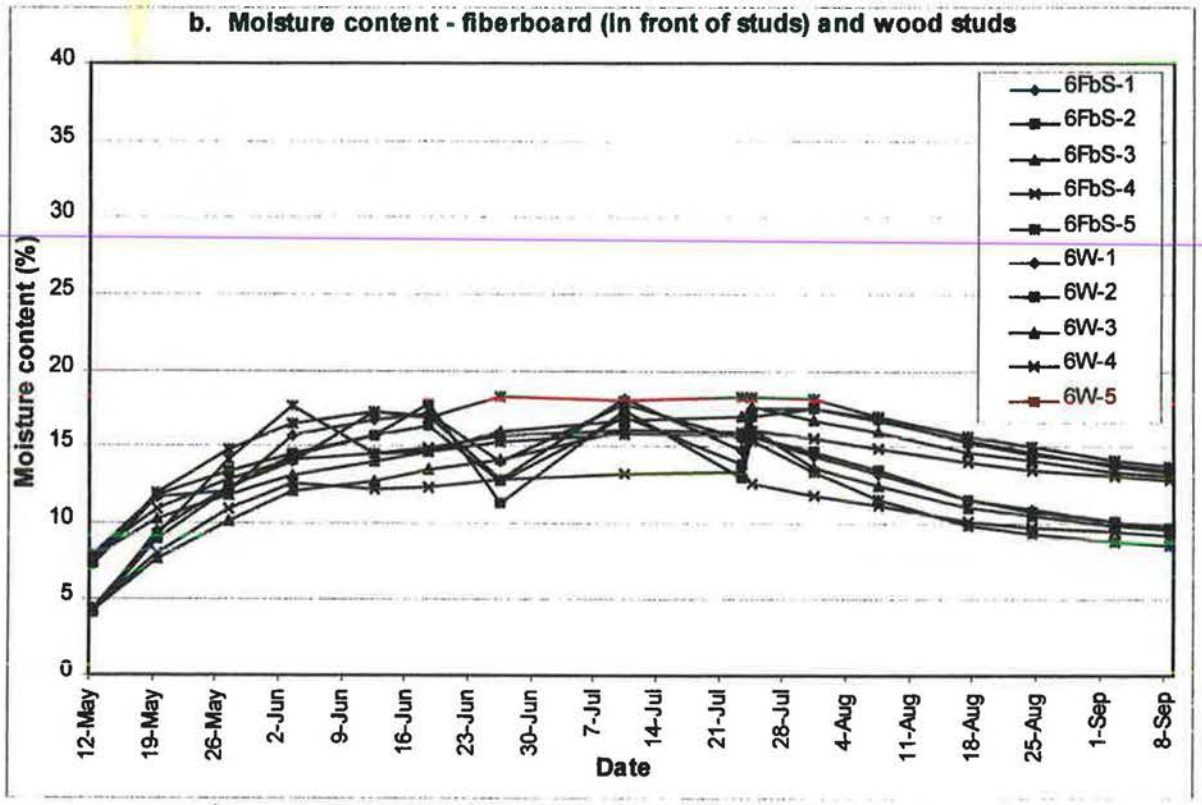

Figure 40. Section with rigid insulation added on the cold side, distributed air leakage path.

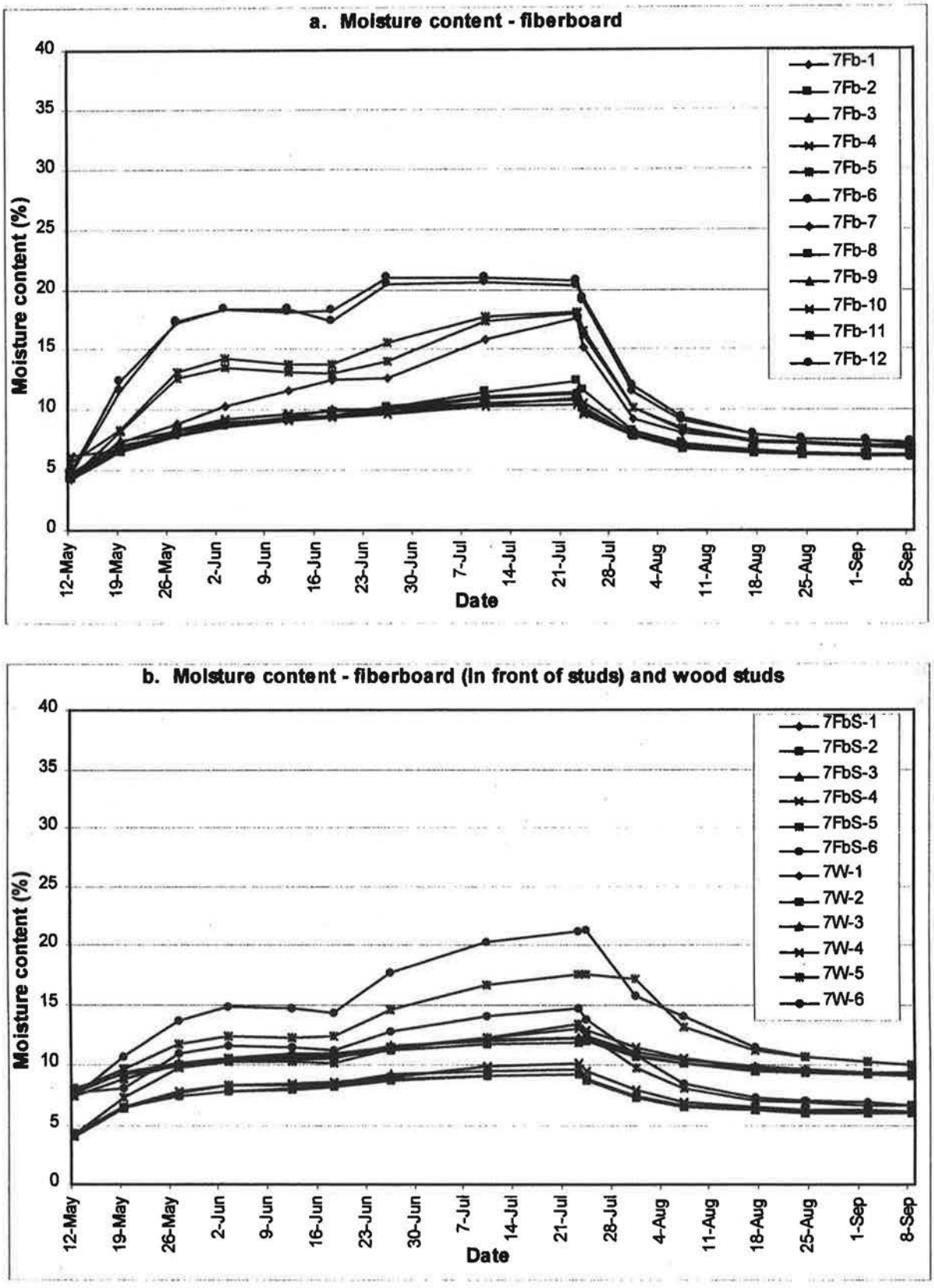

Figure 41. Section with rigid insulation added on the warm side, long air leakage path.

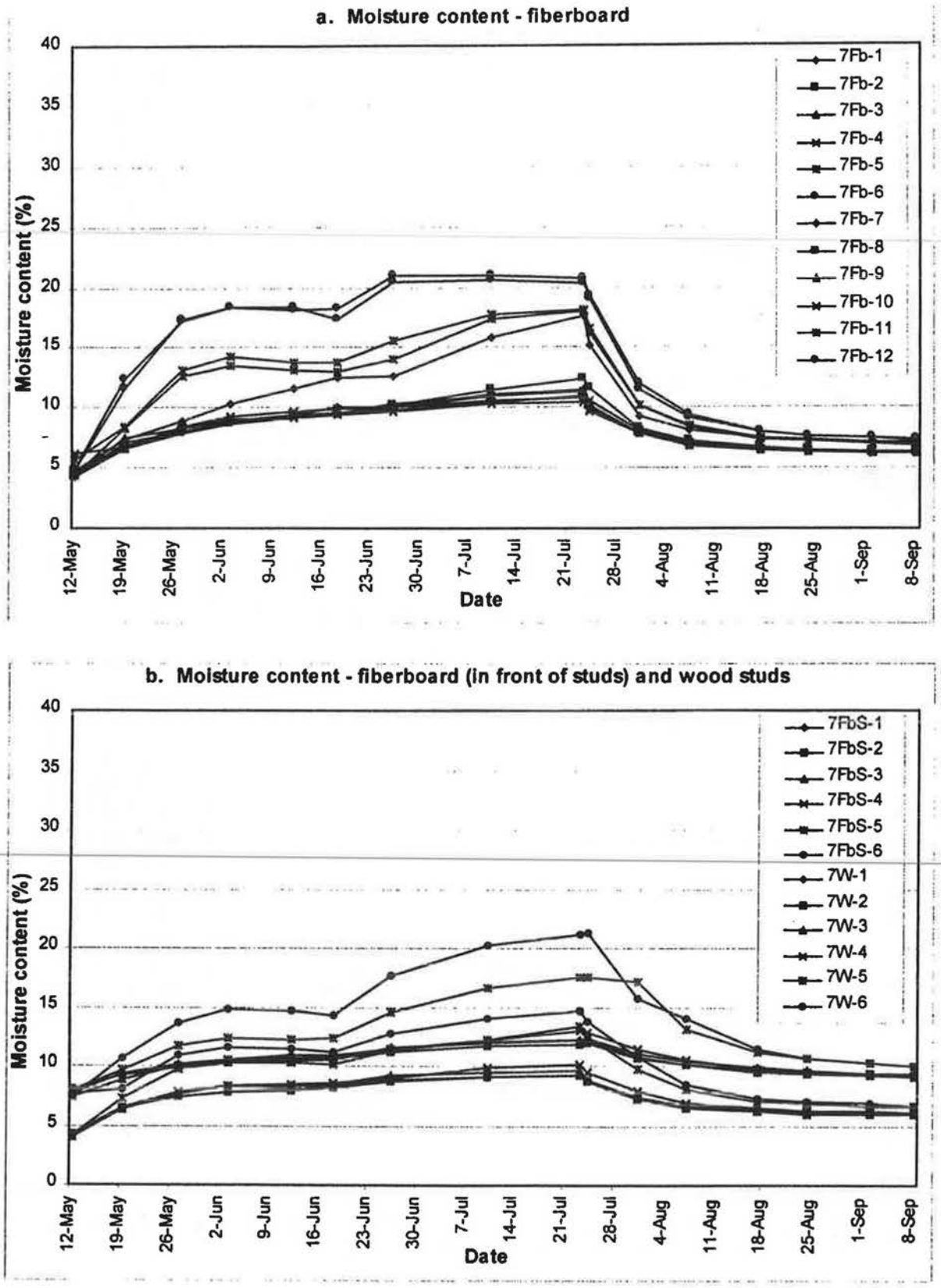

Figure 41. Section with rigid insulation added on the warm side, long air leakage path.

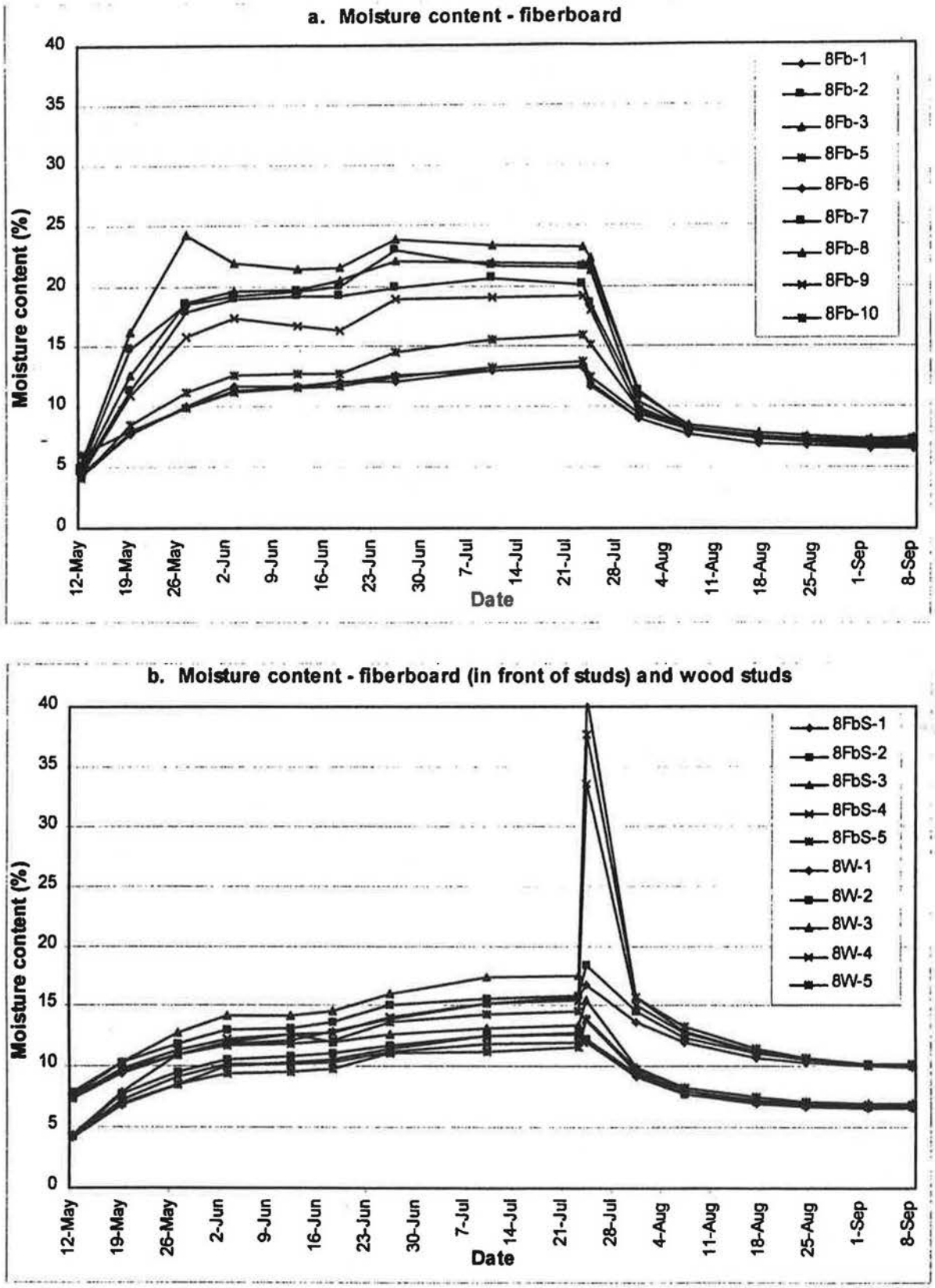

Figure 42. Section with rigid insulation added on the warm side, concentrated air leakage path.

Analysis of the moisture content results can be further continued. In Table 7, the fiberboard moisture content measurements taken on July 10th are averaged for each sample section with fiberglass batt insulation. An overall average is then given for each insulation strategy and leakage path. The overall average moisture content in the sheathing is highest for the sections with rigid insulation added on the cold side, at 23%, and for the sections with the concentrated and distributed air leakage paths, at 21% and 20% respectively. The sheathing in the sections with rigid insulation added on the warm side shows average moisture contents lower than those in the base-case assemblies. The sections where the sheathing had the lowest average moisture content are the airtight section and the section with the long air leakage path and insulation added on the warm side of the fiberglass batt insulation, both at 13% moisture content. The rigid insulation added on the warm side of the fiberglass batt insulation may have helped to decrease the flow of air and therefore the amount of moisture getting inside the wall, while adding rigid insulation on the cold side only trapped the moisture in the fiberboard which was kept at temperatures above freezing.

Table 7. Average of gravimetric moisture contents (%) in the fiberboard for the July 10th.

	Long path	Concentrated path	Distributed path	Airtight	**Average**
Base-case	17%	20%	19%	13%[4]	**17%**
Cold side	22%	27%	20%[4]		**23%**
Warm side	13%	15%			**14%**
Average	**17%**	**21%**	**20%**	**13%**	

The maximum moisture contents measured in the fiberboard on July 10th are presented in Table 8. The sheathing in the sample sections with rigid insulation added on the cold side of the fiberglass batt insulation reached much higher moisture contents than that in the others, particularly those with the long and concentrated air leakage paths (61% and 53% respectively). In organic hygroscopic materials, mold can grow at moisture contents above 25%. Considering this, although average moisture contents do not rise above 25%, local potential problem areas exist for the sample sections mentioned. Table 7 shows lower numbers and a variation of 14% between the lowest and the highest moisture content averages, while Table 8 shows higher numbers and a variation of 45% between the lowest and the highest maximum moisture contents.

Table 8. Maximum gravimetric moisture contents (%) in the fiberboard for July 10th.

	Long path	Concentrated path	Distributed path	Airtight	**Average of maximum**
Base-case	25%	26%	26%	16%[5]	**23%**
Cold side	61%	53%	32%[5]		**49%**
Warm side	21%	23%			**22%**
Average of maximum	**36%**	**34%**	**29%**	**16%**	

[4] Switching samples from the top of these sections did not affect the overall moisture content average by more than 1% for the July 10th measurements. Assuming switched samples would have followed the trends of the others, the average moisture content would be around 12% for the airtight section and 21% for the section with the distributed air leakage path and rigid insulation added on the cold side.

[5] Switching samples from the top of these sections did affect the maximum moisture content in the airtight section on July 10th. Assuming the switched samples would have followed the trends of the others, the maximum moisture content would be around 12% for the airtight section.

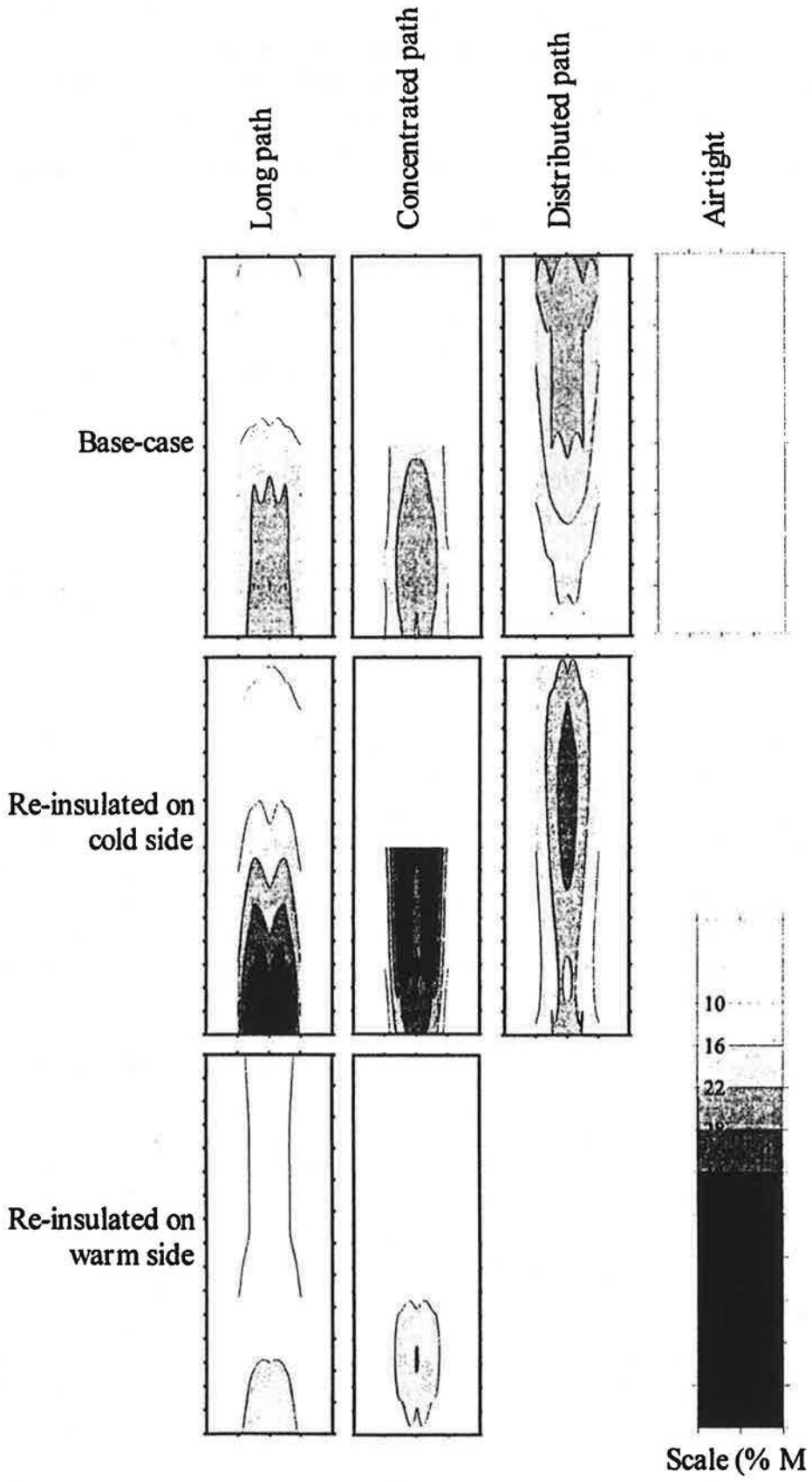

Figure 43. Isohygrons - maps of moisture contents in the fiberboard sheathing.

Figure 43 shows the isohygrons for all sections insulated with fiberglass batt insulation. The same scale is used for all nine assemblies, from 10% to 64% moisture content per dry weight in the fiberboard sheathing, allowing comparison of the moisture contents and of their distribution patterns. Between each curve, there is a 6% moisture content variation. The airtight section is at the very low end of the moisture content scale and has no curves because the moisture content does not vary by more than 6% across the whole section. The sections with added insulation on the cold side have areas with lower moisture contents, but other areas reach the top of the scale. These sections also have the highest number of curves, corresponding to the largest variation in moisture content across the area of the sample sections. The base-case assemblies and the sections with insulation added on the warm side all have moisture contents toward to low end of the scale, and few lines of change in moisture content.

In the case of the five sections insulated with cellulose fiber, cellulose itself was a marker for moisture accumulation due to its change of texture. Qualitative information can be extrapolated from inspection of the cellulose but no numerical characterization is possible (as was done with the isohygrons generated for the fiberglass insulated walls) due to the small number of monitoring points installed in those walls. At high moisture contents, the cellulose agglomerates together. The shape and location of the agglomerated cellulose give an indication of where moist indoor air flowed. From this method and from the measurements performed, it was seen that the fiberboard and wood stud moisture contents did not reach the critical level of 25% in any of the five assemblies insulated with blown cellulose fiber.

6. Conclusion

A full scale test hut, typical of low-rise residential construction in the province of Quebec, was built inside an environmental chamber. This test hut was subjected to 66 days of simulated winter and then to 47 days of late spring conditions to verify the feasibility of different proposed modes of characterizing air exfiltration and to study the modes of dispersion of moisture through different exterior wall assemblies with and without added rigid insulation. By gaining a better understanding of the movement of exfiltrating air through the envelope, the risks related to moisture condensation within the envelope when adding insulation to existing exterior wall assemblies can be better ascertained. The air leakage pattern characterization methods implemented were: (1) 3-dimensional grid temperature monitoring and (2) 2-dimensional grid moisture content monitoring.

The experimental results of these two air leakage characterization methods show that the 3-D grid temperature monitoring and the 2-D grid moisture content monitoring (by gravimetry) can be used to gain information on the path of exfiltrating air through the envelope. It has been demonstrated that there is a correlation between the temperature profiles and the air leakage path, and between the moisture distribution pattern and the air leakage path. The monitored temperature profiles tend to follow the air leakage path of the section. Furthermore, by mapping the difference between the monitored temperature profiles and the calculated temperature profiles, a first attempt toward the graphic representation of the impact of air leakage is obtained. Moisture contents measured by gravimetry according to a 2-dimensional grid are used to generate lines of equal moisture contents. This procedure allows to identify local moisture related problem areas and confirms that moisture tends to accumulate at the entry point of indoor air into the assembly. This type of temperature and moisture content data analysis, and the information it provides, could only be achieved because of the extensive monitoring conducted and the graphic representation of the results. In both cases however, additional analysis of the data would be recommended. For example, analysis of electronic moisture content sensor results

and the development of the differential contour line method (temperature and moisture content) for evaluation of the impact of air leakage would benefit from additional investigation. The analysis of the data collected from the 69 moisture content sensors would provide additional information on the accumulation of moisture into the hygroscopic materials. Moreover, comparison between moisture contents measured by gravimetry and electronically could be used to substantiate the conclusions obtained from the gravimetry measurements only. Differential isotherm lines were produced only for the sections with the long air leakage path. The same could be done for the concentrated and distributed air leakage paths. The comparison between the differential isotherms of the different paths could validate the capacity of this method to capture the impact of air leakage. Differential contour lines could also be produced for the gravimetric moisture content measurements, using the airtight base-case assembly as the reference. The two methods used, 3-dimensional temperature monitoring and 2-dimensional moisture content monitoring, require an important monitoring set-up. A sensitivity analysis could be done to investigate the need of so many points.

The temperature and moisture content results are further used to assess the impact of adding 38 mm of extruded rigid polystyrene insulation to existing exterior wall assemblies with different air leakage characteristics on their moisture contents. As calculated using a 3-dimensional heat transfer modeling approach, which does not include air leakage or moisture transfer, adding insulation to the cold side or the warm side of existing assemblies increases the thermal performance by 55% for those with fiberglass batt insulation, and by 66% for those insulated with blown cellulose fiber. But, experimental results demonstrate that these R-Value numbers do not reflect the global hygrothermal performance of the assemblies. For example, the R-Value is the same whether rigid insulation is added on the cold or on the warm side of the base-case assembly insulated with fiberglass batt insulation. However, the performance of these two assemblies in terms of moisture accumulation is very different. In the case of adding insulation on the warm side, moisture contents mostly do not rise above 25%, while they go up to 70% when insulation is added on the cold side. On the other hand, the section with no insulation added but no air leakage showed the lowest moisture accumulation. Even though its thermal performance is lower, the airtight section performed best in terms of overall hygrothermal performance. From this, it can be concluded that the thermal performance cannot be looked at independently from air and moisture transfer, and that air leakage should be minimized to avoid moisture problems.

Some recommendations related to retrofit work arise from the analysis of the results:

- Increasing the airtightness should be considered before increasing the R-value for existing exterior wall assemblies.
- Adding insulation on the warm side of an existing leaky exterior wall appears to induce less moisture accumulation than adding insulation on its cold side.

It should be kept in mind that these recommendations are applicable to the types of assemblies and materials studied in this research project, i.e. with added insulation with low water vapor permeability and that they cannot be generalized to all existing exterior wall assemblies and all insulation materials.

7. References

Abdul-Nabi, L. 1996. "Modeling of air barrier characteristics in predicting the moisture performance of building envelopes." Thesis, Concordia University, Center for building studies. Montreal. 123 p.

ANSI/ASHRAE. 1992. ANSI/ASHRAE 55-1992 "Thermal Environmental Conditions for Human Occupancy." American Society of Heating, Refrigerating and Air-Conditioning Engineers. 20 p.

ASTM. 1989. ASTM C 236-89 "Standard Test Method for Steady-state Thermal Performance of Building Assemblies by Means of a Guarded Hot Box." American Society for Testing and Materials. Annual Book of Standards, Vol. 4.06, pp. 52-62.

ASTM. 1991. ASTM E 283-91 "Standard Test Method for Determining the Rate of Air Leakage Through Exterior Windows, Curtain Walls, and Doors Under Specified Pressure Differences Across the Specimen." American Society for Testing and Materials. Annual book of Standards, Vol. 04.07, pp. 486-489.

ASTM. 1992. ASTM D 4442-92 "Standard Test Method for Direct Measurement of Wood and Wood-Based Materials." American Society for Testing and Materials. Annual book of Standards, Vol. 04.10, pp. 493-497.

Athienitis, A. Ph.D., "An Electronic Mathcad Book.", Center for Building Studies, Concordia University, Montreal, Canada, 1994, 189 p.

Burch, D.M.; S. Treado. 1978 "A technique for protecting retrofitted wood-frame walls from condensation damage." ASHRAE TRANSACTIONS. Vol. 84, Part 1, pp. 197-206.

Colliver, D.G.; W.E. Murphy; W. Sun. 1994. "Development of a building component air leakage data base." ASHRAE TRANSACTIONS: RESEARCH. Vol. 100, Part 1, pp. 292-305.

Forest, T.W. 1989. "Moisture transfer through walls." Thermal Envelopes IV. ASHRAE, pp. 532-542. "Building science for a cold climate." (SI edition). Hutcheon, N.B.; G.O. Handegord. 1989. Construction Technology Center Atlantic Inc. Fredericton, New Brunswick. Chapter 11.

Kumaran, M.K. 1996. "Taking guess work out of placing air/vapor barriers." Canadian Consulting Engineer. Vol. March/April, pp. 32-33.

Ojanen, T.; R.O. Kohonen. 1995. "Hygrothermal performance analysis of wind barrier structures." ASHRAE TRANSACTIONS: SYMPOSIA. Vol. 101, pp. 595-606.

Ojanen, T.; C. Simonson. 1995. "Convective moisture accumulation in structures with additional inside insulation." Thermal Envelopes VI/ Effects of Air Movement - Principles. ASHRAE. Vol. 2, pp. 745-752.

Simpson, A.; D.E. O'Connor. 1994. "Timber frame wall: Hygrothermal properties and vapor barrier damage." Building Services Engineering Research and Technology. Vol. 15, No. 3. pp. 179-184.

Trechsel, H.R.; P.R. Achenbach; J.R. Ebbets. 1985. "Effect of an exterior air-infiltration barrier on moisture accumulation within insulated frame wall cavities." ASHRAE Technical Data Bulletin Infiltration. ASHRAE. Atlanta. Vol. 1, No. 2, pp. 23-37.

Trechsel, H.R.; P.R. Achenbach; H.J. Knight; G.W. Lou. 1986. "Evaluation of wind effect on moisture content of frame walls with and without an air-infiltration barrier." Thermal Envelopes III/Effects of Air Movement – Principles. ASHRAE. Vol. 2, pp. 648-662.

Verschoor, J.D. 1986. "Measurement of water migration and storage in composite building construction." pp. 140-153.

Zarr, R.R.; D.M. Burch; A.H. Fanney. 1995. "Heat and Moisture Transfer in Wood-Based Wall Construction: Measured Versus Predicted." NIST Building Science Series 173. Building and Fire Research Laboratory, National Institute of Standards and Technology. Gaithersburg, MD. 72 p.

8. Bibliography

"ASHRAE Handbook of Fundamentals" (SI edition). 1993. American Society of Heating, Refrigerating and Air-Conditioning Engineers, Inc. Atlanta, GA., Chapters 20, 21, and 23.

ASTM. 1989. ASTM D 1348-89 "Standard Test Method for Use and Calibration of Hand-Held Moisture Meters." American Society for Testing and Materials. Annual book of Standards, Vol. 06.03, pp. 498-503.

Dumont, R. 1993. "Wood frame wall moisture accumulation study." Saskatchewan Research Council. 31 p.

Fazio, P.; A. Athienitis; C. Marsh; J. Rao. 1997. "An environmental chamber for investigation of building envelope performance." Journal of Architectural Engineering, American Society of Civil Engineers. Vol. 3, No. 2, pp. 97-102.

Janssens, A.; H. Hens; A. Silberstein; J. Boulant. 1992. "The influence of underroof systems on the hygrothermal behavior of sloped insulated roofs". Thermal Envelopes V. ASHRAE. Vol. 1, pp. 368-378.

Jones, D. C. 1995. "Impact of airflow on the thermal performance of various residential wall systems utilizing a calibrated hot box". Thermal Envelopes VI / Heat Transfer in Walls II - Principles. ASHRAE. pp. 247-260.

Kumaran, M.K. 1992. "Heat, air and moisture transport through building materials and components: can we calculate and predict ?" Proceedings of the 6th Conference on Building Science and Technology. Waterloo, Ontario. pp. 130-144.

Straube, J.; E. Burnett. 1995. "Moisture movement in building enclosure wall systems". Thermal Envelopes VI / Moisture and Air Leakage Control III-Practices. ASHRAE. Vol. 1, pp. 177-188.

TenWolde, A. 1989. "Moisture transfer through materials and systems in buildings". Water Vapor Transmission Through Building Materials and Systems: Mechanisms and Measurement, ASTM STP 1039. H.R. Trechsel, M. Bomberg, ASTM. Philadelphia. pp. 11-18.

White, J. 1989. "Moisture Transport in Walls: Canadian Experience". Water vapor transmission through building materials and systems: mechanisms and measurement, ASTM STP 1039. H. R. Trechsel and M. Bomberg, ASTM, Philadelphia, pp. 35-50.

Appendix A

Stack effect calculations:

From "Building for a Cold Climate" (Hutcheon, Handegord 1989), the pressure due to the stack effect can be calculated from the following equation:

$$p_s = g * h\, p_t / R_a\, (1/T_o - 1/T_i) \quad (1)$$

where:
p_s = pressure due to stack effect (Pa);
g = acceleration due to gravity (9.81 m/s^2)
h = height from neutral plane (m);
p_t = barometric pressure (101000 Pa);
R_a = gas constant (287.1 J/kg*K for air);
T_o = outside temperature (264.5K for winter, 289K for spring);
T_i = inside temperature (295K for winter, 296K for spring).

For winter conditions:
$p_s = 9.81 * (2.8 * 101000 / 287.1) (1/264.5 - 1/295)$
$p_s = 9.81 * 985 * (0.0038 - 0.0034)$

p_s = 3.865 Pa or **4 Pa**

For spring conditions:
$p_s = 9.81 * (2.8 * 101000 / 287.1) (1/289 - 1/296)$
$p_s = 9.81 * 985 * (0.0035 - 0.0034)$

p_s = 0.966285 Pa or **1 Pa**

Appendix B

Method to analyze the air leakage measurements data.

The "power law" equation:

$$Q = C(\Delta P)^n \quad (2)$$

where :

Q = airflow, m^3/s ;
ΔP = pressure differential, Pa ;
C = flow coefficient, $m^3/s(Pa)^n$;
n = flow exponent, dimensionless.

Then, the "C" and "n" coefficients are determined by performing a log transformation on the data:

$$\ln Q = \ln C + n * \ln(\Delta P) \quad (3)$$

A least-squares regression is done on the linear transformed data to determine the slope (n) and the intercept (C) of the line. This relationship is not based on any fundamental fluid flow principles. It is expected that the exponent "n" should lie between 0.5 (approximating orifice flow) and 1.0 (approximating fully developed laminar flow) (Colliver 1994).